ฟิล์มบางแบบพรุนของไทเทโนซิลิเกตบนซับสเตรตซิลิกอนเพื่อเป็นตัวเร่งปฏิกิริยาไฮดรอกซิเลชันของฟีนอลในปฏิกรณ์แบบไหลต่อเนื่อง

นางสาวกุสุมา ศรียะนัย

วิทยานิพนธ์นี้เป็นส่วนหนึ่งของการศึกษาตามหลักสูตรปริญญาวิทยาศาสตรมหาบัณฑิต
สาขาวิชาปิโตรเคมีและวิทยาศาสตร์พอลิเมอร์
คณะวิทยาศาสตร์ จุฬาลงกรณ์มหาวิทยาลัย
ปีการศึกษา 2559

TITANOSILICATE POROUS THIN FILM ON SILICON SUBSTRATE AS CATALYST FOR HYDROXYLATION OF PHENOL IN CONTINUOUS FLOW REACTOR

Miss Kusuma Sriyanai

A Thesis Submitted in Partial Fulfillment of the Requirements
for the Degree of Master of Science Program in Petrochemistry and Polymer Science
Faculty of Science
Chulalongkorn University
Academic Year 2016

Thesis Title	TITANOSILICATE POROUS THIN FILM ON SILICON SUBSTRATE AS CATALYST FOR HYDROXYLATION OF PHENOL IN CONTINUOUS FLOW REACTOR
By	Miss Kusuma Sriyanai
Field of Study	Petrochemistry and Polymer Science
Thesis Advisor	Assistant Professor Sukkaneste Tungasmita, Ph.D.
Thesis Co-Advisor	Duangamol Tungasmita, Ph.D.

Accepted by the Faculty of Science, Chulalongkorn University in Partial Fulfillment of the Requirements for the Master's Degree

.....Dean of the Faculty of Science
(Associate Professor Polkit Sangvanich, Ph.D.)

THESIS COMMITTEE

.....Chairman
(Assistant Professor Rattachat Mongkolnavin, Ph.D.)

.....Thesis Advisor
(Assistant Professor Sukkaneste Tungasmita, Ph.D.)

.....Thesis Co-Advisor
(Duangamol Tungasmita, Ph.D.)

.....Examiner
(Associate Professor Voravee Hoven, Ph.D.)

.....External Examiner
(Papapida Pornsuriyasak, Ph.D.)

กุสุมา ศรียะนัย : ฟิล์มบางแบบพรุนของไทเทโนซิลิเกตบนซับสเตรตซิลิกอนเพื่อเป็นตัวเร่งปฏิกิริยาไฮดรอกซิเลชันของฟีนอลในปฏิกรณ์แบบไหลต่อเนื่อง (TITANOSILICATE POROUS THIN FILM ON SILICON SUBSTRATE AS CATALYST FOR HYDROXYLATION OF PHENOL IN CONTINUOUS FLOW REACTOR) อ.ที่ปรึกษาวิทยานิพนธ์หลัก: ผศ. ดร. สุคคเณศ ตุงคะสมิต, อ.ที่ปรึกษาวิทยานิพนธ์ร่วม: ดร. ดวงกมล ตุงคะสมิต, 101 หน้า.

ในงานวิจัยนี้ศึกษาการเตรียมไทเทเนียมซิลิกาไลต์-1 และโลหะไทเทเนียมซิลิกาไลต์-1 วัสดุที่สังเคราะห์ได้แบ่งออกเป็น 2 ประเภทได้แก่แบบผงและฟิล์มบางซึ่งทั้งสองแบบของไทเทเนียมซิลิกาไลต์-1 และโลหะไทเทเนียมซิลิกาไลต์-1แบบฟิล์มบางสังเคราะห์ได้จากวิธีก่อผลึกร่วมกับไฮโดรเทอร์มัล ในขณะที่โลหะไทเทเนียมซิลิกาไลต์-1 แบบผงเตรียมได้จากวิธีไฮโดรเทอร์มัล ซิลิกอนเวเฟอร์ถูกนำมาใช้เป็นตัวสารชั้นฐานในการสังเคราะห์วัสดุฟิล์มบาง โลหะที่สนใจในงานวิจัยนี้คือวาเนเดียมและเหล็ก วัสดุที่สังเคราะห์ได้ทั้งหมดถูกตรวจสอบลักษณะเฉพาะโดยใช้เทคนิคการเลี้ยวเบนของรังสีเอ็กซ์ การดูดกลืนแสงยูวี การดูดซับแก๊สไนโตรเจน กล้องจุลทรรศน์อิเล็กตรอนแบบส่องกราด และอินดักทีฟลีคัปเปิลพลาสมาแมสเปกโทรเมตรี วัสดุที่เตรียมได้ทั้งหมดแสดงถึงโครงสร้างแบบเอ็มเอฟไอ ขนาดของอนุภาคที่เล็กเป็นผลมาจากการเติมสารก่อผลึกในปริมาณที่สูงซึ่งเท่ากับร้อยละ 10 โดยเทียบน้ำหนักของแหล่งซิลิกา หลังจากทำการเติมโลหะเข้าไปความเป็นผลึกของวัสดุที่สังเคราะห์ได้ลดลง วัสดุที่สังเคราะห์ได้ทั้งหมดถูกทดสอบความสามารถในการเร่งปฏิกิริยาไฮดรอกซิเลชันของฟีนอลด้วยไฮโดรเจนเปอร์ออกไซด์ วัสดุแบบผงที่สังเคราะห์ได้ทั้งหมดถูกทดสอบในเตาปฏิกรณ์แบบกะเพื่อศึกษาอิทธิพลของตัวแปรของปฏิกิริยา รวมทั้งอัตราส่วนโดยโมลของฟีนอลต่อไฮโดรเจนเปอร์ออกไซด์ และอุณหภูมิในการทำปฏิกิริยา ในบรรดาขนาดของตัวเร่งปฏิกิริยาไทเทเนียมซิลิกาไลต์-1ที่ต่างกัน สารก่อผลึกไทเทเนียมซิลิกาไลต์-1แสดงค่าการเปลี่ยนไปของฟีนอลสูงที่สุดที่ 30.36 เปอร์เซ็นต์เนื่องจากมีขนาดของอนุภาคเล็กที่สุด นอกจากนี้เหล็กไทเทเนียมซิลิกาไลต์-1 แสดงถึงค่าการเปลี่ยนไปของฟีนอลที่สูงและมีค่าการเลือกจำเพาะต่อคาทิคอลสูงที่ร้อยละ 43.46 และ 64.5 ตามลำดับ ในปฏิกรณ์แบบต่อเนื่องที่อัตราการไหล 4 ไมโครลิตรต่อนาที ให้ค่าการเปลี่ยนไปของฟีนอลสูงสุดเมื่อใช้ตัวเร่งปฏิกิริยาเป็นฟิล์มบางไทเทเนียมซิลิกาไลต์-1 ส่วนค่าการเปลี่ยนไปของฟีนอลในกรณีของฟิล์มบางเหล็กไทเทเนียมซิลิกาไลต์-1ให้ค่าต่ำกว่าฟิล์มบางไทเทเนียมซิลิกาไลต์-1 เนื่องจากฟิล์มบางเหล็กไทเทเนียมซิลิกาไลต์-1มีความหนาของฟิล์ม น้อยกว่า อย่างไรก็ตามฟิล์มบางเหล็กไทเทเนียมซิลิกาไลต์-1 ให้ค่าการเลือกจำเพาะต่อคาทิคอลสูงเช่นเดียวกับปฏิกิริยาในปฏิกรณ์แบบกะ

สาขาวิชา ปิโตรเคมีและวิทยาศาสตร์พอลิเมอร์ ลายมือชื่อนิสิต .....

ปีการศึกษา 2559 ลายมือชื่อ อ.ที่ปรึกษาหลัก .....

ลายมือชื่อ อ.ที่ปรึกษาร่วม .....

5572239423 : MAJOR PETROCHEMISTRY AND POLYMER SCIENCE
KEYWORDS: THIN FILM/TITANIUM SILICALITE-1/IRON-TITANOSILICATE-1/PHENOL HYDROXYLATION

KUSUMA SRIYANAI: TITANOSILICATE POROUS THIN FILM ON SILICON SUBSTRATE AS CATALYST FOR HYDROXYLATION OF PHENOL IN CONTINUOUS FLOW REACTOR. ADVISOR: ASST. PROF. SUKKANESTE TUNGASMITA, Ph.D., CO-ADVISOR: DUANGAMOL TUNGASMITA, Ph.D., 101 pp.

This research investigated the preparation of titanium silicalite-1 and metal titanium silicalite-1 materials. The synthesized materials were applied into 2 parts as powder and thin film forms. Both titanium silicalite-1 form and metal titanium silicalite-1 thin film were synthesized by seeding together with hydrothermal method, while metal titanium silicalite-1 powder was prepared by hydrothermal method. The silicon wafer is used as substrate for synthesizing thin film material. The interested metals in this research were vanadium and iron. All synthesized materials were characterized by X-ray powder diffraction, DR-UV spectrophotometry, N_2 adsorption-desorption, scanning electron microscopy and inductively coupled plasma mass spectrometry. All prepared materials showed characteristic of MFI structure. The smaller particle size was resulted from the higher seed loading as 10 wt.% base on silica source. After metal addition, the crystallinity of synthesized materials was decreased. The catalytic activities of synthesized materials were investigated in phenol hydroxylation with hydrogen peroxide. All powder synthesized materials were carried out in batch reactor. The influence of reaction parameter, including mole ratio of phenol/ hydrogen peroxide and reaction temperature were examined. Among several of particle size of titanium silicalite-1 catalysts, the titanium silicalite-1 seed illustrated the highest phenol conversion at 30.36% due to the smallest of particle size. The iron titanium silicalite-1 demonstrated high phenol conversion and highest catechol selectivity as 43.46 and 64.5%, respectively. In the continuous flow reactor at 4 µl/min displayed the highest phenol conversion when titanium silicalite-1 thin film was used. The phenol conversion of iron titanium silicalite-1 thin film was lower than titanium silicalite-1 thin film due to the thinner film thickness. However, iron titanium silicalite-1 provided the high selectivity to catechol same as in batch reaction.

Field of Study:	Petrochemistry and Polymer Science	Student's Signature	.....
		Advisor's Signature	.....
Academic Year:	2016	Co-Advisor's Signature	.....

ACKNOWLEDGEMENTS

Firstly, I would like to deeply thank Assistant Professor Dr. SukkanesteTungasmita and co-advisor, Dr. Duangamol Tungasmita for help and offering valuable advice in this research and resolve advice of my thesis problem.

I would like to gratitude to Assistant Professor Dr. Rattachat Mongkolnavin, as the chairman, Associate Professor Dr. Voravee P. Hoven and Dr. Papapida Pornsuriyasak who have been members of thesis committee, for all of their kindness and useful advice in the research.

Moreover, I would like to gratefully thank Department of Petrochemistry and Polymer Science, Faculty of Science, Chulalongkorn University for the providing the accommodation in laboratories and instruments. I would like to thank the Graduate School Thesis Grant, Chulalongkorn University for research grants.

Finally, I would like to greatly thank to my family, all of my friends and the members of Materials Chemistry and Catalysis Research Unit for their help and encouragement throughout during my research.

CONTENTS

Page

Page

Page

Page

Page

LIST OF TABLES

Table **Page**

LIST OF FIGURES

Figure **Page**

LIST OF SCHEMES

Scheme **Page**

LIST OF ABBERVITATION

a.u.	Arbitrary unit
BET	Brunauer-Emmett-Teller
℃	Degree Celsius
g	Gram (s)
MS	Mass spectroscopy
μm	Micrometer (s)
ml	Milliliter
nm	Nanometer (s)
Ph	Phenol
HQ	Hydroquinone
CT	Catechol
BQ	Benzoquinone
%	Percentage
XRD	X-ray diffraction
SEM	Scanning electron microscopy

CHAPTER I

Introduction

1.1 Background

Catalysts are a key role in the chemical industry and industrial research. According to the report of global catalyst market, the demand for catalysts in the global market stood at US$19.2 billion in 2012 and is expected to reach US$24.1 billion in 2018. The demand and revenue of catalysts are rising in each year as shown in figure 1.1. The development of catalysts is fulfilling the economic and political. In addition, using catalysts is expected to replace pollution in chemical reaction. In the global catalyst market, environmental application is rapidly growing. The manufacturers are focusing on launch innovative products with thorough research and development catalysts that are environmentally friendly.

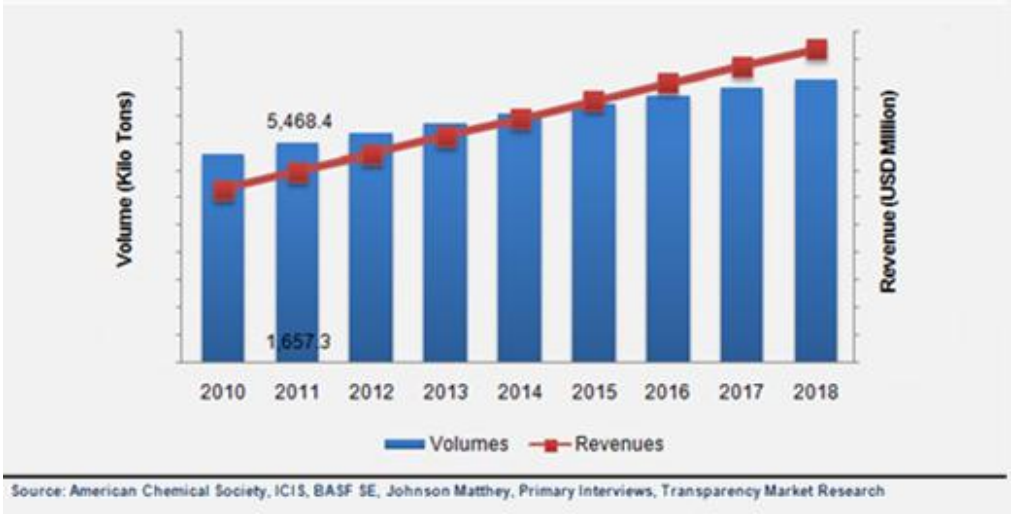

Figure 1.1 Global environmental catalysts market, 2010-2018 (Kilo Tons) (USD million) [1]

Catalysts are broadly classified as heterogeneous and homogeneous. Heterogeneous catalysts are the more mighty used type of catalysts. The advantage of heterogeneous catalyst is friendly environmental. It has become an importance used in the petrochemical, fine chemical and pharmaceutical industries. The industry requires the catalyst for many continuous processes. Normally, catalysts are prepared as fine powders, which quite difficult to use in a continuous flow reactor because the high pressure drop caused by catalyst. Zeolites are also produced as a fine crystalline powder. Previous uses for industrial, zeolites are usually used in the configuration of spheres, pellets or extrudates. In order to make the formation of pellets or extrudates, binder was added to zeolite. Although, the binder can reduce the adsorption properties of the zeolite and can clog the pore of zeolite[2]. Accordingly, the preparation of non-binder zeolite was interested. Zeolite thin film was introduced to use in many industrial applications such as microelectronic-devices[3], membrane[4, 5], sensor[6, 7], and catalyst[8]. The catalyst thin films are usually prepared by pre-seeding the substrate with zeolite nanocrystals then, followed by a hydrothermal synthesis.

The catalysts can also be classified on the basis of materials. This includes zeolites, metals, chemical compounds and others. Even, zeolites were mainly employed in petroleum refineries and chemical synthesis for the last decade. However, chemical compounds dominate the demand for catalysts in terms of both volume as well as revenue. Currently, oxidation reactions are widely used in industry and fundamentally studies in industry laboratory for improvement and other issues. Environmental protection is also another issue to considering in the process. The catalysts of oxidation reaction play a key role for a new selective oxidation processes such as oxidation of aromatic, alkene, and alcohol [9-12]. Among them, hydroxylation of phenol is one of the most important and encouraging chemical process. The main industrial products from phenol are phenol resin, caprolactam, bisphenol A, adipic acid, and alkyl phenol. Catechol and hydroquinone are also high value chemicals. They can be produced by direct hydroxylation of phenol with the favorable oxidant, hydrogen peroxide. These hydroquinone and catechol are widely used as medicine antioxidants, perfumes, polymerization inhibiter, organic synthesis and other

pharmaceutical applications. The phenol hydroxylation with hydrogen peroxide was respected as production process for its outstanding advantage mild condition, shape-selective oxidation as well as simple and environmentally friendly process.

Furthermore, the trend to develop new catalyst with high efficiency and catalytic stability is increasing due to the environmental concerns and economic considerations. The field of heterogeneous catalysis has recently turned its attention to the study of bimetallic catalysts because they offer the potential of increased activities and selectivity combined with enhanced stability as compared to their monometallic counterparts. Several families of bimetallic catalysts have been commercialized for use in industrial environmental treatment, chemical synthesis and petroleum refining processes. Lately, several work studies of the synthesis bimetallic catalyst containing both titanium and heteroatom such as Fe, Al or B in MFI structure have been reported [13-15]. The reactions are usually performed on powder catalyst but only a few reactions had been managed on thin film or membrane forms.

In this thesis, Titanium silicalite-1 is another material in our focus, because of its unique catalytic properties for selective oxidation of organic compound. Titanium silcialite-1 was first synthesis by Taramasso in 1983[16]. It is a microporous material with Mobil Five (MFI) structure for using as selective oxidation of various organic reactants with hydrogen peroxide, in mild condition, for example aromatic hydroxylation, ammoximation of cyclohexanone, oxidation of alkenes and alcohols

1.2 Literature review

1.2.1 Titanium silicalite-1

Titanium silicalite-1 was first discovered by Taramasso in 1983. The titanium silicalite-1 catalyst is constituted by silicon and titanium oxide. The material is usually synthesized by using tetrapropylammonium hydroxide (TPAOH) as structure directing agent, tetraethyiorthosilicate (TEOS) as silica source and tetrabutylorthotitanate (TBOT) as titanium source. The temperature of crystallization is at 130 to 200 ℃ and calcination at 550 ℃. A major problem often received during the synthesis of titanium silicalite-1 is the precipitation of titanium oxide outside the lattice framework, result in inactive of titanium for oxidation reaction. The titanium contents with little or no extra-framework were a suitable titanium silicalite-1 catalyst. According to, tetrapropylammonium hydroxide is an expensive structure directing agent. Titanium silicalite-1 can be synthesized by tetrabutylammonium bromide (TPABr) because of the lower cost but the particle sizes of crystals are larger than the use of tetrapropyl ammonium. Commonly, titanium silicalite-1 synthesized by hydrothermal process that took between 3 and 10 days. The long crystallization time brings about large crystal of titanium silicalite-1. Moreover, the small titanium silicalite-1 particles illustrate high catalytic activity. The small particles of titanium silicalite-1 can be synthesized by adding seeds to the initial solution as it could promote crystal growth and enhance their crystallization rate to decrease of the titanium silicalite-1 crystal size.

Synthesis of a high quality titanium silicalite-1 was studied by Vasile et al. [17]. The tetrapropylammonium bromide was used as structure directing agent, ammonia and sodium hydroxide to provide hydroxide ion are necessary for the crystallization process. In addition, they used amorphous fumed silica as Si source and titanium(IV) butoxide as Ti source. This method avoided the expensive synthesis materials and environmental opponent silica alkoxide. It was found that the large crystals were obtained and the crystal size decreased with increasing titanium

content in this work. The Si/Ti molar ratio of about 25 in the starting gel is the maximum to which well titanium silicalite-1 formation.

Deng et al. [18] reported the hydrothermal synthesis of titanium silicalite-1 with the ultralow of TPAOH/SiO_2 by multistep hydrolysis process. For the first step, a fast hydrolysis and condensation of TEOS observed due to the high ratio of TPAOH/SiO_2, which formed large nuclei. Then, TEOS was added into the first step, the nuclei in the first step used as seed for further crystallization of titanium silicalite-1. It was found that the morphology of titanium silicalite-1 as blackberry with small particle size around 300-400 nm, same as the titanium silicalite-1 synthesized at a high molar ratio of TPAOH/SiO_2. Moreover, the catalytic activity of titanium silicalite-1 synthesized by multiple processes in epoxidation of alkene and ammoximation of ketone was better than synthesized by conventional method titanium silicalite-1.

Zhang et al [19] reported the synthesis of titanium silicalite-1 in the absence of alkali metal ion with the combined effect of seed addition and structure directing agent. Titanium silicalite-1 can be prepared by using hexamethyleneimine (HMI) as structure directing agent and fumed silica as silica source. The titanium silicalite-1 seeds were prepared by conventional method, using tetrapropylammonium hydroxide as a template. The titanium silicalite-1 were prepared by using hexamethyleneimine, 5 wt% of seeds of silica source relative to the total amount of silica in the gel solution were added. They found that, the absence of seed, an amorphous of product was obtained. The crystal size of titanium silicalite-1 was larger, this is because the weak alkalinity of MFI.

Mother liquor of nano-size titanium silicalite-1 used as seed to synthesize the small crystal size titanium silicalite-1 in a TPABr-ethylamine as structure directing agent was discovered by Zuo et al. [20]. The crystal size of titanium silicalite-1 was not affected significantly by the synthesis conditions. However, the crystal size of titanium silicalite-1 depended on the amount of seed addition. From a result, when the small amount of seed with m(seed/SiO_2) = 0.03 added, the large crystal titanium

silicalite-1 was obtained. The catalytic activity of small titanium silicalite-1 with *m*(seed/SiO_2) value of 0.06 exhibited high performance in the epoxidation of propylene.

Titanium silicalite-1 was prepared by seeding to reduce cost and the small crystals obtained. According to the small crystal can improve catalytic activity, Xue et al. [21] synthesized the small crystal titanium silicalite-1 by using the colloid silicalite-1 as seed. The synthesis of small titanium silicalite-1 seed used the tetrapropyl ammonium hydroxide as structure directing agent. The small amount of colloid seeds were added to the initial solution mixture. It was found that the small crystal size of titanium silicalite-1 that synthesized by seeding was about 100-300 nm, which was smaller than the titanium silicalite-1 without seeding. In cyclohexanone ammoxination the small crystal sized titanium silicalite-1 exhibited higher catalytic activity than the large titanium silicalite-1.

1.2.2 Modification and application of titanium silicalite-1

Prasetyoko et al. [22] studied the catalytic performance of Fe_2O_3 titanium silicalite-1 catalyst in phenol hydroxylation. The xFe_2O_3/titanium silicalite-1 was prepared by incipient wetness impregnation method, where x is the amount of iron (II) nitrate in ranges of 0.5-4 wt%. The result showed the catalytic activity of Fe_2O_3/titanium silicalite-1 toward phenol hydroxylation. The test was carried out using hydrogen peroxide as an oxidant and methanol as a solvent at 70 °C. The 1 wt.% of Fe_2O_3 on titanium silicalite-1 exhibited the highest formation rate of hydroquinone. In case of the large amount of Fe_2O_3 in the titanium silicalite-1, it decreased the rate formation of hydroquinone because Fe_2O_3 can block the pore of titanium silicalite-1.

Wu et al. [23] prepared metal loading on titanium silicalite-1 and used as a catalyst in butadiene epoxidation with hydrogen peroxide. The 1% of various metals (metal = V, Cr, Mn, Fe, Co, Ni, Cu, Zn, Cd and La) were loaded into the titanium silicalite-1. It was found that the hydrogen peroxide was decomposed by V, Cr and Mn because of the high conversion of hydrogen peroxide but utilization was relatively low. The introduction of Fe, Co, Ni, Cd and La into titanium silicalite-1 promoted activity in butadiene epoxidation.

The vanadium oxide supported on surface of titanium silicalite-1 was studied by Mulyatun et al. [24]. The vanadium oxide titanium silicalite-1 was prepared by impregnation method. The amount of vanadium loading was varied in ranges 0.5 – 4 wt%. The characterization of the structure of titanium silicalite-1 after loading vanadium oxide found that the structure of titanium silicalite-1 was still remained. By increasing the vanadium oxide on the titanium silicalite-1, the hydrophobicity character of titanium silicalite-1 was increased. The vanadium oxide showed the higher activity than titanium silicalite-1 because of the more hydrophobicity of vanadium titanium silicalite-1.

1.2.3 Phenol hydroxylation

The phenol hydroxylation with hydrogen peroxide over Ti-MSU were investigated by Song et al. [25]. The Ti-MSU catalyst was synthesized by direct hydrothermal synthesis system. The conversion of Ti-MSU was a little bit lower than titanium silicalite-1 at reaction temperature at 60 ℃ for 4 hour over 1:10 of catalyst: phenol mass ratio and 3:1 of phenol: hydrogen peroxide mole ratio which gave 19.6% conversion, hydroquinone selectivity of 48.9%.

Wróblewska et al. [26] used the Ti-MWW heterogeneous catalyst for the production of hydroquinone and catechol. The effect of introduced water to the reaction was investigated. In addition, the other effect of the reaction also studied

such as the reaction temperature 50 to 100 °C, phenol to hydrogen peroxide mole ratio 0.5 to 3, catalyst content 3 to 15 wt% and reaction time 15 to 300 min. The introduction of the additional amounts of water into the reaction mixture caused a slight decrease in the molar ratio of hydroquinone/pyrocatechol. The optimum reaction at the temperature of 100 °C, phenol/hydrogen peroxide mole ratio 1, water content 62%, catalyst content 8wt% and reaction time of 180 min gave the final conversion of phenol of 28 mol% with the selectivity of hydroquinone 43 mol%.

Jiang et al. [27] synthesized the iron containing MCM-41 nanoparticles for phenol oxidation. It was found that decreasing the iron content decreased the Fe-MCM-41 nanoparticle size. After reaction time of 20-30 min, the selectivity of hydroquinone and catechol were 55-65% and 35-45%, respectively. Fe-MCM-41 nanoparticles showed higher conversion than Fe-MCM-41 with larger particle size. This suggests that the particle size of Fe-MCM-41 has an influence on the reaction, indicating that small particle size is important for the reaction.

Ti-SBA-12 and Ti-SBA-16 were prepared by Kumar et al. [28]. They were used as catalyst for phenol hydroxylation with hydrogen peroxide. It has been provide that the characteristic feature of Ti-SBA-12 and Ti-SBA-16 are similar to titanium silicalite-1. The phenol conversion increased with increasing the Ti content in the catalyst. The influence of reaction temperature was studied. The phenol conversion was increased with increasing temperature in ranges of 60 to 90 °C. In addition, when the catalyst amount was increased, the phenol conversion was also increased. The high concentration of hydrogen peroxide gave higher phenol conversion while HQ/CT mole ratio was decreased. It was found that an optimum condition was at 3:1 of phenol: hydrogen peroxide mole ratio at 80 °C for 24 hours, the phenol conversion of Ti-SBA-12 was 24.1% and selectivity of hydroquinone was 53.9%.

1.2.4 Thin film catalyst

Wang et al. [29] synthesized the titanium silicalite-1 on alumina tube by hydrothermal treatment using silicalite-1 and titanium silicalite-1 particles as seed. The titanium silicalit-1 film was used as membrane for phenol hydroxylation. It was found that the titanium silicalite-1 film did not grow on tube without seed. Nevertheless, titanium silicalite-1 film can grow on tube with silicalite-1 and titanium silicalite-1 seed. The synthesis composition was 1 SiO_2: 0.02 TiO_2: 0.18 TPA_2O: 250 H_2O. For the phenol hydroxylation, it was found that the thickness of titanium silicalite-1 increased, the phenol conversion was increased due to the mass of the catalyst increases and also increased in active site.

Jiang et al. [30] studied the phenol oxidation on ultrafine titanium silicalite-1 in a side-stream ceramic membrane separation reactor. The operation conditions were determined. The suitable pore size of the membrane was 200 nm. The optimum condition of titanium ceramic membrane was residence time 8 h, temperature 80 ℃, catalyst concentration 14.1 $kg.m^{-3}$ and phenol to hydrogen peroxide molar ratio 7. The side-stream ceramic membrane reactor system can maintain a steady production of CA and HQ over 20 h. This work demonstrated that the developed side-stream ceramic membrane reactor system, possibly be used for continuous heterogeneous catalytic reactions over ultrafine catalysts.

Yan et al. [31] synthesized the novel Fe-ZSM-5 membrane catalyst for oxidation of phenol. The Fe-ZSM-5 was fabricated on the sintered stainless steel fibers with a thickness of 6 μm. The Fe was loaded on the surface and well dispersed on the surface of ZSM-5 membrane support. The Fe_2O_3 can block the pores of ZSM-5 and the reducing efficiency of catalytic activity was observed. The highest phenol conversion of Fe-ZSM-5 was about 95% with a Fe loading of 25%. The optimum condition was carried out at temperature of 80 ℃, feed flow rate of 2 mL/min and catalyst bed height of 2.0 cm after continuously ran for 7 h.

From the literature reviews, that were mentioned earlier, we can see that the titanium silicalite-1 was suitable for phenol hydroxylation. Thus in this research, the titanium silicalite-1 and metal titanium silicalite-1 were chosen as a catalyst in phenol hydroxylation reaction. Moreover, the titanium silicalite-1 thin films were prepared as catalyst for the continuous reactor. The catalytic activities between batch reaction and flow reaction were investigated and compared in the phenol hydroxylation reaction.

1.3 Objectives

1. To synthesize and characterize titanium silicalite-1 and metal titanium silicalite-1 powder and thin film.
2. To study the optimum condition of phenol hydroxylation in batch reactor.
3. To study for the optimum condition of phenol hydroxylation in flow reactor.

1.4 Scope of work

1. Synthesize titanium silicalite-1 by hydrothermal and seeding methods
2. Synthesize metal titanium silicalite-1 both in powder and thin film forms
3. Material characterizations by using XRD, N_2 adsorption-desorption, DR-UV spectroscopy and SEM
4. Examine the reaction parameters of phenol hydroxylation with hydrogen peroxide, following these fixed parameters:
   - Mole ratio of phenol to hydrogen peroxide; 1:2 to 1:12
   - Reaction temperature; 55 to 65 ℃
   - Flow rate of reactant; 4-8 µl/min
   - Type of metal of catalyst

CHAPTER II
THEORY

2.1 Type of catalysts [32]

2.1.1 Homogeneous catalyst

Homogeneous catalyst is a catalyst in the same phase as the reactants. The catalyst is a molecule which can be compatible in the reaction mixture. The catalyst usually introduced and accelerates reaction with reactants to form target products. However, the homogeneous catalyst is difficult to separate from the product.

2.1.2 Heterogeneous catalyst

Heterogeneous catalyst is in a different physical phase to the reactants and products. The heterogeneous catalytic reaction relates to adsorption of reactants from a fluid phase onto a solid surface, surface reaction of adsorbed species, and desorption of products into the fluid phase. The advantage of using the heterogeneous catalysts is the relative ease of catalyst separation from the product by a simple method such as filtration or centrifugation that could be assisting in the manufacture of continuous chemical process.

2.2 Zeolites [33]

Zeolites are aluminosilicate minerals, microporous materials containing aluminium, silicon, and oxygen in their regular framework as shown in Figure 2.1. The structures of zeolites are aluminosilicate framework, which related three-dimensional network of AlO_4 and SiO_4 tetrahedral linked to each other by sharing all of the oxygen. Zeolites have large cages in their structure that form pore channels. The molecules and ions could pass through of these channels. Moreover, the presence of negative charges in their structure, the charge could be balanced by group I and group II elements such as sodium, magnesium, calcium and barium.

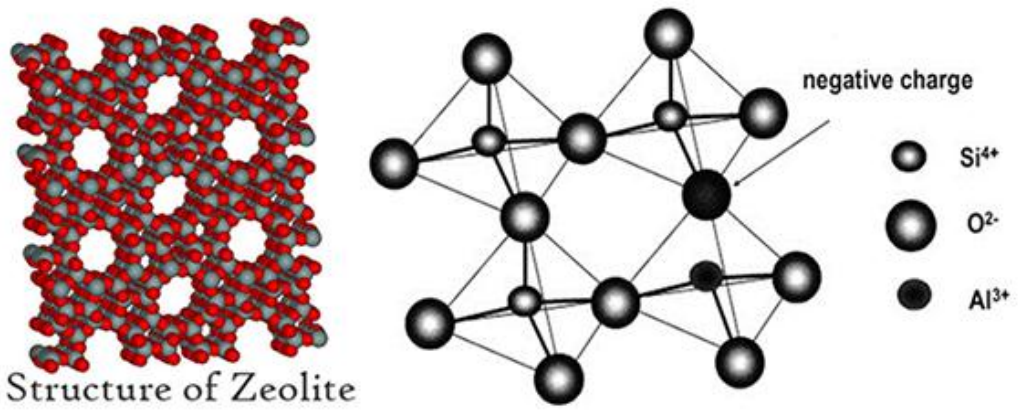

Figure 2. 1 Structure of zeolites[34].

The framework charge of AlO_2^- tetrahedral in the structure is balanced by cation that inhabits nonframework position. The common formula of zeolite is

$$M_{x/n} = [(AlO_2)_x(SiO_2)_y].\ w\ H_2O$$

Where M is cationic of valence n, normally from group I or II ions, and other metals and organic cations are also possible, w is the number of molecules of water. The cations balance the negative charge of AlO_2^- tetrahedral in the structure. x+y is the number of tetrahedral atom. The tetrahedral atoms of the structure of zeolites are specific for a structure such as the MFI structure has number of x+y equal to 96 although FAU structure has number of x+y equal to 192.

2.2.1 Structure of zeolites

Structures of zeolites are three-dimensional framework of the tetrahedral primary building units when tetrahedral atoms are silicon and aluminum, as shown in Figure 2.2. All zeolite structures have in common the primary building unit.

Structures of zeolites are based on a secondary unit (SBU) which consists of selected geometric groupings of these tetrahedral. There are nine such building units, which can be used for describing all of the known zeolite structures. The secondary building units consists of 4,6 and 8-member single ring, 4-4, 6-6 and 8-8 member double rings, and 4-1, 5-1 and 4-4-1 building rings as illustrated to Figure 2.2

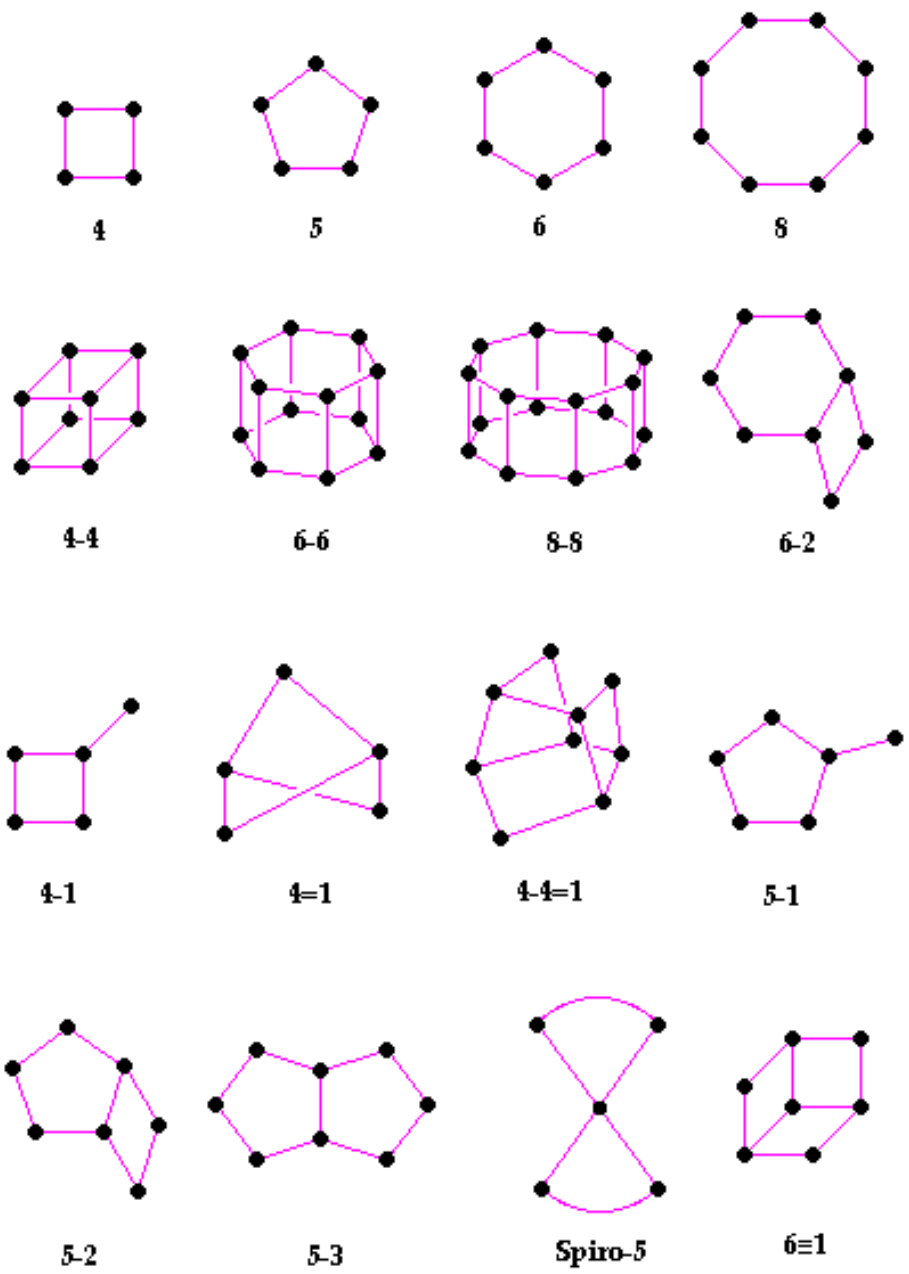

Figure 2. 2 Secondary Building Units (SBU's) in zeolites [35]

The number of oxygen atom relates to the number of tetrahedral atoms which indicated the pore size or the pore opening of zeolite. In the different pore sizes, typical zeolite pore sizes can be divided into 3 groups as shown in Figure 2.3. They include small pore zeolites with 8-ring pores with free diameters of 0.30 - 0.45 nm, zeolite A. The medium pore zeolites formed by a 10-ring, 0.45 - 0.60 nm in free

diameter for ZSM-5 and TS-1. The large pore zeolite with 12-ring opening pores larger than 0.6-0.8 nm such as beta and faujasite[36].

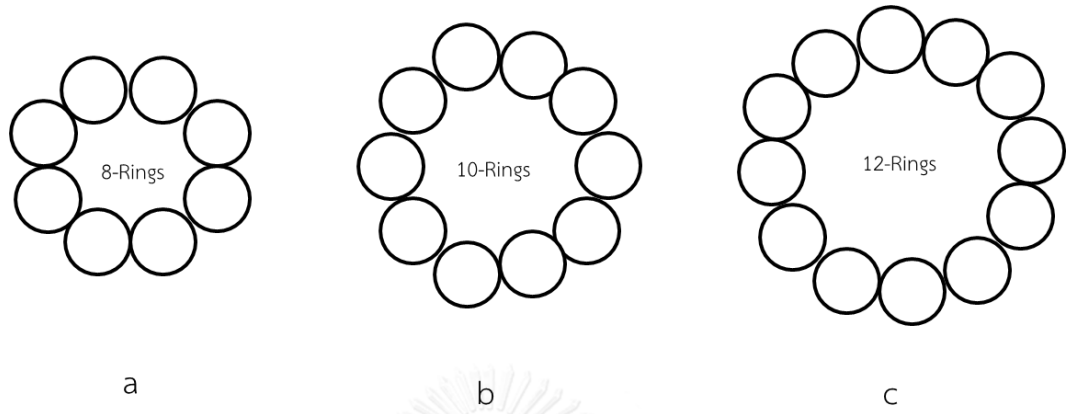

Figure 2. 3Three type of pore opening in zeolite framework (a) small pore (b) medium pore (c) large pore

2.2.2 Shape Selectivity of Zeolites

Shape and selectivity of zeolite catalyst is very important. Zeolite have regular structures and highly crystalline that use as catalyst. Shape and selectivity can be separated into 3 types: reactant shape selectivity, product shape selectivity and transition-state shape selectivity as shown in Figure 2.4. Due to the inflexible pore of any zeolite, only suitable shape and size of reactant can productively diffuse and enter inside in the zeolite pore. Therefore, the reactant molecules with a larger size than the zeolite pore cannot reach the active site, thus the reaction cannot occur. The product will be selected by shape and size where the products of reaction are obtained inside the zeolite pore. Some of the product cannot leave from the zeolite pore. Restricted transition-state selectivity will take place when certain reactions will be interrupted as the transition-state necessary for them to proceed will not be reached due to steric and space restriction.

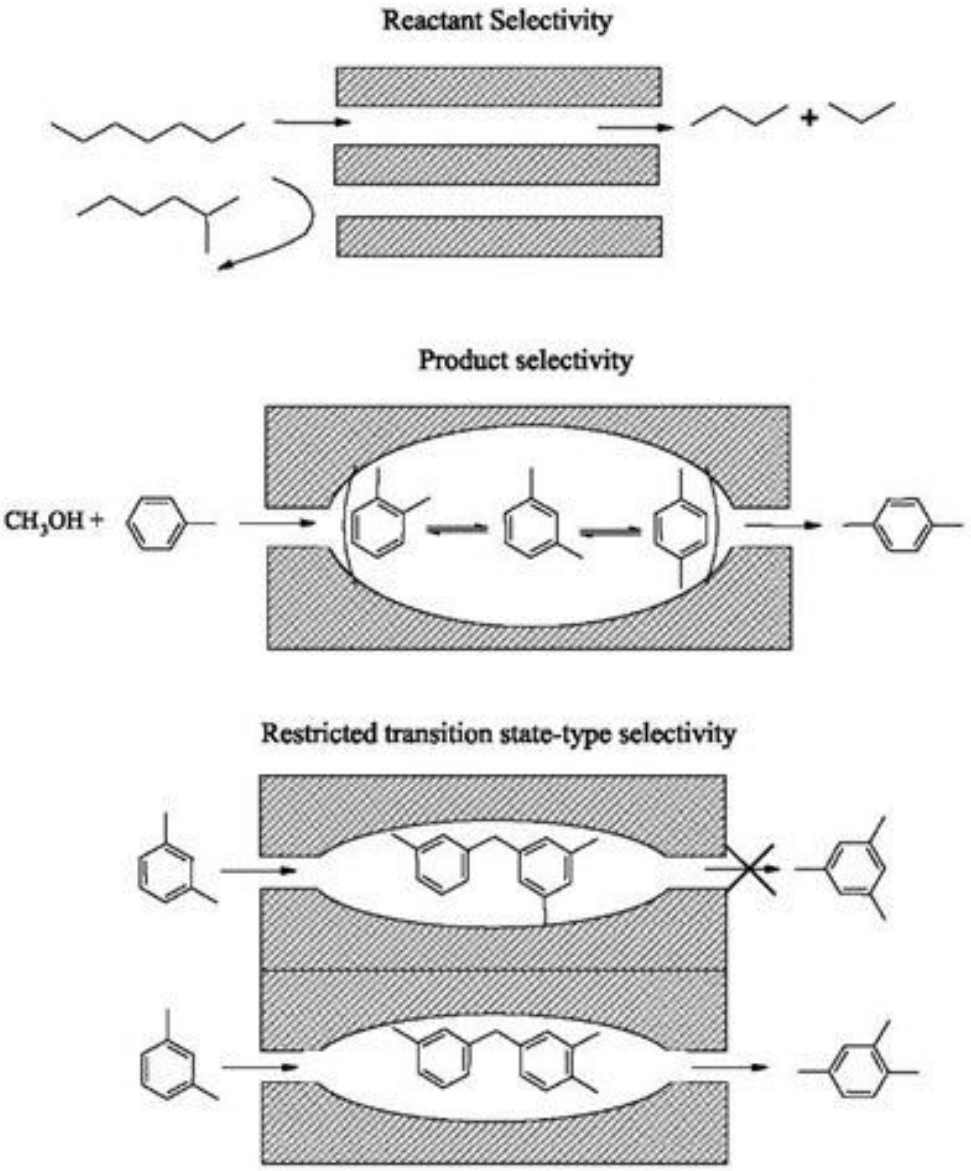

Figure 2. 4 Three types of selectivity in zeolites: reactant, product and transition-state shape selectivity [37]

2.3 Titanium-containing zeolites [38]

Redox zeolite catalysts are one of the excellent in the industry of recent year. The zeolite exists little amount of transition metal ion isomorphously substituted for Si^{4+} in a pure silica framework. The example of titanium silicalite-1 has the structure of MFI with Ti^{4+} in the framework. It demonstrated specific catalytic properties which have been taken advantage in function of oxidation reaction.

Titanium containing materials has been studied for a variety of reactions. Although the selective oxidation with hydrogen peroxide as the oxidant have attracted the most interest. For the formation of surface titanium peroxo compounds with hydrogen peroxide and subsequent transfer of the peroxidic oxygen to the organic reactants have been presented to describe the mechanism by which titanium participates in the catalyst cycle.

2.3.1 Titanium silicalite-1

Titanium silicaite-1 was first synthesized by Taramasso in 1983. The structure of titanium silicalite-1 is MFI structure. The chain type building blocks are from the tetrahedral linkage. Ring consisted of five oxygen atoms are observed in the structure. Titanium silicalite-1 is a medium pore zeolite having an orthorhombic crystalline structure. The pore opening is composed of a 10 membered ring. The MFI framework contains two types of intersection channels: one type is straight, has elliptical (5.3-5.6 Å) opening, and run parallel to the b-axis of the orthorhombic unit cell. The other has near circular (5.1-5.5 Å) opening, is sinusoidal (zigzag) and directed along the a-axis. Figure 2.5 illustrates structure of MFI and schematic of three-dimensional channel.

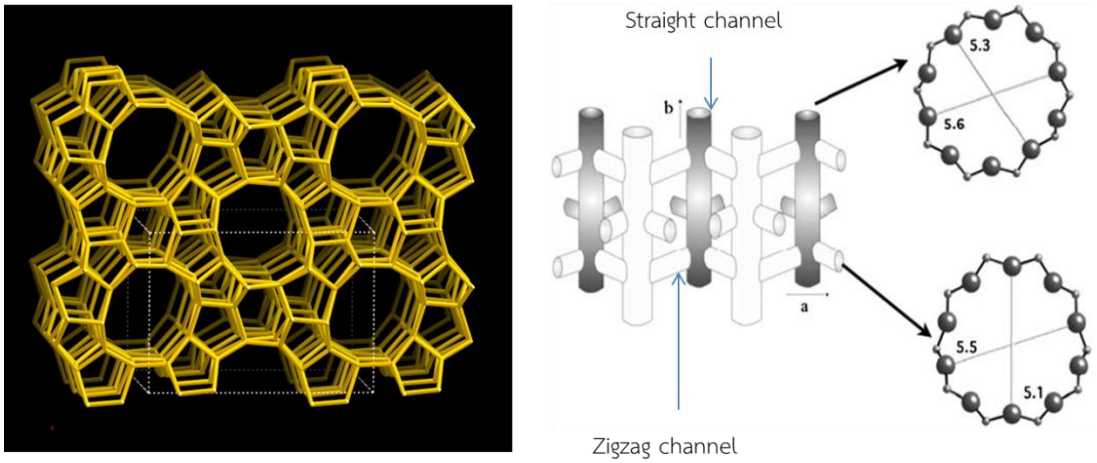

Figure 2. 5(a) Structure of MFI structure[39] (b) Schematic illustration of the three-dimensional channels in titanium silicalite-1 [40]

2.4 Catalytic Sites [41]

Titanium silicalite-1 has Ti^{IV} site in the framework as described the active site, due to pure silicalite-1 are all inactive. In the crystalline structure, Ti^{IV} is present in the structure randomly. More likely, titanium in the precursor reagent is maintained in the solid. In the synthesis solution, each Ti^{IV} is expected to be surrounded by O-Si^{IV} groups and separated from other Ti^{IV} ions by long O-Si-O-Si-O order. It has been offered that Ti^{IV}, in this state of dispersion and tetrahedral coordination, has properties different from those of other materials having Ti^{IV} sites with octahedral coordination and are not isolated from each other. It has been presented that isolated Ti^{IV} sites have a low activity for H_2O_2 decomposition[42]. Furthermore, isolation alone is not enough to describe all the observed properties. The hydrophobic condition current inside the catalyst pores and the multiplex Ti-O-Si bonds that permit interaction with reactants but prevent complete hydrolysis of the Ti^{IV} sites in titano silicates must also play a role in stabilizing the dispersed Ti^{IV} sites. In addition, the formation of peroxo complex caused by addition the hydrogen peroxide to titanium silicates. It has been offered that the active species transfer oxygen from the oxidant to the reactant.

2.5 Phenol Oxidation [43]

The oxidation reaction of phenol with hydrogen peroxide in the presence of a catalyst is the most acceptable way to producing hydroquinone and catechol. The phenol oxidation reaction with hydrogen peroxide is shown in Scheme 2.1. The interaction of catalysts and hydrogen peroxide gives •OH and HO2• species by a redox mechanism. •OH radicals interact to aromatic ring to obtain hydroquinone and catechol, the further oxidation of hydroquinone can form benzoquinone. Moreover, over oxidation of benzoquinone can be observed to yield a little tar during the reaction of phenol oxidation. Beside, water and oxygen could be obtained by hydrogen peroxide decomposition.

The phenol oxidation reaction could occur through homogeneous or heterogeneous catalyst. For homogeneous catalyst, reactant and product are in the same phase as it would be difficult to separate the product and recover the catalyst from the reaction mixture and it can be corrode the reactor. Therefore, numerous heterogeneous such as metal oxide, supported metal complexes, metallosilicalites, hydrotalcite-like compounds, metal-bearing, mesoporous materials, metal hydroxylphosphates and heteropoly compounds have been attracting research interest recently.

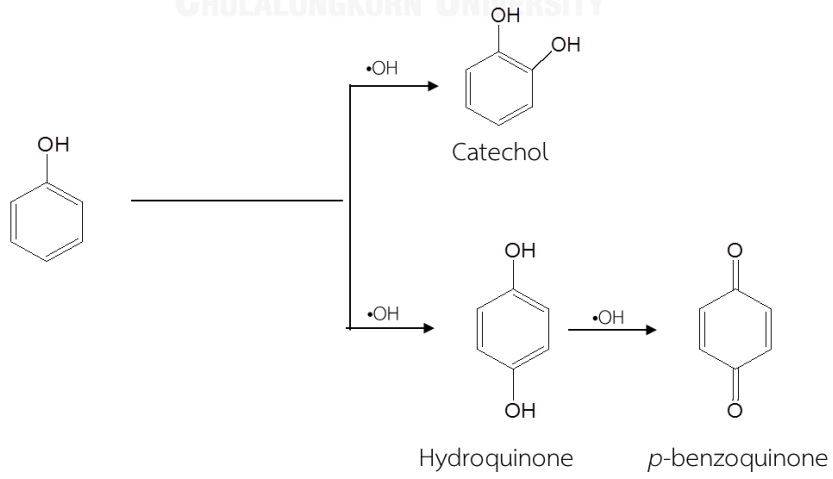

Scheme 2. 1 Phenol hydroxylation with hydrogen peroxide [44]

2.5.1 Reaction mechanism for the hydroxylation of phenol on TS-1 catalyst[45]

The reaction mechanism for the process of oxidation of phenol is not yet fully understood. The protic solvent such alcohol and water can interacted with titanium site. The protic molecules coordinate to titanium which is the active center of the catalyst, expending its coordination sphere 5 or 6. The active intermediate complex for TS-1 catalyst formed a five-membered ring at the titanium site with hydrogen bond between methanol and peroxo group. Possible configurations of the titanium active site without (species c) and with coordination of 1 or 2 protic solvent molecules (species a and b) was demonstrated in Scheme 2.2.

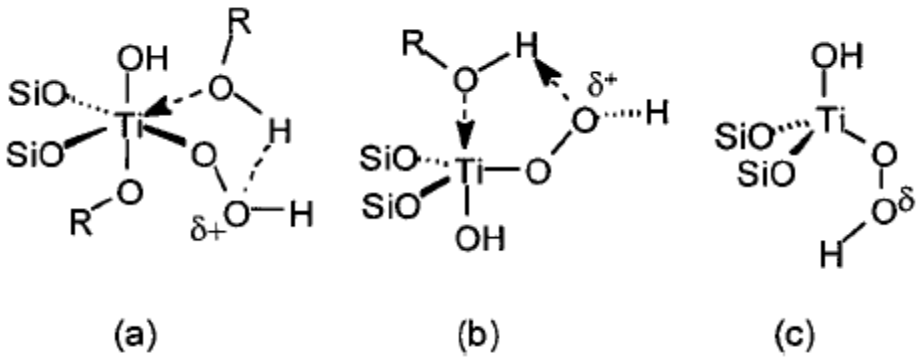

Scheme 2. 2 Possible configurations of the hydroperoxo-titanium active site of TS-1: (a) hexacoordinate octahedral, (b) pentacoordinate trigonal bipyramidal, and (c) tetracoordinate tetrahedral. [45]

Increase the active titanium site caused the coordination of protic solvent molecules. The channels of Titanium silicalite-1 are narrow according to a geometric constraint for an approaching phenol molecule. The phenol molecule is more bulky to form the hydrogen bonds of the phenolic-OH with OH of the solvent groups. Phenol, hydrogen-bonded to the solvent OH groups, will approach the bulky titanium site with the OH group pointing away from the titanium site (Scheme 2.3) yielding hydroquinone. In addition, hydrogen bond formation with the active site (species a and b in Scheme 2.2) leading to the presence of coordinated protic

molecules close to the peroxo group, destabilizing H-bonding with the phenol molecule assisting in o-hydroxylation (as shown in Schemes 2.4A and 2.4B)

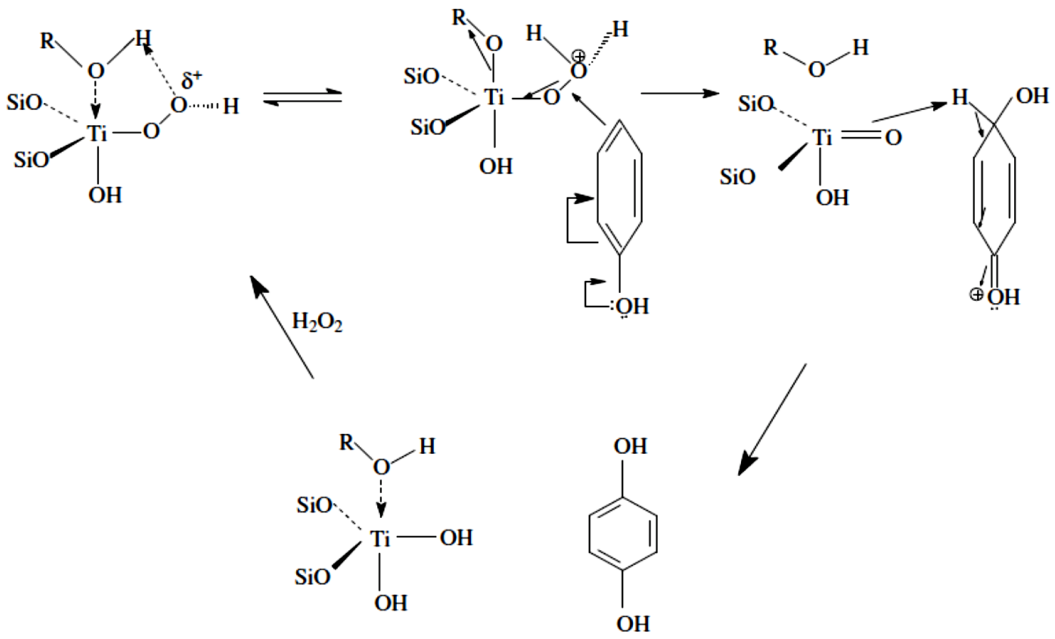

Scheme 2. 3The mechanism of phenol hydroxylation for the formation to hydroquinone [26]

On the other hand, in nonprotic solvents, phenol can take over the role of the protic solvent molecule. Although water is always present, its concentration in the hydrophobic titanium silicalite-1 pores is expected to be low. Thus, the existence of titanium sites without protic molecules coordinated is proposed (Scheme 2.2, species c). In that case, another reaction pathway is opened, i.e., the conversion via pentacoordinated (trigonal bipyramidal) Ti site, involving coordination of phenol to Ti peroxo species yielding catechol (Scheme 2.4A). This will be the case in aprotic solvents, such as acetone. Protic solvents will compete with phenol, so that this pathway is not dominant in these solvents.

Formation of catechol without coordination of phenol to the active titanium site takes place via a six-membered transition state involving phenol (see Scheme 2.4B).

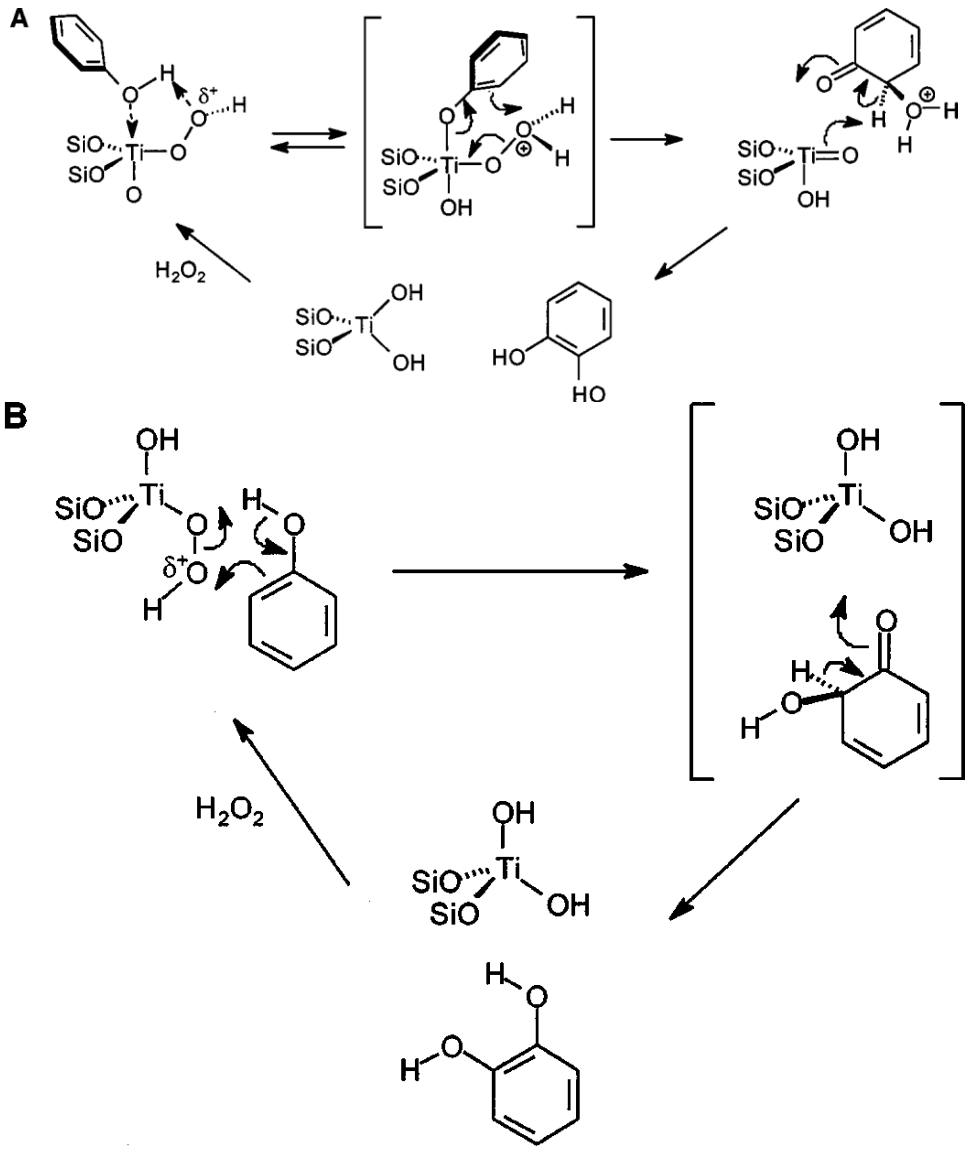

Scheme 2. 4 The mechanism of phenol hydroxylation for the formation to catechol [26]

2.6 Characterizations of catalysis structure

2.6.1 Powder X-ray diffraction (XRD) [46]

The structural of crystalline materials can be identified by using X-ray diffraction technique in powder which is a non-destructive technique. This technique can also determine lattice parameters and interplanar spacing between lattice planes. Furthermore, X-ray powder diffraction can provide the degree of crystallinity of sample relative to a reference compound. The X-ray region falls in the range of electromagnetic spectrum between ultraviolet and gamma-rays. The X-ray wavelength about 0.1 nm is approximately similar for structural examination in a wide range of materials. The X-ray is produced when high energetic electrons collide with a metal target which usually copper (Cu) material. As high accelerating voltage is applied to tungsten filament as the cathode and Cu target as the anode, the high energetic electrons are produced and then collide with the Cu target. These electrons strike on inner core electrons of the target atom, the energy is transferred to the core electrons and the core electrons with excess energy are forced to eject from the atom, leaving a space behind. Electrons from and outer shells, the higher energy shells then fills the space and reduces it extra energy by emitting X-ray with a characteristic wavelength. The energy (E) and wavelength (λ) of X-ray photon are related by the equation $E = hc/\lambda$, where h is Planck's constant and c is the light speed.

Figure 2.6 shows a monochromatic beam of incident X-ray on the surface of crystal at an angle 2θ. The scattered intensity can be measured as a function of scattering angle 2θ. The peaks in x–ray diffractogram or "pattern" directly depend on the interplanar and *d* spacing of the sample. The d-spacing value of sample can be examined by using Braggs' law;

$$n\lambda = 2d\sin\theta, \qquad \text{(Equation. 1)}$$

Where *n* is the order of diffraction beam, λ is the X-ray wavelength, d is the interplanar spacing and 2θ is the angel between the detector position and extrapolation of the incident beam, that is, θ is the angel between incident beam and the lattice plane.

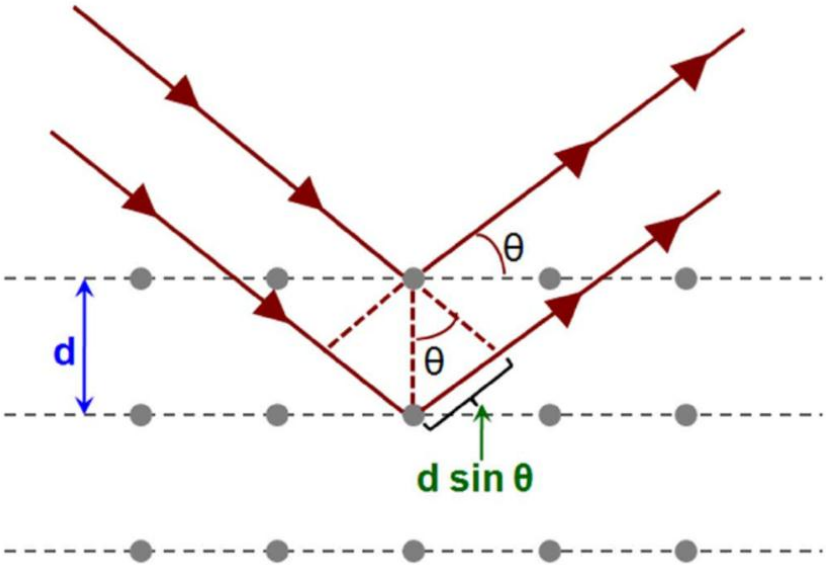

Figure 2. 6 Diffraction of X-ray by regular planes of atoms [45]

X-ray diffractogram is the relationship plotted between peak intensities and direction of wave in angel of 2θ, so call "2θ-scan'. In this work, the structural characterization of our zeolite is determined by this X-ray powder diffraction technique. The X-ray diffractogram is also beneficial for identification of framework

type of zeolite, based on the reference database. The crystallinity of zeolite is related to the XRD peak positions and its relative intensities. Moreover, the size of unit cell can be indicated by peak position and the crystal size can be informed by peak width (FWHM).

2.6.2 Diffuse reflectance-ultraviolet spectroscopy (DR-UV) [47]

Conventionally, the UV-vis analysis can be used to determine the characteristic of the liquid sample. However, the DR-UV cell in this day can be used to analyze the solid sample. The various metals containing zeolite catalyst sample was examined by DR-UV. Expressions are obtained for Kubelka-Munk constants and the remission function in terms of fundamental optical parameter. In general, in a DR-UV spectrum the ratio of the light reflected from the sample and from an ideal non-absorbing reference standard is measured as a function of wavelength (λ). This can be expressed by Kubelka-Munk equation:

$$f(R) = \frac{(1-R)^2}{2R} = \frac{K}{S} \qquad \text{(Equation. 2)}$$

Where *R* is the ratio of the reflectivity of an infinitely thick layer of the sample and the one of a standard, *K* is the apparent absorption coefficient and *S* is the apparent scattering coefficient.

2.6.3 Nitrogen adsorption-desorption technique [48]

The IUPAC classification of porous materials can be derived in to three types as shown in table 2.1. In the adsorption, the adsorbate was adsorbed on the surface of adsorbent. The nitrogen was adsorbed on the surface of materials as the physical adsorption or physisorption due to van der Waals force, which is an attractive force between the nitrogen molecules and the surface of solid materials. Consequently, this attractive force is weak; those adsorbed nitrogen molecules on the surface can be easily desorbed by decreasing the pressure or heating.

Table 2. 1 The IUPAC classification of porous materials

Type	Pore width
Micro pore	< 2 nm
Mesopore	2-50m
Macropore	> 50 nm

Nitrogen adsorption-desorption technique can be used to determine the physical properties as surface area, pore volume, pore diameter and pore size distribution of solid catalyst. Adsorption isotherm describes the adsorption behavior, a plot of the amount of adsorbed gas by the surface of adsorbent at a constant temperature, as a function of relative pressure. Different types of absorbate show many different types of adsorption isotherms, the type of adsorbent and interaction of nitrogen gas on the surface. The IUPAC classification of adsorption isotherms is presented in Figure 2.7. The isotherm type I is the characteristic of microporous materials such as zeolite, and activated carbon. For the micro pore, the nitrogen gas can reach the saturation very fast at the very low relative pressure. The isotherm type II, the adsorption raised at the high relative pressure is designated to porous materials with high external surface area. The isotherm of type III is a signature for the macroporous or non-porous materials, only a small adsorption capacity can be

observed. Type IV and V isotherms are mesoporous materials. Type IV is the adsorption of mesopous containing micropores. In type V isotherm not observe any micropores.

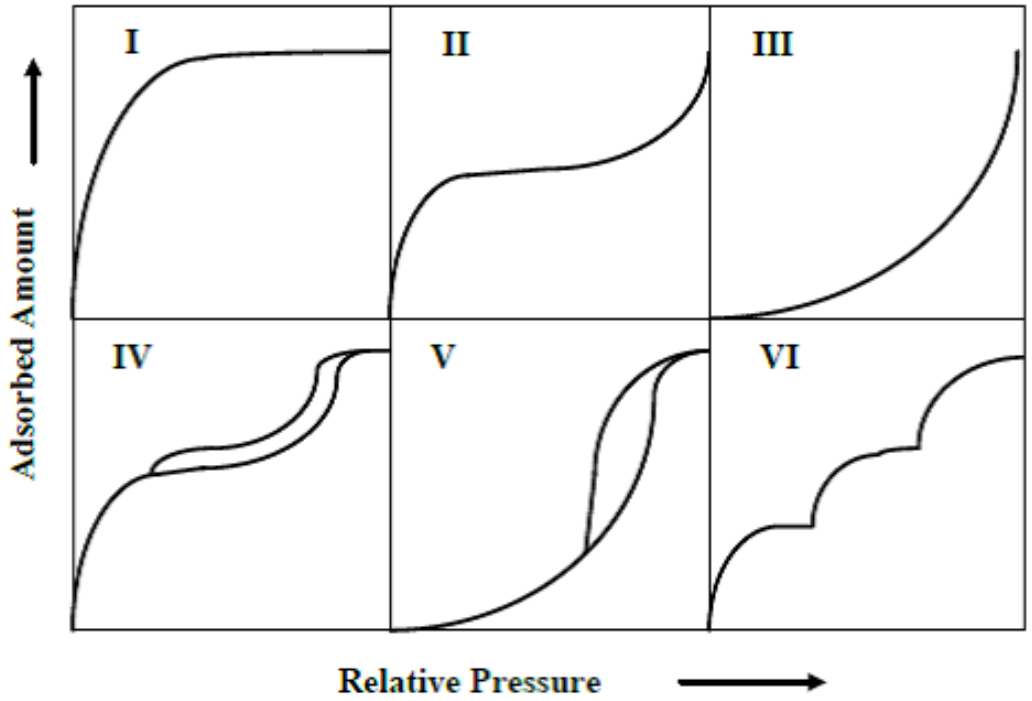

Figure 2. 7 The IUPAC classification of isotherms [49]

In figure 2.8 shows IUPAC classification of hysteresis loops. The shape of the hysteresis loops (types H1–H4) are related with the texture properties of the adsorbent. Type H1 is often associated with porous materials exhibiting a narrow distribution of relatively uniform (cylindrical-like) pores. Hysteresis of type H2 contain a more complex pore structure in which network effects are important. The very steep desorption branch can be attributed to pore blocking. Isotherms with type H3 hysteresis do not exhibit any limiting adsorption at high P/P_0. This behavior can be caused not only by the existence of non-rigid aggregates of plate-like particles but also if the pore network is formed of macropores which are not completely filled with pore condensate. The H4 hysteresis loops are generally observed with complex materials containing both micropores and mesopores. The more pronounced uptake at low P/P_0 can be associated with the filling of micropores. The aggregated crystals

of zeolites, some mesoporous zeolites, and micro-mesoporous carbons discover H4 loop frequently [48].

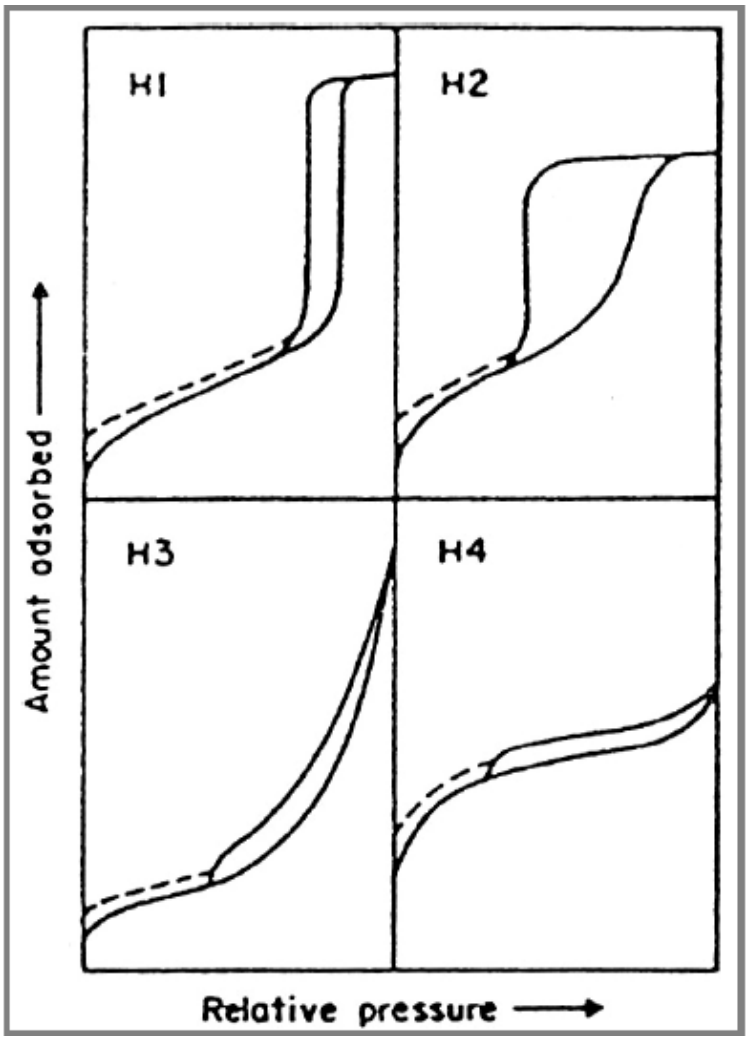

Figure 2. 8 The IUPAC classification of hysteresis loop [48]

Nitrogen adsorption/desorption isotherm at liquid nitrogen temperature (77K) and relative pressure (P/P_0) ranging from 0.05-0.1 is measure pore size distribution. The Brunauer, Emmett and Teller (BET) method is generally used to determine of the specific surface area of porous materials. The BET model was assumed on multilayer adsorption which is different from Langmuir monolayer adsorption. The BET specific

surface area can be obtained from the measurement of adsorption isotherm. The adsorption isotherms are carried out by the BET equation,

$$\frac{P}{V[P_0-P]} = \frac{1}{V_m C} + \frac{C-1}{V_m C}\left(\frac{P}{P_0}\right) \qquad \text{(Equation. 3)}$$

Where V is the volume of adsorbed gas. P and P_0 are the equilibrium and atmospheric pressure of adsorbed gas at the adsorption temperature, and V_m is the monolayer adsorbed gas, and C is the BET constant that is related to the heat of adsorption. The slope ($(C-1)/V_mC$) and intercept ($1/V_mC$) are used to examined the quantity of nitrogen adsorbed in the monolayer and calculate the surface area. The surface area can be calculated by using the equation below, where S_{total} is total surface area, N is Avogadro's number and σ is the gas cross section which is 0.162 nm^2 for the molecules of nitrogen gas.

$$S_{total} = \frac{V_m N \sigma}{M} \qquad \text{(Equation. 4)}$$

2.6.4 Scanning electron microscope (SEM) [50]

The scanning electron microscope (SEM) is one of the most widely used to provide the information detail about the microstructure of materials such as morphology, homogeneity and purity. SEM result brings about the significant information of crystal size, shape and distribution. The SEM shows the 3-dimension black and white magnified image by using electrons instead of light waves as use by traditional microscope. The samples are sputtering coated with a thin layer of gold or other conductive metals if the samples are not conductive. The sample is transferred into the microscope's vacuum chamber trough and airtight door. A beam of high-energy is emitted by an electron gun from the top after the air is pumped out. This beam down the column through a series of magnetic lens made to focus the electrons to an extremely tiny point. The scanning coil is set to move the focused

beam rearward and outward across the specimen, row by row. When the electron beam beats each point on the sample, secondary electrons are leaved from its surface. These electrons are counted by detector and send the signal to amplifier. The amount of electron illuminated from each point on the sample creates the final image, as electron micrograph.

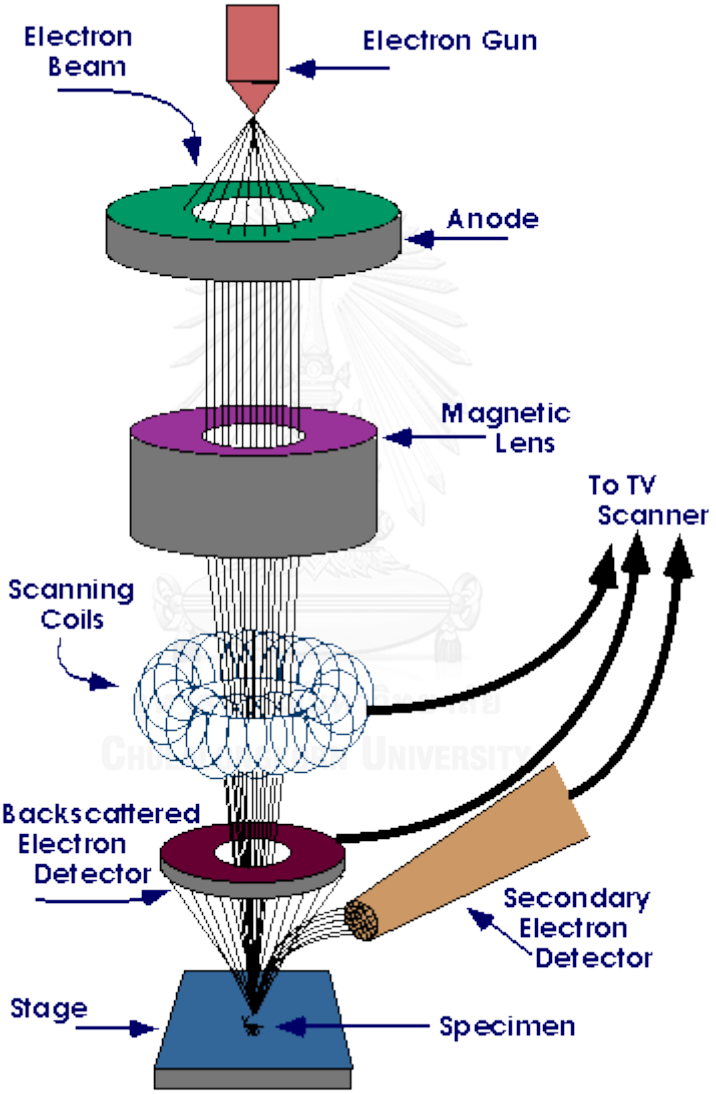

Figure 2. 9 The operating concept of SEM. [51]

2.6.5 Inductively Coupled Plasma-Mass Spectroscopy (ICP-MS) [52]

Inductively coupled plasma-mass spectroscopy (ICP-MS) is multi-elemental analytical technique with very low detection limits in the range of parts per brilliant to part trillion levels. Modern ICP-MS combines a high temperature ICP source with a mass spectrometer. ICP source in ICP-MS was illustrated in Figure 2.10. Argon gas is flow inside the concentric channels of the ICP torch. Electrons are removed from the argon atom to produce argon ion when the flame is hit to the argon flowing through the ICP torch. These ions are taken in the oscillating fields and run into other atoms to generate plasma.

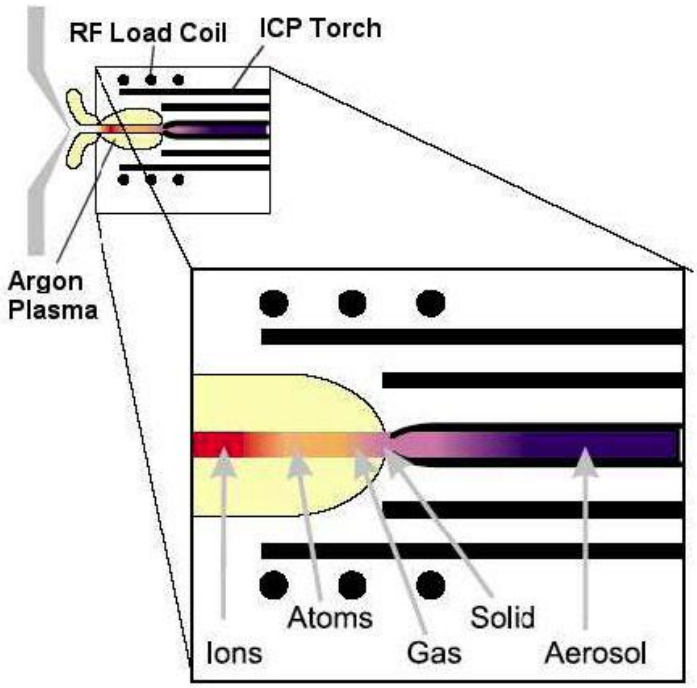

Figure 2. 10 The ICP torch demonstrating the state of the sample. [53]

The sample is introduced through nebulizer into the ICP plasma as aerosol. After that, the sample enters to the center of ICP torch, it evaporates and the elements in the aerosol are changed into gaseous atoms before ionization toward the end of the plasma. Quadrupole mass spectrometers extract the singly-charge ion from the plasma. These ions are separated its mass-to-charge ratio by using quadrupole mass filter which only allow ions of a single mass-to-charge ratio pass the tube to the detector at a given time. Figure 2.11 exhibits the system of ICP-MS.

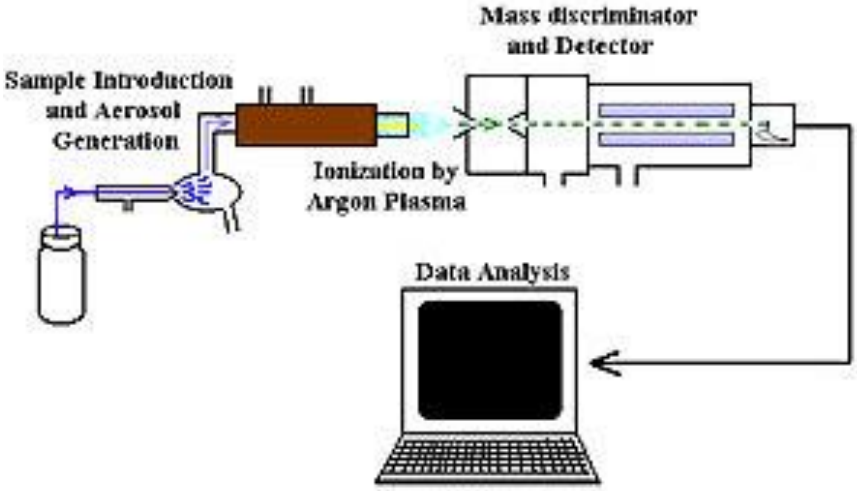

Figure 2. 11 The system of ICP-MS [53]

2.7 Types of reactors [54]

2.7.1 Stirred tank reactors

Stirred tank agitated reactors consist of a tank fitted with a mechanical agitator and a cooling jacket or coils. They are operated as batch reactors or continuous reactors. Several reactors may be used in the series. The stirred tank reactor can be considered the basic chemical reactor; modeling on a large scales the conventional laboratory flask. Tank sizes range from a few liters to several thousand liters. They are used for homogeneous and heterogeneous liquid-liquid and liquid-gas reactions and for reactions that involve freely suspended solids, which are held in suspension by the agitation. As the degree of agitation is under the designer control, stirred tank reactors are particularly suitable for reactions where good mass transfer or heat transfer is required. When operated as a continuous process the composition in the reactor is constant and the same as the product stream and except for very rapid reactions, this will limit the conversion that can be obtained in one stage.

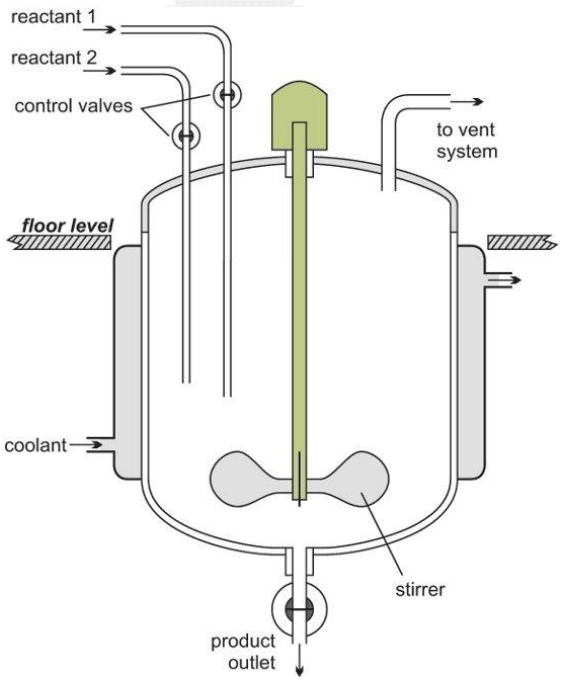

Figure 2. 12 Illustrating a Stirred tank reactors [55]

2.7.2 Tubular reactors

Tubular reactors are generally used for gaseous reactions, but are also suitable for some liquid phase reactions. If high heat transfer rates are required in small diameter tubes are used to increase the surface area to volume ratio. Several tubes may be arranged in parallel, connected to a manifold or fitted into a tube sheet in a similar arrangement to a shell and tube heat exchangers. For high temperature reactions, the tubes may be arranged in a furnace.

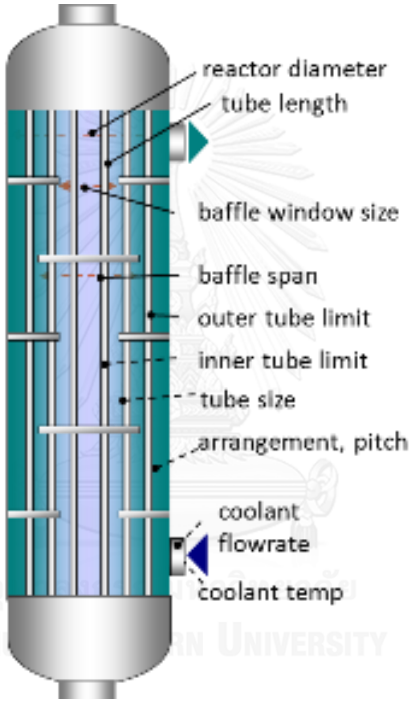

Figure 2. 13 Illustrating a turbular reactor [56]

2.7.3 Packed bed reactors

There are two basic types of packed bed reactor; those in which the solid is a reactant and those in which the solid is a catalyst (Fig.11). In chemical process industries, the emphasize is mainly on the designing of catalytic reactors. Industrial packed bed catalytic reactors range in size from small tubes, a few centimeters diameter to large diameter packed beds. Packed-bed reactors are used for gas and gas-liquid reactions. Heat-transfer rates in large diameter packed beds are poor. Therefore, where high heat-transfer rates are required, fluidized beds should be considered.

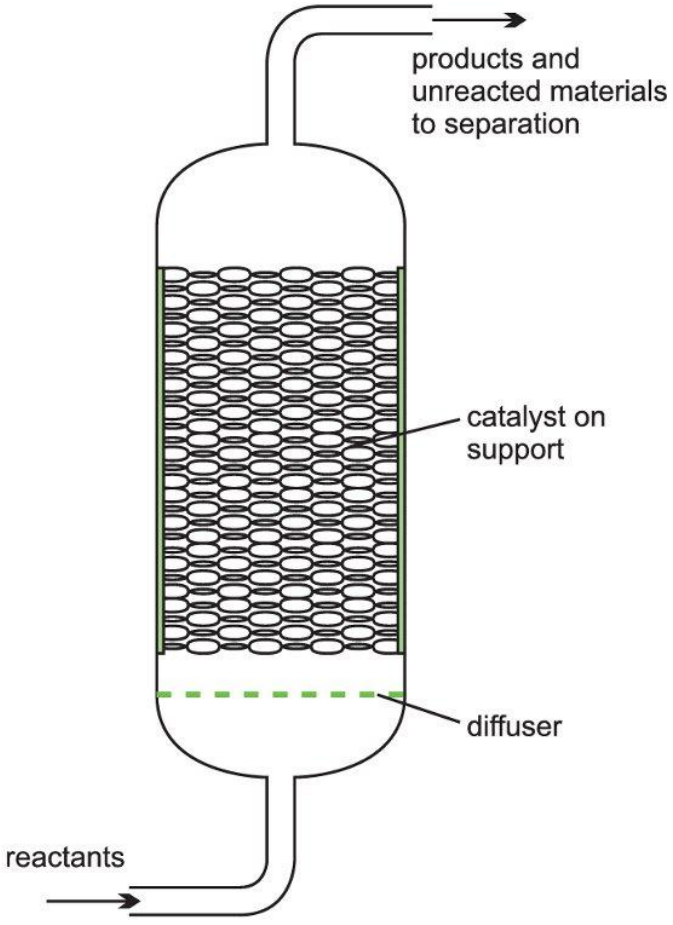

Figure 2. 14 Illustrating a packed bed reactor [57]

2.7.4 Fluidized bed reactors

A fluidized-bed reactor (Fig. 14 is a combination of the two most common, packed-beds and stirred tank, continuous flow reactors. It is very important to chemical engineering because of its excellent heat and mass transfer characteristics. The essential feature of a fluidized bed reactor is that the solids are held in suspension by the upward flow of the reacting fluid. This promotes high mass and heat transfer rates and good mixing. The solids may be a catalyst, a reactant in fluidized combustion processes or an inert powder, added to promote heat transfer. Though the principal advantage of a fluidized bed over a fixed bed is the higher heat transfer rate, fluidized beds are also useful where it is necessary to transport large quantities of solids as part of the reaction processes, such as where catalysts are transferred to another vessel for regeneration. Fluidization can only be used with relatively small a sized particle, that is less than 300μm. This is the limitation of the process.

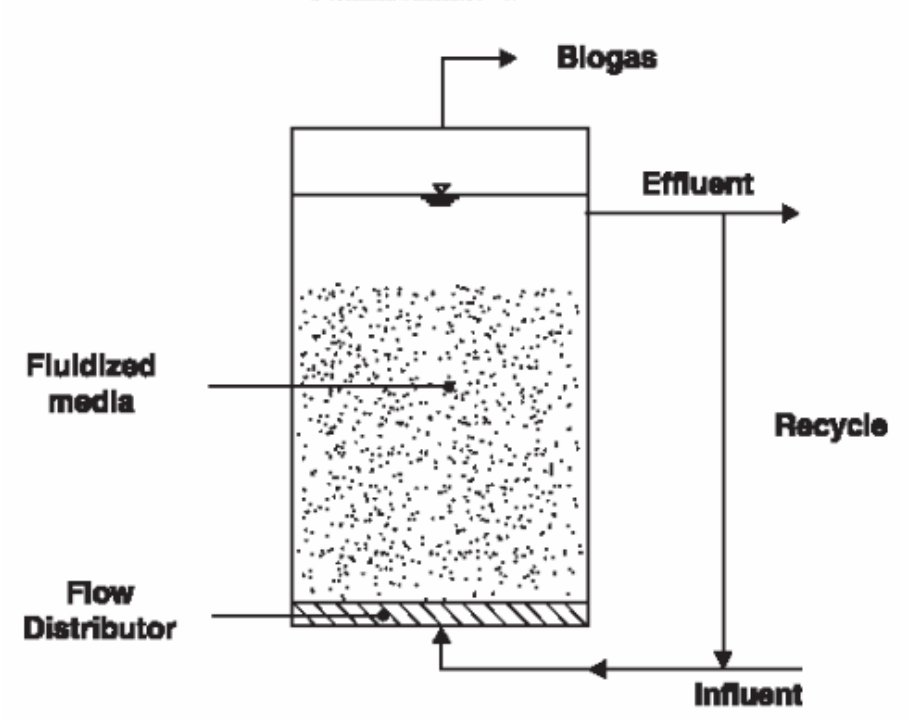

Figure 2. 15 Illustrating a fluidized bed reactor [58]

CHAPTER III
EXPERIMENTAL

3.1 Instruments, apparatus and analytical techniques

3.1.1 Powder X-ray diffraction (XRD)

The X-ray diffractograms or "patterns" of materials were measured by using a Rigaku, Dmax 2200/Ultima^{+} diffratometer, equipped with a monochromator and Cu Kα radiation source. The tube voltage and current were set at 40 kV and 30 mA, respectively. The diffractograms were recorded in the 2-theta ranged from 5 to 50 degree with scan speed 5 degree/min and scan step of 0.02 degree. The scattering slit, divergent slit and receiving slit were fixed at 0.5 degree, 0.5 degree and 0.3 mm, respectively.

3.1.2 Scanning electron microscope (SEM)

Scanning electron micrograph for investigation of morphology and particle size of catalyst were taken by using a JEOL JSM-5410 LV scanning electron microscope (SEM). The powder samples were sprinkled on carbon tape. On the other hand, the film samples were stick on carbon tape. Then, the samples were coated with sputtering gold under vacuum previous analysis to reduce charging effect in SEM.

3.1.3 N_2-adsorption/desorption

N_2 adsorption-desorption isotherm, BET specific surface area, and pore size distribution of the materials were done on the BEL Japan, BELSORP-moni instrument. The powder samples were weighted about 40 mg and weighted precisely after pretreated at 400 °C for 3 hrs. The weight of the thin film materials on the substrate was measured before hydrothermal and after hydrothermal.

3.1.4 DR-UV spectroscopy

Diffused reflectance ultraviolet (DR-UV) in the range of 200-700 nm was used to determine the metal coordination of catalyst. This experiment was done by using the Shimadzu UV-2550 UV-visible spectrophotometer equipped with a 60 °C integrating sphere and pressed powder of Barium sulfate was used as reference.

3.1.5 Micro flow reactor

Oxidation of phenol reaction was carried out in a column reactor. Diameter of reactor tube is 0.6 cm and height is 10 cm.

3.1.6 Elemental analysis

The Si to Ti mole ratio was investigated by ICP-MS. The sample was soaked with 10 mL of conc HCl and 10 mL of 48% hydrofluoric acid in Teflon beaker. The sample was heated but not boiled until the solution was dried. This step was repeated twice or more for all silica atoms were removed as volatile SiF_4 species. Then, the mixture solution of 6M HCl: 6M HNO_3 = 3:1 v/v was added and was heated until dry. In the last step, 10 mL of deionized water was added and was warmed at 150 °C for 5 minutes. The sample solution was transferred into a 50 mL Teflon volumetric flask then water was added to the mark.

3.2 Chemicals

3.2.1 Chemical for Substrate cleaning

1. Trichloroethylene (Unilab, 95 wt.%)
2. Acetone (Merck)
3. Isopropanol (Merck)
4. Trichloroethylene (Unilab, 95 wt.%)
5. Sulfuric acid (Merck)
6. Ethanol
7. Hydrogen peroxide (Merck, 30 wt.%)
8. Hydrofluoric acid (Merck, 48 wt.%)
9. Silver nitrate
10. Nitric acid (Merck, 65%)

3.2.2 Chemicals for synthesis catalyst

1. Trichloroethylene (Unilab, 95 wt.%)
2. Acetone (Merck)
3. isopropanol (Merck)
4. Hydrofluoric acid (Merck, 48 wt.%)
5. 3-Mercaptopropyltrimethoxysilane (Aldrich)
6. Tetrapropyl ammonium hydroxide (Merck, 40 wt.%)
7. Tetraethyl-orthotitanate (Merck, 95 wt.%)
8. Tetraethyl-orthosilicate (Merck, 99 wt.%)
9. Triethoxy-methylsilane (Fluka, 95 wt.%)
10. Iron (III) nitrate (Merck)
11. Vanadium (IV) oxide sulfate (Aldrich)

3.2.3 Chemicals for phenol hydroxylation

1. Phenol (Merck)
2. Hydrogen peroxide (Merck, 30wt %)

3.3 Preparation of substrates

Silicon (002) wafer was used as substrates and cut into 0.5×0.5 cm^2. These silicon substrates were ultrasonic cleaned with trichloroethylene, acetone, iso-propanol and DI water, respectively. The surface of substrates were etched by immersion in 10% hydrofluoric acid for 15 second and then rinsed before dried by nitrogen gas. The process of cleaning of the substrate is shown in Scheme 3.1. Next, the substrates were treated with 3-mercaptopropyl-trimethoxysilane (50mM) for 10 min, and then dried in an oven at 200 ℃ for 2 h.

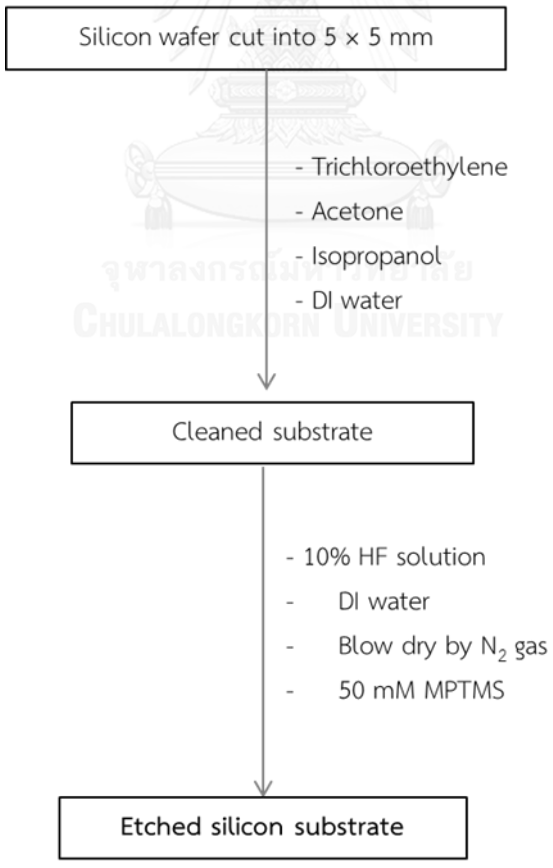

Scheme 3. 1 Preparation of silicon substrates

3.4 Preparation of silicon nanowires substrates

The silicon nanowires were prepared by three different cleaning steps. Firstly, the organic on surface of silicon substrates were removed by acetone. Secondly, the acetone was washed off by ethanol and then the substrates were cleaned with acidic solution which is 3:1 mixture of sulfuric acid and hydrogen peroxide in order to remove metal particle on the substrate surfaces. Lastly, the substrates were cleaned with deionized water. The pre-cleaning method is shown in Scheme 3.2.

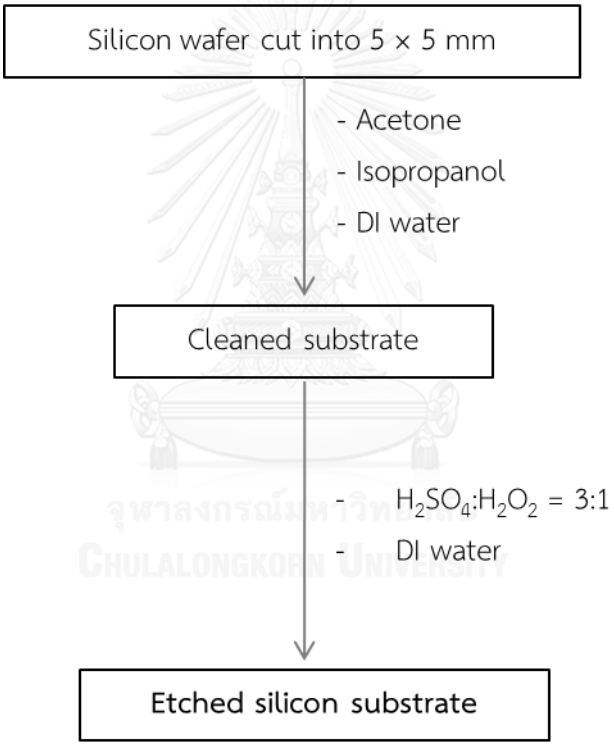

Scheme 3. 2 Pre-cleaning method before etching the silicon substrates.

The etching step has three main parts: oxide removal, nanowire forming, and silver (Ag) clusters removal. First, the silicon substrates were dipped in 2% hydrofluoric acid solution in Teflon beaker for 2 minutes to remove the oxide layers on the substrate surfaces. Then, the substrates were etched in the etching solution which is a mixture of silver nitrate and hydrofluoric acid (0.2 M $AgNO_3$ in 4.6 M HF) at room temperature for 10 minutes, the silicon nanowires was obtained. The silicon nanowires were rinsed with deionized water to stop the reaction step. Finally, the Ag layers was removed by nitric acid solution and then rinsed with deionized water to clean the substrates.

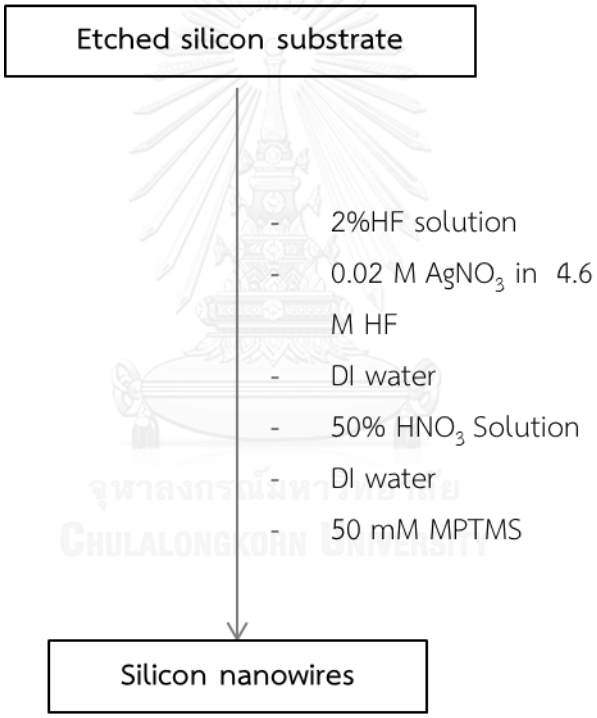

Scheme 3. 3 Etching method to form the nanowires structure.

3.5 Synthesis of titanium silicalite-1 films

3.5.1 Preparation of titanium silicalite-1 seed

Titanium silicalite-1 seeds were synthesized by modified hydrothermal method from previous literatures [59]. In a typical synthesis, 27.1 g tetrapropylammonium hydroxide was dissolved in 108.2 g water in a 500 ml three-necked round bottom flask. Then, 62 g of tetraethylorthosilicate was added dropwise to the mixture, followed by the addition of 3.77 g of tetraethylorthotitanate. The molar composition was 20TEOS: 0.75 TEOT: 9TPAOH: 404H_2O. The mixture solution was vigorously stirred at room temperature for 24 h. Finally, this gel was placed into a Teflon-line autoclave for hydrothermal treatment at 125°C for 96 h. After hydrothermal process, the solid was washed with deionized water before drying at 70°C overnight. The dried solid is described as titanium silicalite-1 seed.

The seeds were diluted with absolute ethanol to give 2wt % suspension of the seed solution. Seeds were deposited onto the silicon substrates by immersion small pieces of silicon wafer in the seed solution for 1 h, following by drying at 60°C overnight and calcination at 550°C for 6 h.

3.5.2 Preparation of titanium silicalite-1 by seeding method

In order to prepare the titanium silicalite-1 crystal from titanium silicalite-1 seed was investigated. The effect of seed amount was studied. From an initial gel with the gel composition of 40 TEOS: 1.6TEOT: 0.4 TEMS: 14TPAOH: 10000H_2O. The amount of titanium silicalite-1 seed was added into the initial gel, of which seed mass was 5 and 10%wt based on the amount of tetraethylorthosilicate. The gel mixture was crystallized at 175 ^{o}C for 24 h. The solid products were denoted as titanium silicalite-1-5% and titanium silicalite-1-10%.

3.5.3 Preparation of titanium silicalite-1 films

Titanium silicalite-1 films growth were prepared by hydrothermal method. Titanium silicalite-1 solution was prepared with composition 40 TEOS: 1.6TEOT: 0.4 TEMS: 14TPAOH: 10000H_2O. 2.97 g of tetrapropylammonium hydroxide were added to 188 g of water. 8.70 g of tetraethylorthosilicate were added dropwise to this solution. Next, 0.380 g of tetraethylorthotitanate and 0.075 g of triethoxymethylsilane were added. The solution mixture was vigorously stirred at room temperature for 24 h. After that, the silicon substrates were placed in a Teflon stand and dip into a Teflon-line autoclave, aged at 175°C for 24 h. As-deposited titanium silicalite-1 films were rinsed with water, dried at 60°C overnight and calcined at 550 °C for 6 h.

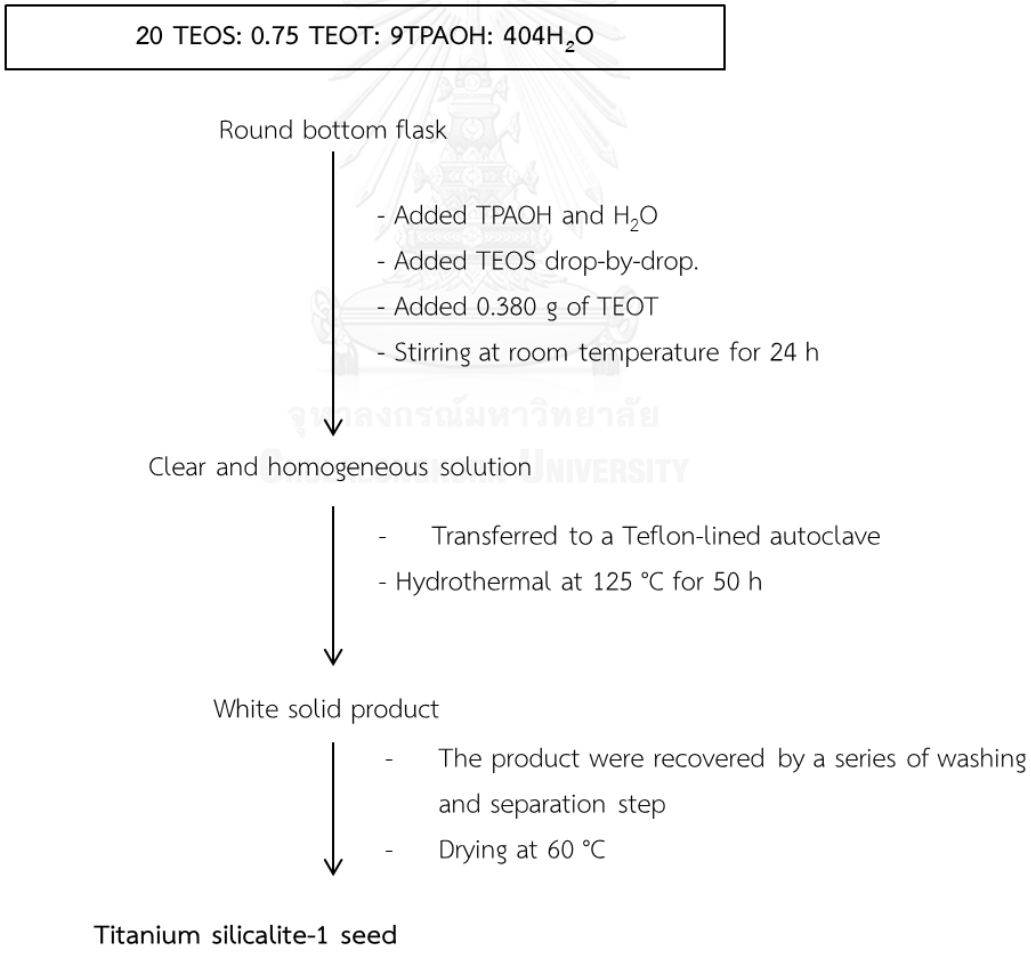

Scheme 3. 4 Preparation diagram for titanium silicalite-1 powder

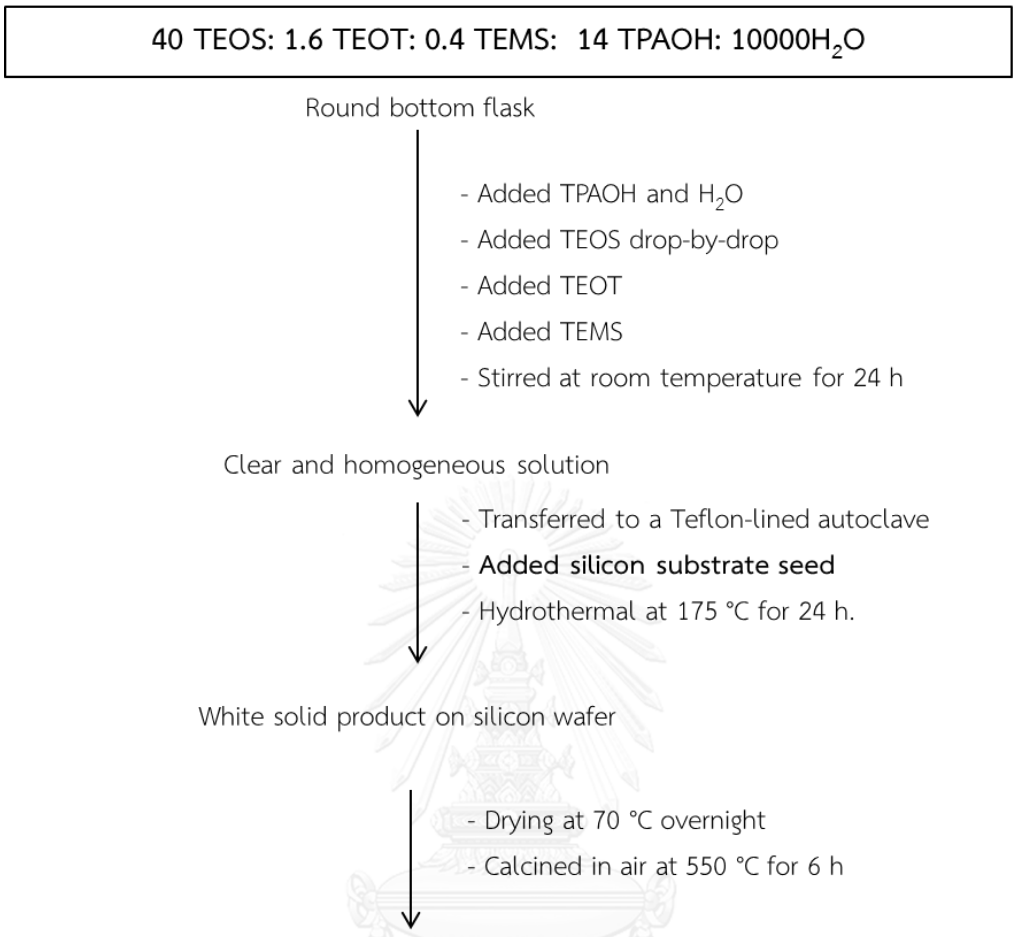

Scheme 3. 5 Preparation diagram for titanium silicalite-1 film

3.6 Preparation of iron titanium silicalite-1 films

3.6.1 Synthesis of iron titanium silicalite-1 and vanadium silicalite-1 powder

Iron-titanium silicalite-1 seeds were synthesized in basic condition using a gel composition of 20TEOS: 0.75TEOT: 0.2$Fe(NO_3)_3$: 9TPAOH: 404H_2O modifying from the previous work [60]. The solution was prepared by dissolving 3.75 of tetraethylorthotitanate in 62 g of tetraethylorthosilicate by dropwise while stirring at room temperature for 2 h. After that, 1.19 g of $Fe(NO_3)_3$ was mixed with tetrapropylammonium hydroxide and then added into the solution of silicon and titanium alkoxide, stirred at 60 ℃ for 2 h and further stirring at room temperature for 24 h. The solution was placed into Teflon line-autoclave, and held at 125 ℃ for 96 h. When the synthesis was completed, the autoclave was quenched by cold water. After the hydrothermal treatment, the crystals were rinsed with deionized water and the solid was separated by centrifugation. The solid was dried at 70 ℃ and then calcined at 550 ℃ for 6 h to burn out the tetrapropylammonium hydroxide that was used as template. This solid product is described as iron-titanium silicalite-1 seed. For vanadium titanium silicalite-1, the source of metal was changed to the vanadyl (IV) sulphate.

The iron titanium silicalite-1 seed substrates were prepared. The iron-titanium silicalite-1 seeds were suspended in ethanol solution. The concentration of iron-titanium silicalite-1 seed solution was 2wt.%. Next, the silicon substrates were immersed in iron-titanium silicalite-1 seed solution for 1 h. Then, the silicon substrates with iron-titanium silicate-1 seeds were dried at 60 ℃ overnight and calcined at 550 ℃ for 6 h.

3.6.2 Synthesis of iron titanium silicalite-1 films

The iron titanium silicalite-1 films were grow from seeds that adsorb on silicon substrates by hydrothermal process. The iron titanium silicalite-1 solution was preparing the same procedure as described in section 3.6.1. In this solution $Fe(NO_3)_3$ was added in the solution. Therefore, the gel composition for synthesized iron titanium silicalite-1 films was 40 TEOS: 1.6TEOT: 0.4$Fe(NO_3)_3$: 0.4 TEMS: 14TPAOH: 10000H_2O. 0.380 g of Tetraethylorthotitanate was add dropwise to and dissolved in 8.70 g of tetraethylorthosilicate by stirred at room temperature for 2 h. 2.97 g of Tetrapropylammonium hydroxide and $Fe(NO_3)_3$ were dissolved in the 188 g of water. The solutions were mixed together. After that 0.075 g of triethoxymethylsilane was added to the solution mixture. The solution was stirred at 60 ℃ for 2 h and stirred at room temperature for 24 h. Next, the silicon substrates were held in Teflon stand and place into a solution in a Teflon-line autoclave, age at 175℃ for 24 h. After that, the as-deposited iron titanium silicalite-1 films were rinsed with deionized water and dried in air at 60℃ overnight then calcined at 550℃ with heating rate of 1 ℃/min for 6h.

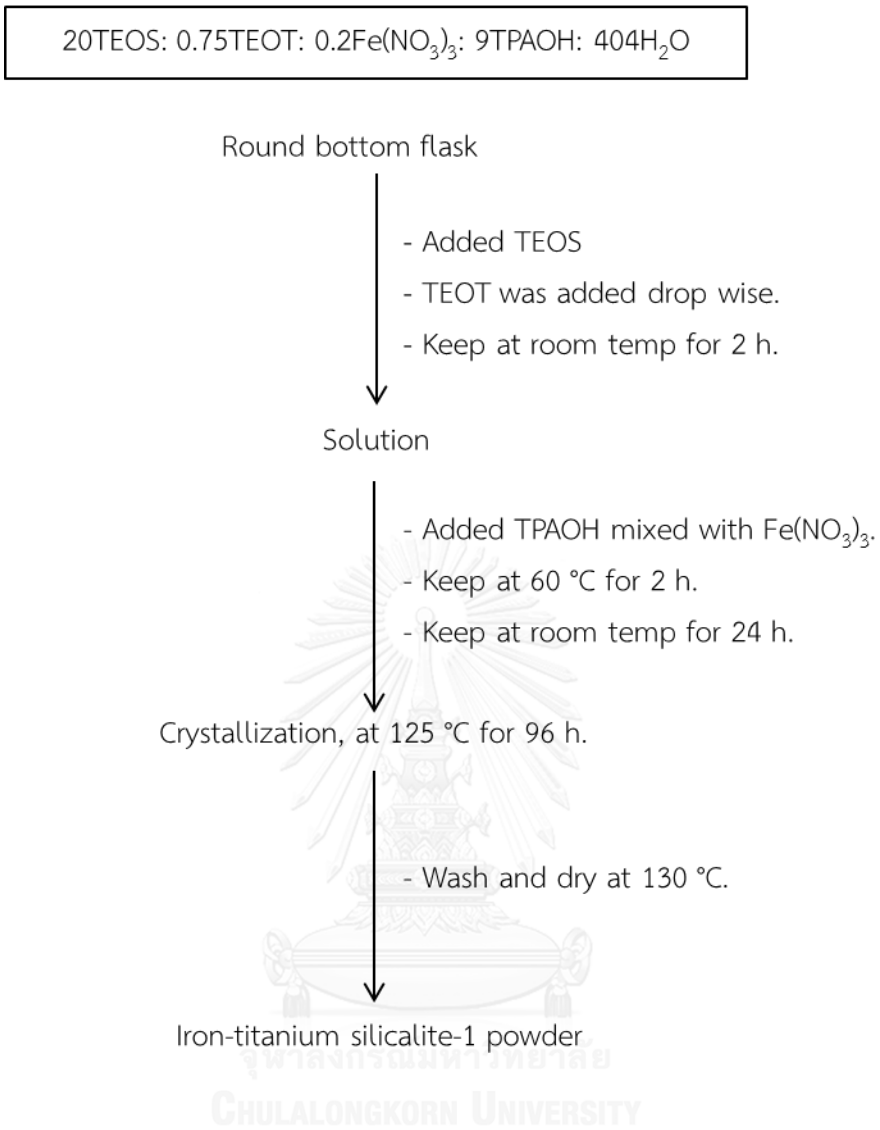

Scheme 3. 6 Preparation diagram for Iron titanium silicalite-1 and vanadium titanium silicalite-1 powder

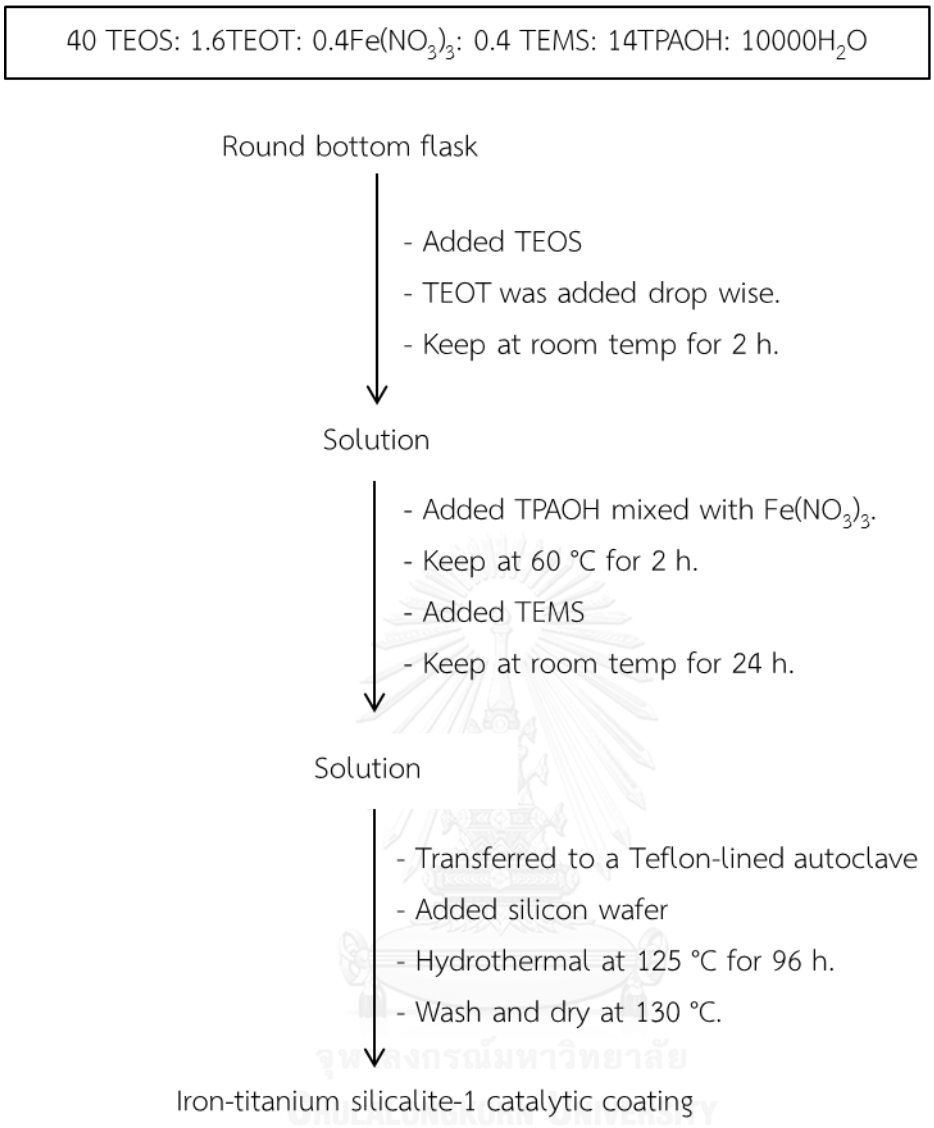

Scheme 3. 7 Preparation diagram for Iron titanium silicalite-1 film

3.7 Catalytic Activity Test for Phenol Hydroxylation

The phenol hydroxylation reaction in batch reactor was carried out in a 50 ml three-neck round bottom flask equipped with a magnetic stirrer and cooling condenser. A typical reaction was carried out as the following: 50 mg of catalyst, 0.94 g of phenol (0.01 mol) and 10.8 g of deionized water were added into the flask. After heating the mixture to setting temperature (55 – 65^{o}C), 30 wt.% of hydrogen peroxide was added dropwise. Then, the reaction mixtures were further stirred for 4 hours. After the reaction completed, the reaction mixture was cooled down and then the catalyst was separated from the reaction mixture by centrifugation.

For the phenol hydroxylation in continuous flow reactor was done in column reactor. The catalyst thin films were packed into the reactor. The reactant mixture of phenol, water and hydrogen peroxide was feed into the reactor under the optimum temperature. All the reaction mixtures were quantitatively analyzed by gas chromatography compared with calibration curve.

3.7.1 Parameters affecting oxidation in batch reaction

The study of parameter effecting on phenol hydroxylation was usually fixed amount of 0.05 g of powder catalyst, 10.8 g of water and reaction time 4 h.

3.7.1.1 Effect of phenol to hydrogen peroxide mole ratio

In order to study the effect of phenol to hydrogen peroxide mole ratio, the reaction parameter was varied the phenol to hydrogen peroxide mole ratio in a range of 1:2 to 1:12 at fixed catalyst as 0.05 g, 60°C for 4 hours.

3.7.1.2 Effect of reaction temperature

To determine the effect of temperature in phenol hydroxylation reaction, the reaction was carried out at three reaction temperatures as 55, to 65°C, phenol to hydrogen peroxide mole ratio at 1:2, catalytic amount 0.05 g and reaction time 4 hour.

3.7.2 Parameter affecting oxidation in continuous flow reactor

3.7.2.1 Effect of reaction flow rate

The effect of flow rate was examined at 4, 6, 8 µL/min at 60 °C.

CHAPTER IV

Results and discussions

4.1 Characterization of materials

4.1.1 Powder X-ray Diffraction

4.1.1.1 Effect of seed amount on the formation of titanium silicalite-1

The effect of various amounts of titanium silicalite-1 seed to the formation of titanium silicalite-1 was a prior studied. The amount of titanium silicalite-1 seed was added with a variation of mass about 5 and 10 wt. %, bases on relative to the total amount of silica source in the initial gel solution. These samples were denoted as titanium silicalite-1-5% and titanium silicalite-1-10%, respectively. In Figure 4.1, the five main diffraction peaks at 2θ of 7.9°, 8.9°, 23.2° and 23.9° were observed. They were attributed to (010), (200), (501), (303) and (133) orientation of MFI structure to all samples[61]. The appearance of peak 2θ at 24.4° is attributed to the orthorhombic symmetry of titanium silicalite-1. The results suggested that the titanium silicalite-1-5% and titanium silicalite-1-10% still have the same crystal structure as titanium silicalite-1 seed.

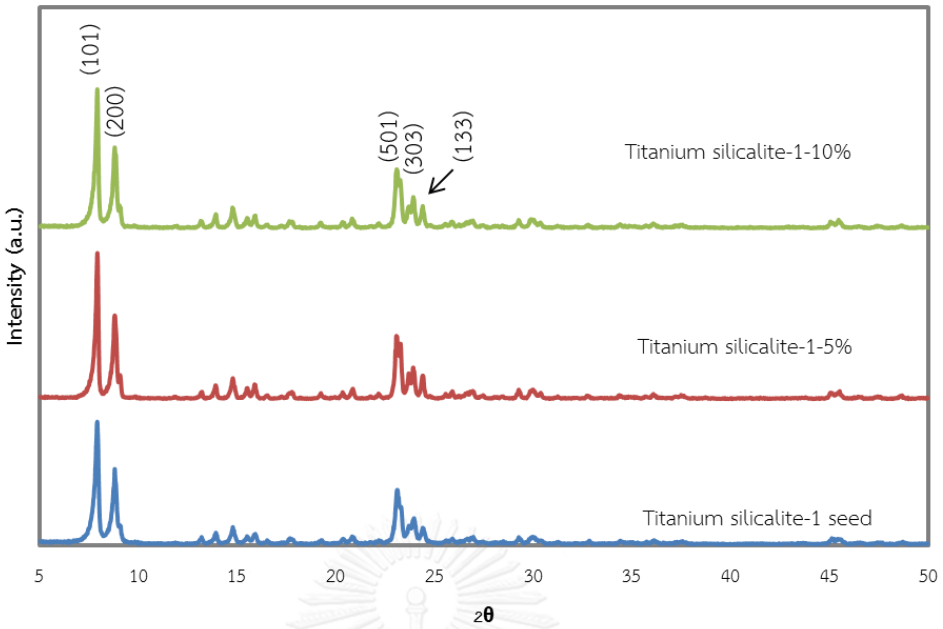

Figure 4. 1 X-ray diffractogram of Titanium silicalite-1 products prepared in presence of seed amount

4.1.1.2 Effect of metal containing on the titanium silicalite-1

X-ray diffractogram of titanium silicalite-1 seed, iron titanium silicalite-1 and vanadium titanium silicalite-1 are showed in the Figure 4.2. All samples exhibited characteristic peaks that referred to high ordered crystallinity of MFI structure. The structure of MFI still remained with an obtained the vanadium and iron in the materials. There is no characteristic peaks of vanadium oxide and iron oxide on the diffractogram indicated that vanadium and iron are well introduce and/or dispersed the titanium silicalite-1 framework [62].

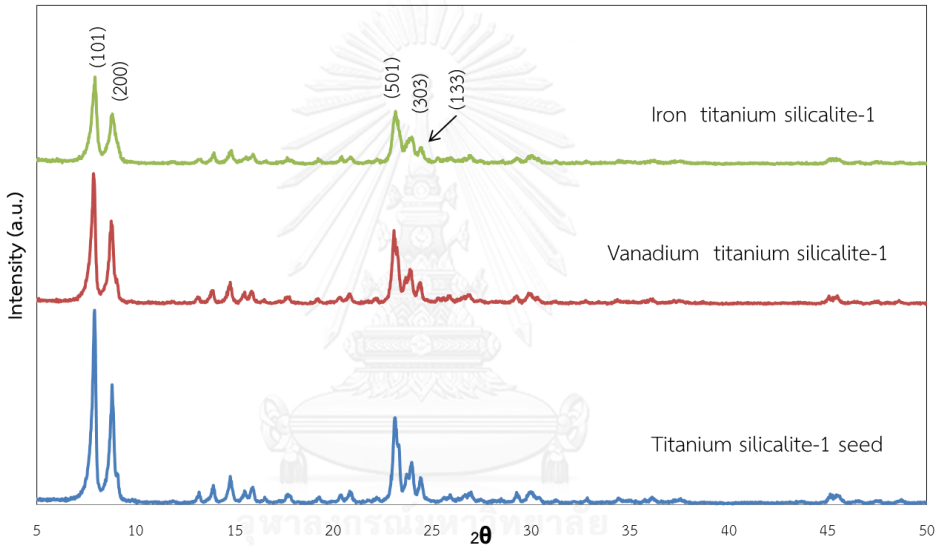

Figure 4. 2 X-ray diffractogram of metal titanium silicalite-1

4.1.1.3 Catalyst thin films

X-ray diffractograms of titanium silicalite-1 thin films and Iron titanium silicalite-1 thin films are presented in Figure 4.3. All the films show typical of characteristic peaks of MFI structure as a powder form. The presence of iron in the titanium silicalite-1 not only the same crystal structure but also the same prefer orientation.

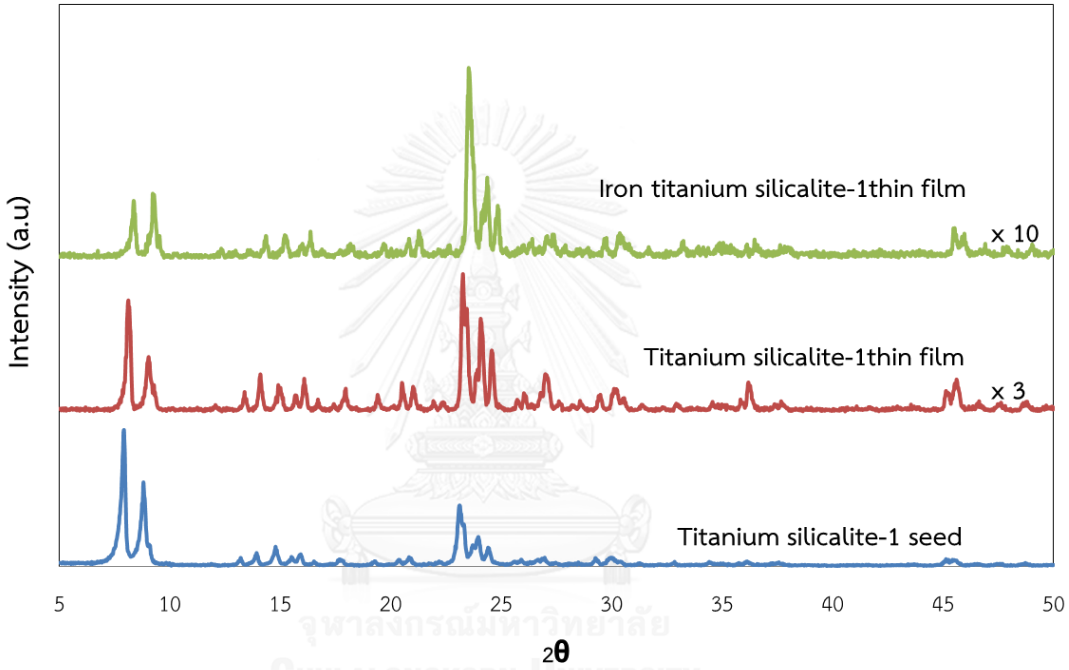

Figure 4. 3 X-ray diffractograms of thin film materials

4.1.2 UV-VIS Spectroscopy Spectra

4.1.2.1 Effect of seed amount on formation of titanium silicalite-1

UV-VIS spectroscopy is widely used to investigate the coordination environment and oxidation states of metal ions. The effect of amount of titanium silicalite-1 seed formatted to titanium silicalite-1 crystal was also investigated, using this technique. Figure 4.4 shows the UV-VIS spectrogram of titanium silicalite-1 seed, titanium silicalite-1-5% and titanium silicalite-1-10%, respectively. All materials showed the clear absorption band at 210 nm that referred to isolated Ti(IV) tetrahedral specie in the framework. There was no shoulder band of the octahedral species, at about 260 nm, in the materials[20, 63]. On the other hand, the band at 330 nm was observed for the titanium silicalite-1-5% and titanium silicalite-1-10%. These attributed to the added amount of seed provides the TiO_2 anatase structure. According to seed, this can directly provide crystal nucleation sites which improve crystallization rate. The introduction of Ti into the framework should occur at suitable condition of crystallization rate to prevent the formation of transition metal oxide. As the crystallization rate is too fast, Ti ions have not enough time to be incorporated into the framework [64].

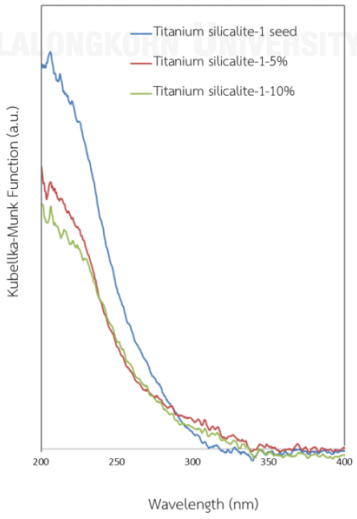

Figure 4. 4 DR-UV spectrogram of seed and synthesized products by various seed amount.

4.1.2.2 Effect of metal containing on the titanium silicalite-1

Figure 4.5 shows the UV-VIS spectrogram of metal titanium silicalite-1. The titanium silicalite-1 seed showed an absorption band at 210 nm, which can referred to isolated Ti(IV) tetrahedral coordination specie. In addition, there is no sign of other band in titanium silicalite-1 seed which indicate that Ti(IV) species can incorporated into the silicate framework. [65]. The vanadium silicalite-1 displayed a wide band at 200-700 nm. The absorption band at 250 nm corresponds to tetracoordinated V(V) in the framework. The position at 400 nm can be referred to the hexa-coordinated V (V) species which dispersed on the surface of titanium silicalite-1. However, the band at about 210 nm of vanadium titanium silicalite-1 demonstrated the isolated Ti(IV) tetrahedral coordination in the framework[66]. The iron titanium silicalite-1 exhibits a broad absorption band at 200-700 nm, which referred to the charge transition between tetrahedral oxygen and the central Ti(IV) and Fe^{3+}, overlapped at the same wavelength position. Nevertheless, the bands at 320 and 500 nm can be assigned to an extra framework iron oligomer or aggregated oxide cluster[65].

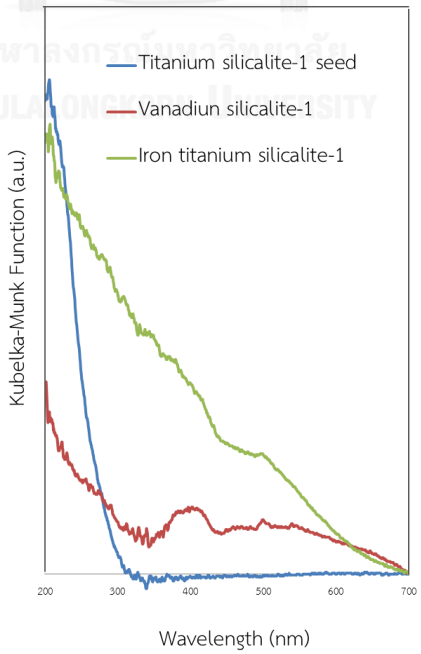

Figure 4. 5 DR-UV spectrogram of metal titanium silicalite-1

4.1.2.3 Catalyst films

Besides, the UV-VIS spectrogram of titanium silicalite-1 and iron titanium silicalite-1 film were shown in Figure 4.6, presented an adsorption band at 210 nm which was referred to isolated Ti(IV) tetrahedral coordination specie. It also displayed shoulder bands around 260 nm and around 300 nm, represented the octahedral-coordination and anatase phase of bulk TiO_2, respectively. This confirms the results from the section of 4.1.2.1. By adding the amount of seed, it can enhance crystallization rate, causes the Ti ions would not have enough time to incorporate in the framework. Moreover, the spectrum of iron titanium silicalite-1 films showed the same band position, which indicated that the introduction of iron does not affect the coordination of situation of titanium. This might be due to the iron was added in initial synthesis solution was trace amount.

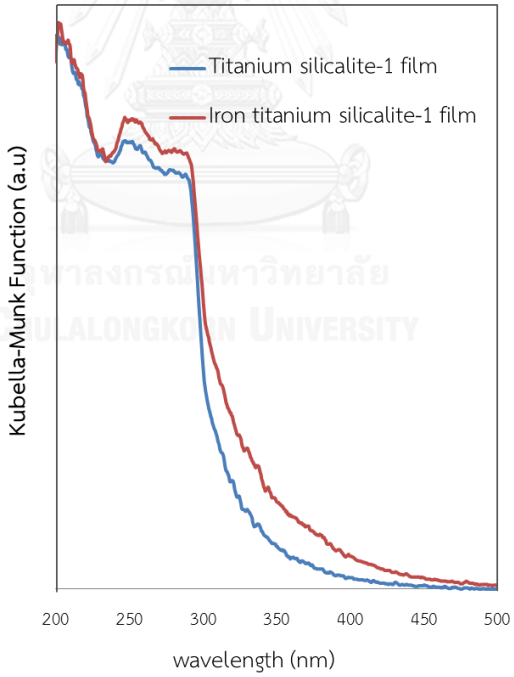

Figure 4. 6 DR-UV spectrogram of metal titanium silicalite-1 thin films

4.1.3 Scanning Electron Microscopy results

4.1.3.1 Effect of seed amount on formation of titanium silicalite-1

The morphology of titanium silicalite-1 crystal prepared by different amount of seed: 5 seed and 10 wt.% seed were investigated by using SEM. From scanning electron micrograph in Figure 4.7, it demonstrated the morphology of seed and the hexagonal prism crystal of titanium silicalite-1 with difference size in the decreasing order of titanium silicalite-1-5% and titanium silicalite-1-10%. The titanium silicalite-1-5% displayed larger crystal average size which was about 0.87 μm in widths and 1.25 μm in lengths, as shown in Figure 4.7(a, b). The crystal of titanium silicalite-1-10% was ca. 0.61 μm widths and 0.78 μm lengths as shown in Figure 4.7 (c, d). It found that the crystal size depending on amount of seed added. From the micrographs, It can be seen that the amount of seed obviously affect the crystal sizes counting on crystallization rate. As the more amounts of seeds were added into the initial gel, crystallization rate of titanium silicalite-1 formation became faster, leading to the smaller crystal size. The large amount of crystalline seed provided large numbers of nuclei, which leading to the shortened of nucleation step[67]. However, the excess of seeds were introduced in the initial gel can be seen in the final product. From the result above, we show that the titanium silicalite-1 crystal could be prepared by seeding method, which can develop to use in other applications.

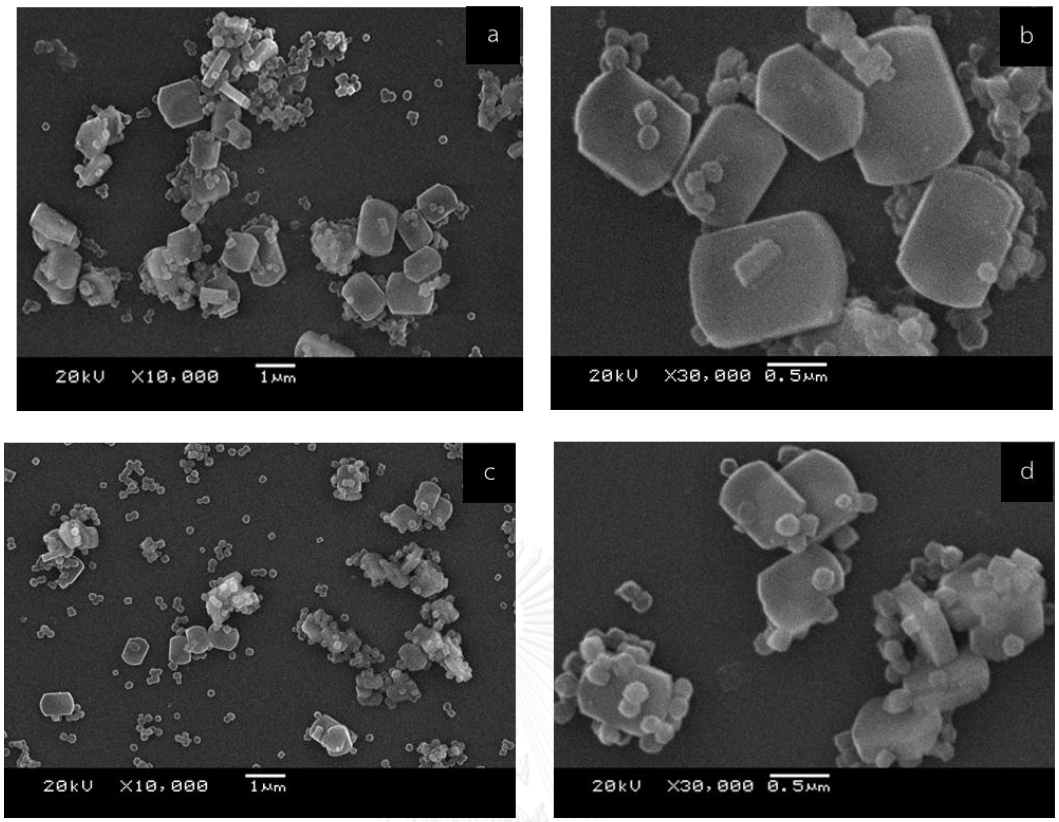

Figure 4. 7 Scanning electron micrographs of the Titanium silicalite-1-5% (a, b), Titanium silicalite-1-10% (c, d)

4.1.3.2 Effect of metal containing on the titanium silicalite-1

The scanning electron micrographs of titanium silicalite-1 seed, vanadium silicalite-1 and iron-titanium silicalite-1 powder were shown in figure 4.8. All three samples have a spherical shape with average diameter about 0.3 μm. However in case of Fe-TS-1, the particles were more aggregated due to the iron highly dispersed on the surface of the materials.

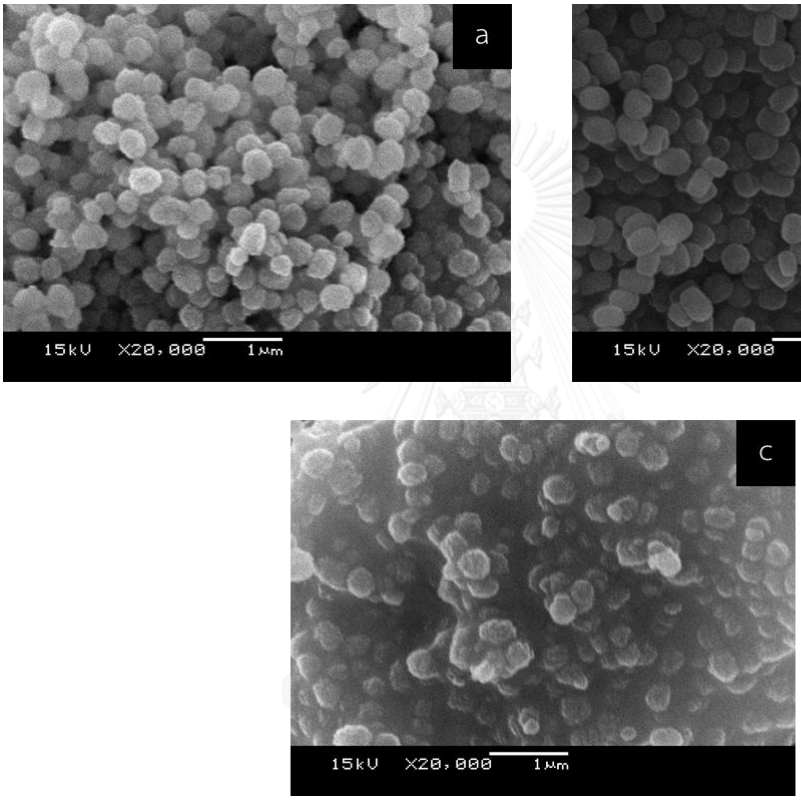

Figure 4. 8 Scanning electron micrographs of (a) titanium silicalite-1 seed (b) vanadium-titanium silicalite-1 (c) iron-titanium silicalite-1

4.1.3.3 The Etching the Silicon substrate

In this work, the silicon wafer was used as substrates. The modification of the substrate surface was investigated to see the potential to apply silicon nanowire (SiNW) arrays for preparing the catalyst film. In Figure 4.9a, the surface morphology of bare silicon wafer exhibited clean and smooth surface. After etching with Ag, the silicon surface has changed into Si nanowire structure. The long nanowires are slightly bended toward the others and cause the bundle structure instead of vertically aligned individual nanowires as shown in figure 4.9b, and the cross-sectional image of the silicon nanowires in Figure 4.9c. As seen from the micrograph, the average length of the nanowires was about 8.5 μm.

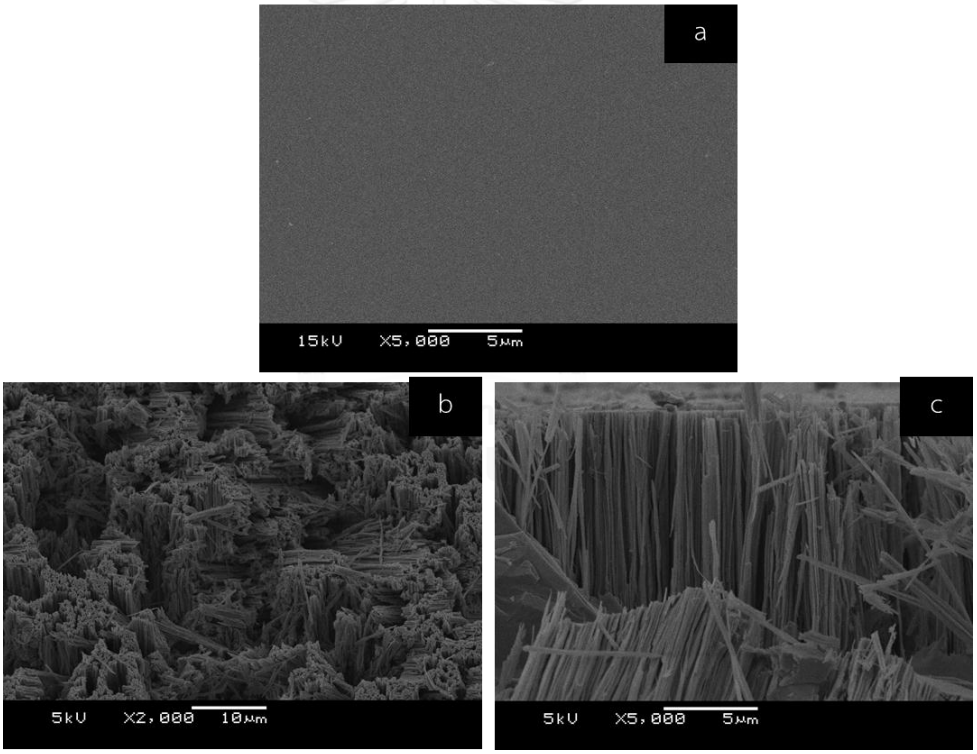

Figure 4. 9 Scanning electron micrographs of (a) top-view of bare silicon wafer (b) top-view of silicon nanowires (c) cross-sectional of silicon nanowires

4.1.3.4 Effect of metal containing on the titanium silicalite-1 thin film

Figure 4.10 shows the top view of titanium silicalite-1 film, iron-titanium silicalite-1 and titanium, deposited on nanowires substrates. It could be seen that the crystals shape become a staurolite-liked crystal morphology. The crystal size of titanium silicalite-1 on silicon substrate as shown in Figure 4.10a has the average dimension of ca. 6.1 μm in lengths, ca. 3.05μm in widths and 1.1 μm in thicknesses. The crystals of iron titanium silicalite-1 deposited on silicon wafer, as seen in Figure 4.10b, have smaller crystal size than the titanium silicalite-1, with the average dimension of ca. 3.1 μm in length, ca. 2.1 μm in widths and 0.43 μm in thicknesses. It is apparent from that the iron titanium silicalite-1 crystal size is smaller for initial gel containing of iron precursor. As reported from Au et al. [68], adding the vanadium in the initial gel was inhibited crystal growth, leading to smaller crystal particle size. Moreover, the scanning electron micrograph show that the averages dimension of titanium silicalite-1 crystal deposited on silicon nanowires (Figure 4.10c) was ca. 7.1 μm in lengths, ca. 3.4 μm in widths and 1.3 in thicknesses.

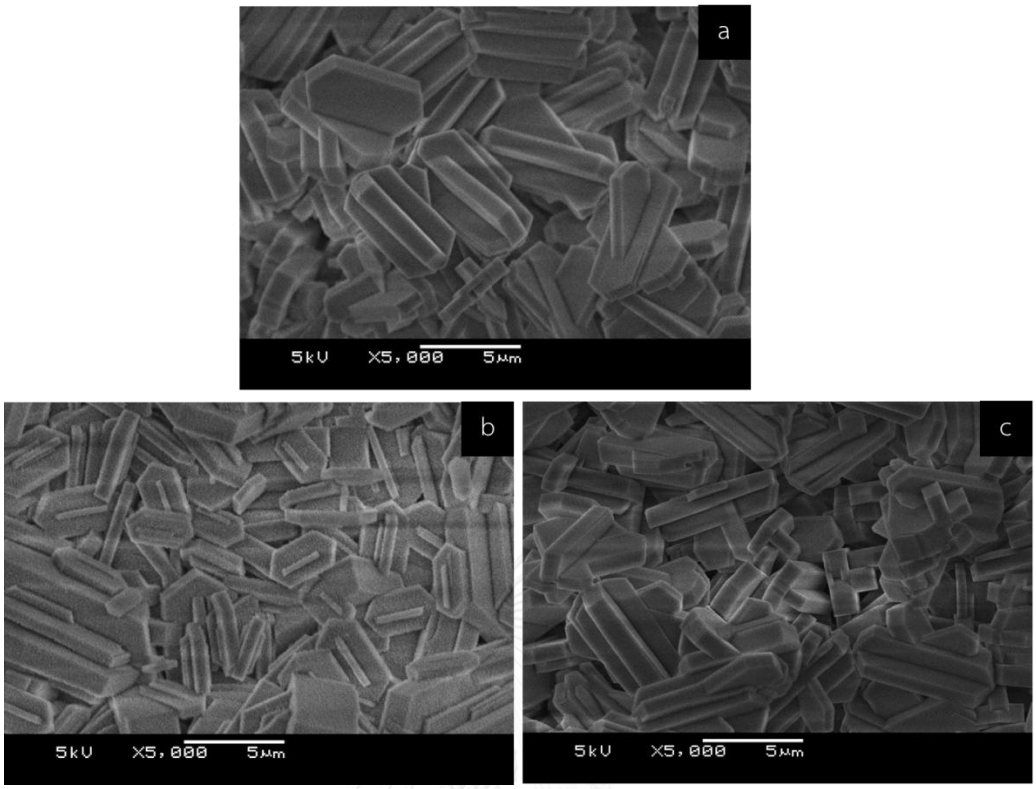

Figure 4. 10 Scanning electron micrograph of (a) titanium silicalite-1 film and (b) iron titanium silicalite-1 film (c) titanium silicalite-1 on silicon nanowires

The cross-section micrographs of titanium silicalite-1 and iron titanium silicalite-1 that deposited on silicon substrate are shown in Figure 4.11. The thickness of titanium silicalite-1 and iron titaniumsilicalite-1 deposited on silicon nanowires were ca. 83 and μm, 55 μm, respectively. Additionally, the thickness of titanium silicalite-1 deposited on nanowires substrate was ca. 31 μm. For titanium silicalite-1 on silicon nanowires, the film was thinner to compare with deposited on bare silicon wafer. This suggests that the seeds were absorbed on the surface on silicon nanowires, it could not grow between nanowires, but on the top of nanowires crystal can be growth of the bigger crystal.

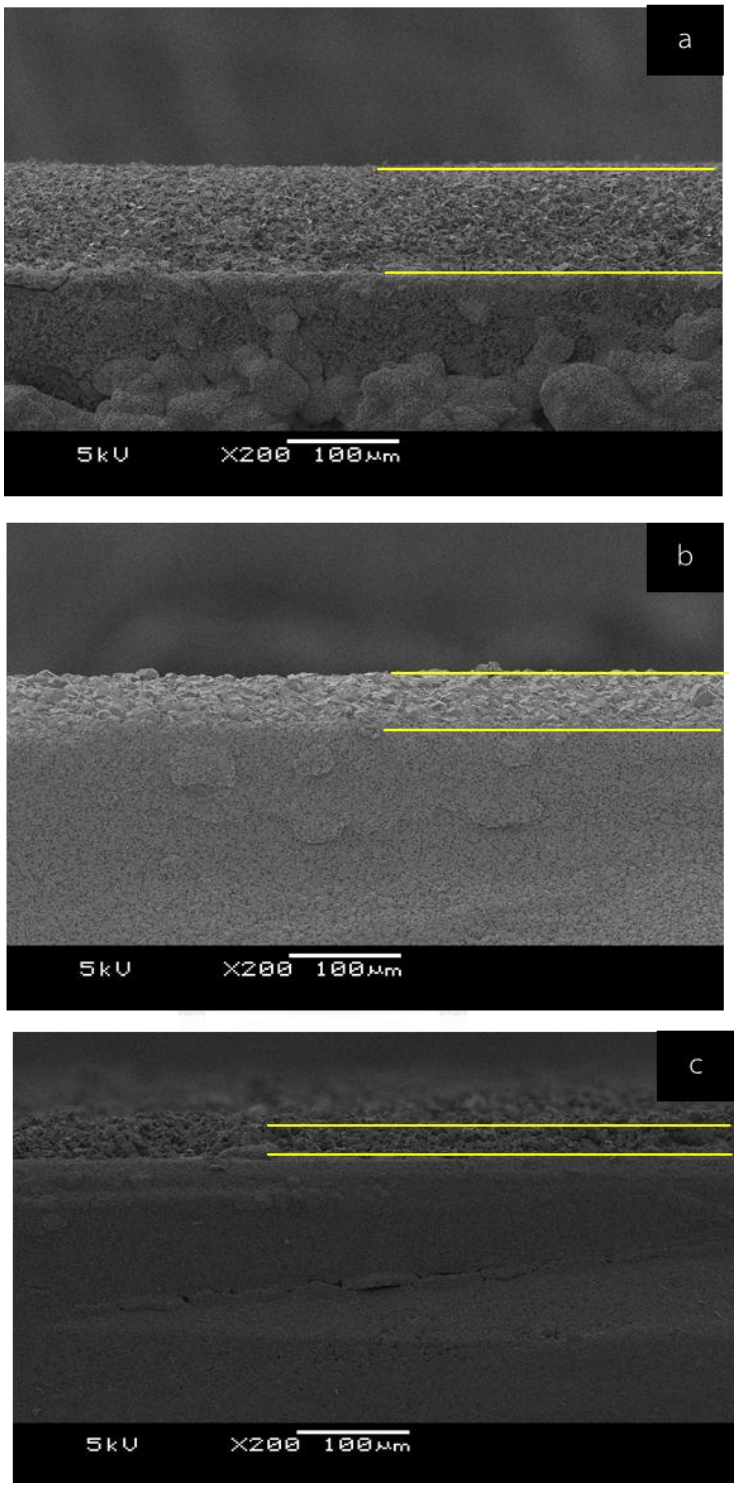

Figure 4. 11 Cross-sectional scanning electron micrographs of (a) titanium silicalite-1 film and (b) iron titanium silicalite-1 film (c) titanium silicalite-1 on silicon nanowires

4.1.4 Nitrogen Adsorption/Desorption Isotherms

4.1.4.1 Effect of seed amount on formation of titanium silicalite-1

The textural properties of titanium silicalite-1 seed, titanium silicalite-1-5% and titanium silicalite-1-10% were determined. Figure 4.12 demonstrates the nitrogen adsorption-desorption isotherm of those three samples which are Type I that referred to the microporous materials corresponding the IUPAC classification[48], A very low relative pressure the micropores were full filled very fast caused the strong capillary effect. The adsorption isotherm-desorption isotherm of titanium silicalite-1 seed and titanium silicalite-1-10% shows no hysteresis loop indicating the uniform pore size. In case of titanium silicalite-1-5% illustrates hysteresis loop showing non-uniform pore size. Table 4.1 exhibits the textural properties of titanium silicalite-1 seed, titanium silicalite-1-5% and titanium silicalite-1-10%. The BET specific surface area of silicalite-1, titanium silicalite-1-5% and titanium silicalite-1-10% are 452, 436 and 449 m^2/g, respectively. The BET specific surface area of titanium silicalite-1-10% is a little bit higher than titanium silicalite-1-5% samples because the smaller particle size of materials showing the higher surface area. Three samples have similar micropore volume and pore size distribution to confirm the same type of material structure.

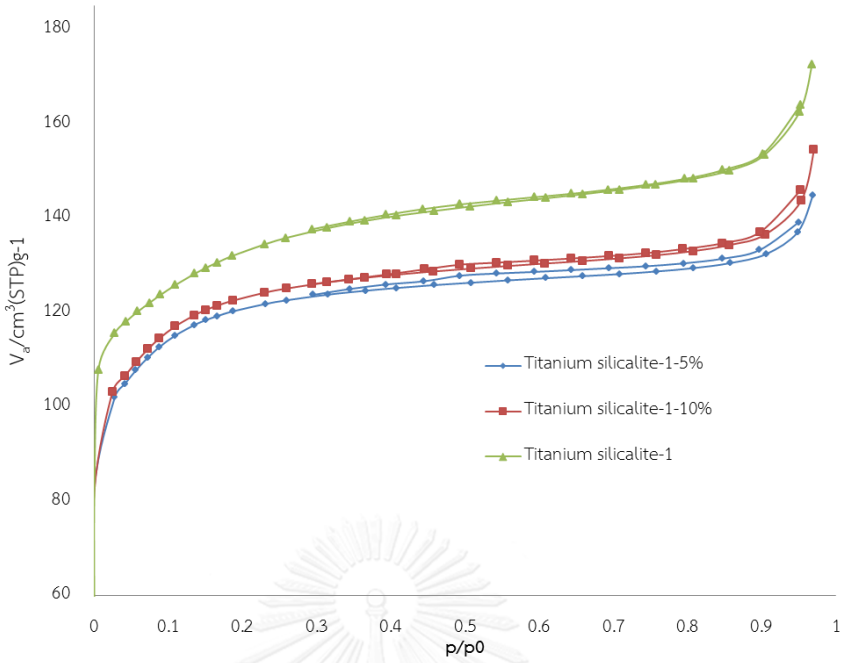

Figure 4. 12 Nitrogen adsorption-desorption isotherms of product

Table 4. 1 Textural properties of titanium metal titanium silicalite-1

Catalyst	N_2 Adsorption/desorption			
	BET surface area (m^2/g^{-1})[a]	External surface area ($m^2 g^{-1}$)[b]	Total pore volume ($cm^3 g^{-1}$)[c]	Average pore diameter (nm)[c]
Titanium silicalite-1 seed	452	36	0.2	0.7
Titanium silicalite-1-5%	436	16	0.2	0.7
Titanium silicalite-1-10%	449	18	0.2	0.7

[a]Reported by BET method

[b]Reported by t-plot

[c]Reported by MP plot

4.1.4.2 Effect of metal containing on the titanium silicalite-1

Nitrogen adsorption/desorption isotherms for the titanium silicalite-1 seed, vanadium titanium silicalite-1 and iron titanium-silicalite-1 were shown in Figure 4.13 The result indicated isotherm type I that referred to the microporous materials corresponding the IUPAC classification[48]. The hysteresis loop at a high pressure of each sample demonstrated H4-type that showing a characteristic of microporous material The hysteresis loop of iron titanium silicaite-1 and vanadium silicalite-1 are much larger than the titanium silicalite-1 seed, which could be due to the existence of the metal oxide particles[31]. The properties of titanium silicalite-1 seed, vanadium titanium silicalite-1 and iron-titanium silicalite-1 results were summarized in table 4.2. The amount of vanadium or iron into the titanium silicalite-1 had a significant influence on the specific surface area and pore volume of the materials. The total specific surface area of titanium silicalite-1 seed, iron titanium silicalite-1 and vanadium silicalite-1 were calculated by using Brunauer Emmett-teller (BET) equation, which were shown as 452, 440 and 405 m^2/g, respectively. The micropore volume was determined by MP plot. The micropore volume of titanium slicalite-1 seed, vanadium titanium silicalite-1 and iron-titanium silicalite-1 were 0.20, 0.19 and 0.14 cm^3/g, respectively. Obtaining of vanadium and iron in the titanium silicalite-1, the pore volume decrease which compared with the titanium silicalite-1 seed. These indicated that vanadium and iron in titanium silicalite-1 could block of pores channel Moreover, the pore size of these materials was the same size as the average size of the MFI structure.

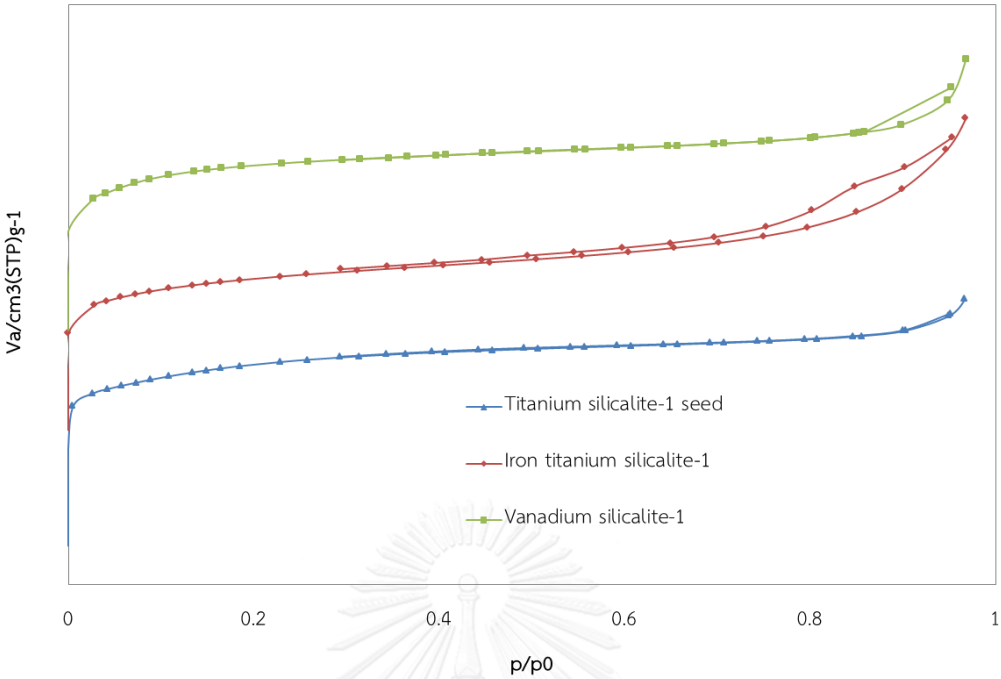

Figure 4. 13 Nitrogen adsorption-desorption isotherms of seed and metal titanium silicalite-1

Table 4. 2 Textural properties of titanium silicalite-1, vanadium-titanium silicalite-1 and Iron-titanium silicalite-1

Catalyst	N_2 Adsorption/desorption			
	BET surface area (m^2/g^{-1})[a]	External surface area ($m^2 g^{-1}$)[b]	Total pore volume ($cm^3 g^{-1}$)[c]	Average pore diameter (nm)[c]
Titanium silicalite-1 seed	452	36	0.20	0.7
Vanadium-titanium silicalite-1	440	56	0.19	0.7
Iron-titanium silicalite-1	405	92	0.14	0.7

[a]Reported by BET method

[b]Reported by t-plot

[c]Reported by MP plot

4.1.4.3 Catalyst thin films

The nitrogen adsorption-desorption isotherm of titanium silicalite-1 and iron titanium silicalite-1 are shown in Figure 4.14, and their textural properties are displayed in Table 4.3. From the adsorption-desorption isotherm shows at the beginning, the volume adsorbed increased with increasing relative pressure which due to the volume filling of micropore. The nitrogen adsorption-desorption isotherms of the both of thin film samples indicated that type I isotherm that referred to the microporous materials corresponding the IUPAC classification. The iron titanium silicalite-1 shows a hysteresis loop at a high relative pressure as describe for type IV of desorption isotherm. The BET specific surface area of iron titanium silicalite-1 (384 $m^2 g^{-1}$) is higher than titanium silicalite-1 thin film (350 $m^2 g^{-1}$) because of the existence of Fe_2O_3 particle on the surface on the catalyst[31]. Besides, the particle size of iron-titanium silicalite-1 is smaller than titanium silicalite-1, illustrated in Figure 4.10b, that might refer to the smaller particle size response to a larger surface area.

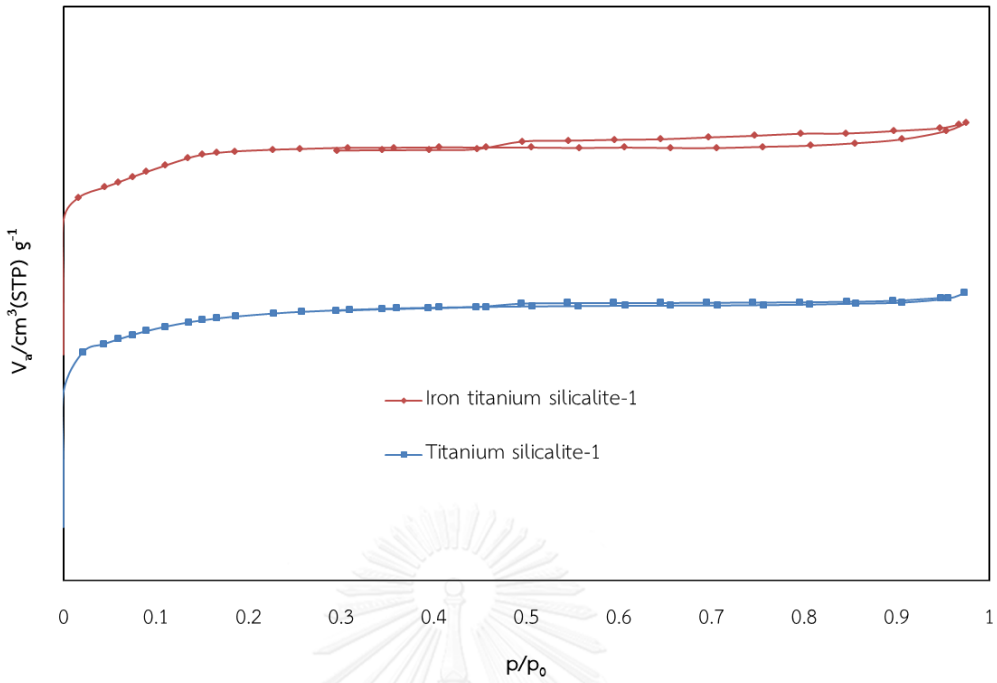

Figure 4. 14 Nitrogen adsorption/desorption isotherm of thin film materials

Table 4. 3 Textural properties of the thin film sample

Catalyst	BET surface area (m^2g^{-1})[a]	External surface area (m^2g^{-1})[b]	Total pore volume (cm^3g^{-1})[c]	Average pore diameter (nm)[c]
Titanium silicalite-1 thin film	350	5.7	0.18	0.7
Iron-titanium silicalite-1 thin film	384	5.7	0.19	0.7

[a]Reported by BET method

[b]Reported by t-plot

[c]Reported by MP plot

4.1.5 Elemental analysis

The all catalysts were investigated by ICP-MS. The elemental analysis results are summarized in table 4.4. The Si/Ti mole ratio of the initial gel was lower than in the final products because Ti cannot fully incorporate in the framework. As the Si/Fe and Si/V mole ratio which are higher than the initial gel.

Table 4. 4 Mole ratio of ICP-MS of prepared material under different composition

Sample	Mole ratio in initial gel[a]			Mole in catalyst[b]		
	Si/Ti	Si/Fe	Si/V	Si/Ti	Si/Fe	Si/V
Titanium silicalite-1	25	-	-	39	-	-
Titanium silicalite-1-5%	25	-	-	38	-	-
Titanium silicalite-1-10%	25	-	-	44	-	-
Iron Titanium silicalite-1	25	100	-	39	120	-
Vanadium Titanium silicalite-1	25	-	100	38	-	142
Titanium silicalite-1 thin film	25	-	-	54	-	-
Iron Titanium silicalite-1 thin film	25	100	-	66	130	-

[a]Calculated from initial gel

[b]Mole ratio was determined by ICP-MS

4.2 Catalytic activity of powder in phenol hydroxylation

4.2.1 Effect of Crystal Size

The effect of crystal size of titanium silicalite-1 over phenol hydroxylation was studied. All of reaction gave nearly different phenol conversion, as shown in Table 4.5. For comparison of reaction of titanium silicalite-1-5% and titanium silicalite-1-10%found that the slightly higher activity of titanium silicalite-1-10%than titanium silicalite-5% due to the smaller particle could easily diffused to the reactant molecule. In addition, phenol conversion of titanium silicalite-1 seed showed the highest phenol conversion due to the smallest of particles size, as illustrate excess of seed in Figure 4.2. Considering the total product yield similar trend like phenol conversion, the titanium silicalite-1 exhibited the highest total products yield of 16.85% and 28.49% selectivity to hydroquinone. As reported by Zuo et al.[20], the catalytic activity of small titanium silicalite-1 exhibited high performance in the epoxidation of propylene.

Table 4. 5 Effect of crystal size of titanium silicalite-1 over phenol hydroxylation

catalyst	Phenol conversion	%selectivity			%total oxidation product
		HQ	CT	BQ	
Titanium silicalite-1 seed	30.36	53.3	33.6	12.7	16.9
Titanium silicalite-1-5%	24.45	47.4	39.4	13.2	12.4
Titanium silicalite-1-10%	28.86	51.3	36.7	12.0	14.9

Reaction condition: Phenol/hydrogen peroxide = 1:2, temperature 60°C, 5 mg of catalyst, 10.8 g of water, time 4h

4.2.2 Effect of mole ratio of phenol/hydrogen peroxide

Table 4.6 and Figure 4.15 exhibited the effect of phenol: hydrogen peroxide molar ratio of phenol hydroxylation. When the mole ratio of phenol to hydrogen peroxide was enhanced from 1:0.5 to 1:12, phenol conversion was slightly increase. This effect might be explained by high amount of hydrogen peroxide which could increase hydroxyl radical and interact with phenol. At the mole ratio of phenol to hydrogen peroxide is 1:2, highest selectivity of hydroquinone was observed. However, when the amounts of hydrogen peroxide increasing, the selectivity of hydroquinone was decreased. In addition, the selectivity of benzoquinone was increased from 8.5 to 40% with 1:0.5 to 1:12 of phenol to hydrogen peroxide and hydrogen peroxide efficiency was slightly changed. Furthermore, even the amount of hydrogen peroxide increasing, the selectivity of hydroquinone and catechol were decreased from 50.8 to 31.3% and 40.7 to 28.8%, respectively. According to the selectivity of hydroquinone was decreased when hydrogen peroxide concentration increasing because hydroquinone was further oxidized by excess hydroxyl radical to form benzoquinone. Hence, the mole ratio of phenol: hydrogen peroxide should be controlled at 1:2 in order to obtain a higher selectivity of hydroquinone under this catalytic system.

Table 4. 6 Effect of mole ratio of phenol/hydrogen peroxide for phenol hydroxylation over titanium silicalite-1 seed

Phenol/ H_2O_2	% Phenol conversion	% selectivity			Total oxidation product	$\%H_2O_2$ efficiency
		HQ	CT	BQ		
1:0.5	27.6	50.8	40.7	8.5	17.7	74.7
1:1	28.0	50.4	37.7	11.9	17.3	73.2
1:2	30.4	51.3	36.7	12.0	16.9	71.8
1:4	30.1	37.4	34.2	28.4	15.9	71.0
1:6	31.0	36.6	31.3	32.1	13.8	72.6
1:8	32.1	35.0	29.1	35.9	12.5	72.6
1:10	33.0	31.5	28.2	40.1	12.0	70.3
1:12	33.0	31.3	28.8	39.9	11.8	72.4

Reaction condition: temperature 60°C, 5 mg of catalyst, 10.8 g of water, time 4h

HQ = hydroquinone CT = catechol, BQ= benzoquinone

%Hydrogen peroxide efficiency =100 × (moles of initial hydrogen peroxide – moles of final hydrogen peroxide)/moles of initial hydrogen peroxide

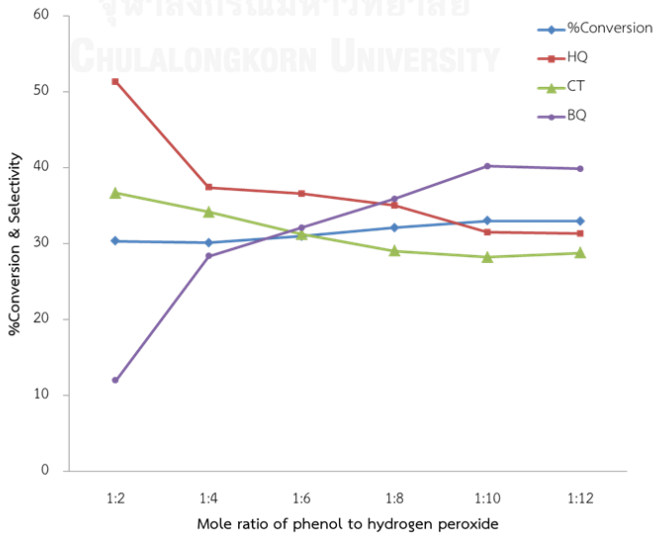

Figure 4. 15 Effect of molar ratio of phenol: hydrogen peroxide

4.2.3 Effect of temperature

The effect of temperature from 55 to 65 ºC of phenol hydroxylation reaction was shown in Table 4.7 and Figure 4.16. Phenol conversion increased up to 60 ºC but decreased at a higher temperature. Meanwhile, hydrogen peroxide efficiency increases with temperature from 56.4% at 55 °C to 80.3% at 65°C. At higher temperature, the hydrogen peroxide may be decomposed to H_2O and O_2 which decrease the conversion of phenol [69]. Therefore, the optimum reaction temperature is at 60 ºC, leading to the high selectivity of hydroquinone and catechol.

Table 4. 7 Effect of temperature for phenol hydroxylation over titanium silicalite-1 seed

Temperature (°C)	% Phenol conversion	% selectivity			Total oxidation product	$\%H_2O_2$ efficiency
		HQ	CT	BQ		
55	26.65	51.4	35.7	12.9	14.3	56.4
60	30.36	51.3	36.7	12.0	16.9	71.76
65	24.26	50.4	32.8	16.8	11.3	80.3

Reaction condition: Phenol/hydrogen peroxide = 1:2, 5 mg of catalyst, 10.8 g of water, time 4h

HQ = hydroquinone CT = catechol, BQ= benzoquinone

%Hydrogen peroxide efficiency = 100 × (moles of initial hydrogen peroxide moles of final hydrogen peroxide)/moles of initial hydrogen peroxide

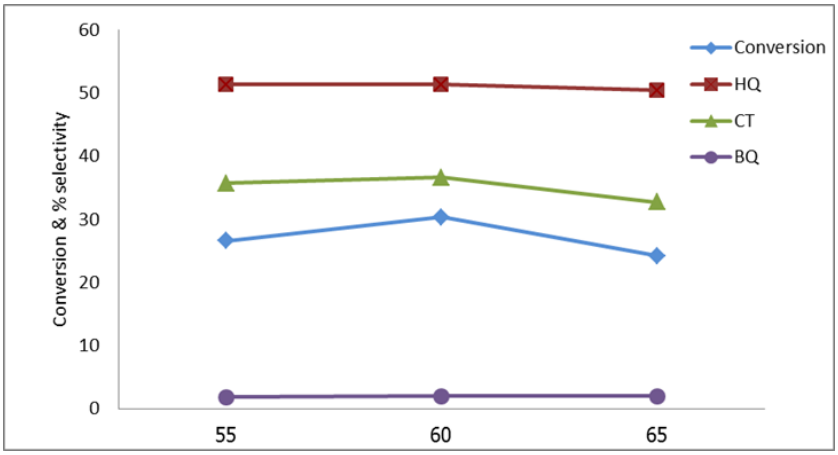

Figure 4. 16 Effect of temperature of Titanium silicalite-1 powder over phenol hydroxylation

4.2.4 Effect of second metal containing in titanium silicalite-1

The reactions were studied type of catalyst between titanium silicalite-1 and iron titanium silicalite-1. Normally, the catalytic reaction by heterogeneous catalysts, the first step of the reaction involve adsorption of the substrate on the surface of catalysts to form intermediate, followed by reaction in the catalyst, and finally desorption of the product from the catalyst. Table 4.4 showed the effect of catalyst, it was found that vanadium titanium-silicalite-1 gave higher phenol conversion and total products yield than titanium silicalite-1 and iron silicalite-1. On the other hand, the selectivity of benzoquinone was higher than other catalysts. This suggests that the vanadium titanosilicalite-1 was more active to oxidation reaction at the same condition. For the iron titanium silicalite-1 was more selective to catechol. This might be explained by Fenton's reagent which hydrogen peroxide was oxidized by ferrous ion to give a hydroxyl radical and then added to phenol molecule to produce the mainly catechol product. On the other hand, titanium silicalite-1 catalyst, the selectivity of hydroquinone was higher than catechol. Due to the Ti in the framework might weakly coordinate to hydrogen peroxide, the low concentration of •OH might be observed. The ortho-hydroxylation of phenol to catechol was a difficult process over titanium silicalite-1 to arise from the coincident coordination of phenol and hydrogen peroxide to Ti species in the framework was hardly occurring[70]. In addition, hydrogen peroxide efficiency of vanadium titanium silicalite-1 and iron titanium silicalite-1 reached to 100% which due to the second metal on the catalyst enhanced the catalytic activity of the system.

Table 4. 8 Effect of iron containing in titanium silicalite-1 on product and yield product

Catalyst	%Conversion	% selectivity			%Total yield of product	%Hydrogen peroxide efficiency
		HQ	CT	p-BQ		
Titanium silicalite-1 seed	30.36	51.4	36.6	12.0	16.85	71.75
Vanadium titanium silicalite-1	50.11	38.8	34.9	26.3	20.45	100
Iron titanium silicalite-1	43.46	35.5	64.5	-	20.3	100

Reaction condition: temperature 60°C, Phenol/hydrogen peroxide = 1:2 by mole, 5 mg of catalyst, 10.8 g of water, time 4h

HQ = hydroquinone CT = catechol, BQ= benzoquinone

%Hydrogen peroxide efficiency = 100 × (moles of initial hydrogen peroxide – moles of final hydrogen peroxide)/moles of initial hydrogen peroxide

4.4 Catalytic activity of thin film

4.4.1 Effect of flow rate

The effect of flow rate of phenol hydroxylation reaction in continuous micro-flow reactor was shown in Figure 4.17. The phenol conversion was increased when decreasing feed flow rate. At flow rate 4 µl/min exhibited the highest total product yield and total product yield was decreased immediately until 24 h and slightly decreases with increasing operating time. It's also showed in the reaction feed flow of 6 and 8 µl/min. In addition, at the feed flow rate 4 µl/min exhibited the yield of hydroquinone decreasing until 24 h. Furthermore, the yield of hydroquinone and catechol at feed flow rate 4 µl/min were decrease by increasing the operation time. Moreover, the %total product yield of feed flow rate at 6 and 8 µl/min are lower than feed flow rate at 4 µl/min. To more specific, the high feed flow rate, the reactants might flow through the space between the packed catalysts more than the zeolite pores. Besides, the activity drop when increasing the flow rate was attributed to the fact that high flow rate of the reactants did not spend enough time to reach the active site inside the catalyst porosity. Thus, the suitable flow rate for this catalytic flow reaction was 4 µl/min.

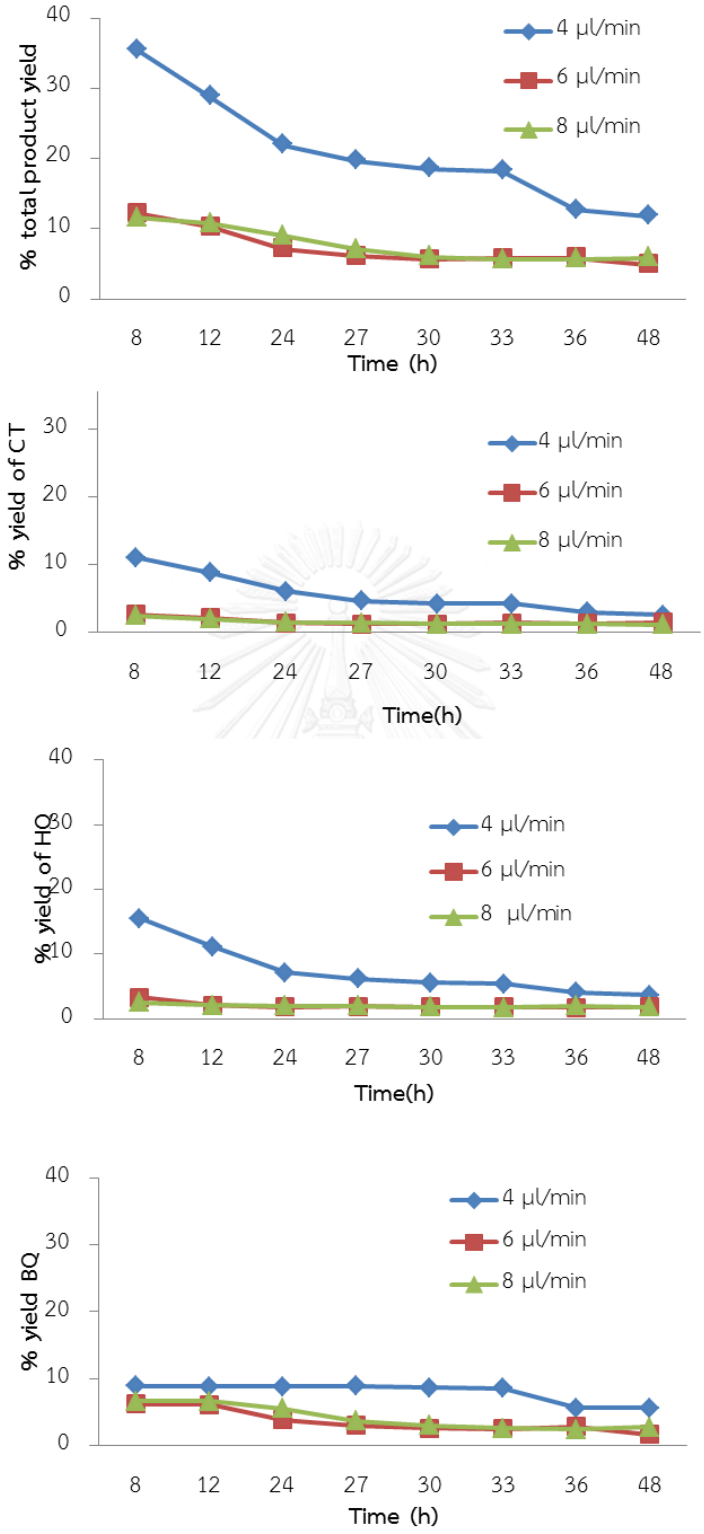

Figure 4. 17 Effect of flow rate of phenol hydroxylation reaction using titanium silicalite-1 thin film as catalyst

Table 4.9 lists the typical results from this work and compares with other results from previous study of using TS-1 films in various reactors under their optimal reaction conditions. It was noted that the phenol conversion of this work was lower than Fe-ZSM-5 membrane. However the present work was carried out at lower reaction temperature that caused less other by-products and also gave higher selectivity of oxidation products. In case of TS-1 wall in micro-reactor, which exhibited a bit higher phenol conversion and oxidation products than our case that mainly caused by the catalyst was packed on the wall of micro-reactor. In addition, the phenol conversion of TS-1 on Al_2O_3 tube was lower than present work due to the thinner of the catalyst membrane. Moreover, the phenol conversion and selectivity also depended on phenol to hydrogen peroxide mole ratio and reaction temperature.

Table 4. 9 Comparison of phenol conversion and selectivity over titanium silicalite-1 film in various reactor

No.	Catalyst	Reaction condition	% phenol conversion	Result (% selectivity)			Ref.
				HQ	CT	BQ	
1	Fe-ZSM-5 on stainless steel fiber	Phenol/H_2O_2 = 1:5 Temperature = 80 ℃	95	45		-	[71]
2	TS-1 wall micro reactor	Phenol/H_2O_2 = 0.55:1 temperature = 60 ℃	44.6	98.4		-	[72]
3	TS-1 thin film on silicon substrate	Phenol/H_2O_2 = 1:2 temperature = 60 ℃	40.4	38.5	27.3	20.7	This work
4	TS-1 on Al_2O_3 tube	Phenol/H_2O_2 = 1:0.5 temperature = 85 ℃	10.2	95.6		-	[29]

4.4.2 Effect of titanium silicalite-1 coated on silicon nanowires

The effect of catalyst thin film on silicon nanowires substrate was determined over phenol hydroxylation, as shown in Figure 4.18. The phenol conversion and total products yield of titanium silicalite-1 on silicon nanowires were lower than titanium

silicalite-1 on non-modified substrate. At the same operating time 8 h, phenol conversion of titanium silicalite-1 nanowires was 25.54% while phenol conversion of titanium silicalite-1 thin film was 40.4%. This might be caused by the thickness of the film affect to the catalytic performance. The thicker film has more active sites of catalyst and resulting to increase activity at first 24 hours.

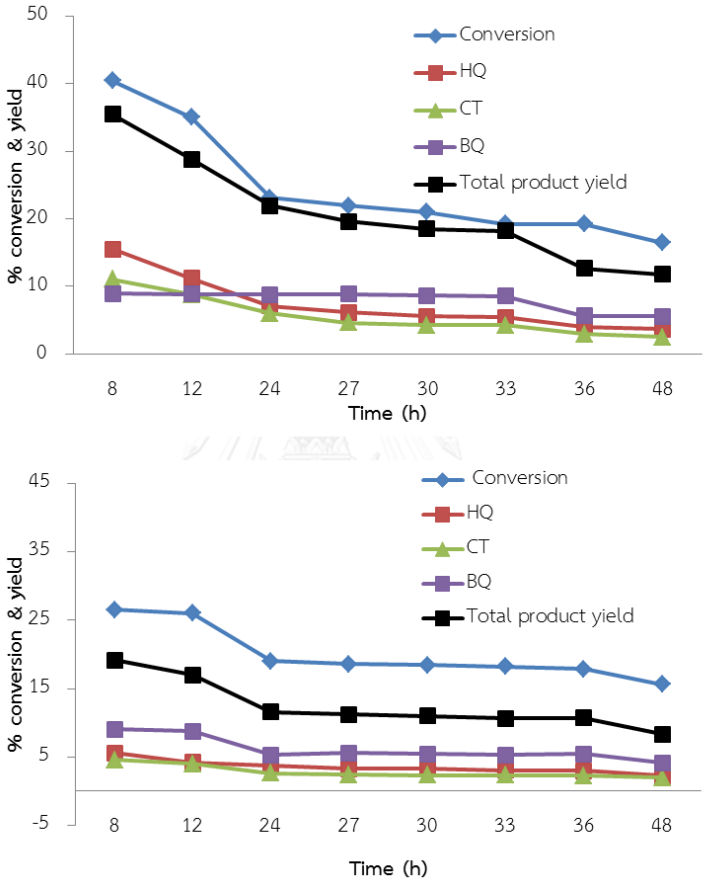

Figure 4. 18 Effect of substrate modifying (a) non-modified silicon wafer (b) silicon nanowires

4.4.3 Effect of iron containing in titanium silicalite-1 thin film

Figure 4.19 showed the effect of iron containing in titanium silicalite-1. The condition of reaction is mole ratio of phenol: hydrogen peroxide = 1:2, temperature at 60°C and flow rate 4 µl/min. Phenol conversion and total product yield of titanium slicalite-1 were higher than iron titanium silicalite-1 it might be the thickness of Iron titanium silicalite-1 thin film which deposited on silicon substrate was thinner than titanium silicalite-1. This effect of thickness film for reaction also reported in previous work [29]. The mass of the thicker film was higher hence it could promote the catalytic activity. However in the presence of iron in catalyst, high total products yield of catechol was observed until 24 hours reaction time. This total product yield showed the same trend as in batch reaction of iron titanium silicalite-1 powder which indicated that the selectivity depend on the property of the catalyst.

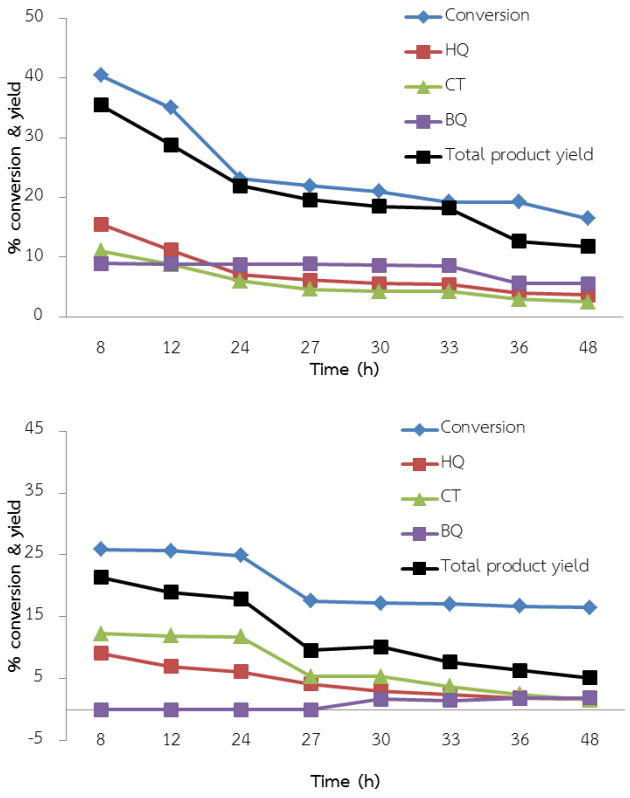

Figure 4. 19 Effect of type of catalyst thin film (a) titanium silicalite-1 thin film and (b) iron titanium silicalite-1 thin film

CHAPTER V
CONCLUSION

Titanium silicalite-1 was successfully synthesized by hydrothermal with seeding method. Adding the seed into initial gel played an important role in crystallinity. Titanium silicalite-1 crystal was synthesized by adding 10wt.% of seed giving the smaller crystal size than adding 5wt.% of seed. All prepared titanium silicalite-1 exhibited a good crystallinity and placed mainly at tetrahedral titanium in MFI framework. In addition, titanium silicalite-1 showed the N_2 adsorption-desorption isotherm of type I, characteristic of microporous material. All synthesized materials were carried out as catalyst in phenol hydroxylation. The optimum of hydroxylation condition was 1:2 mole ratio of phenol to hydrogen peroxide, 60 °C, 4 h. The results found that the titanium silicalite-1 seed demonstrated the highest phenol conversion (30.36%) due to the smallest of particle size.

In addition, the metal titanium silicalite-1 was synthesized by direct hydrothermal method. The iron and vanadium were chosen as the second metal adding into the initial gel of titanium silicalite-1. After iron and vanadium loading, the characteristic of MFI structure was still remained but decreasing in crystallinity. Both of metal titanium silicalite-1 materials demonstrated type I isotherm that related to the microporous structure. The catalytic activity under the optimum condition, iron titanium silicalite-1 gave the highest selectivity to catechol as 64.5%.

Furthermore, the titanium silicalite-1 film and iron titanium silicalite-1 film were prepared by seeding and hydrothermal method using silicon wafer as substrate. These films indicated good crystallinity of MFI structure. The characteristic of microporous material was observed as N_2 adsorption-desorption isotherm of type-1. The continuous flow reaction of iron titanium silicalite-1 thin film displayed the higher catechol selectivity than hydroquinone same as batch reaction. This is because of the property of Fenton reagent produces the mainly catechol product. Moreover in case of the continuous flow reaction, titanium silicalite-1 thin film

exhibited higher phenol conversion than iron titanium silicalite-1 films due to the thicker film of the titanium silicalite-1.

The suggestion of future work

1. To modify the catalyst thin film by improving the thickness in order to enhance the oxidation product yield.
2. To prepare the iron titanium silicalite-1 catalysts with different Si/Fe mole ratio in order to modify the film thickness and obtain higher selectivity of catechol.

REFERENCES

[1] Matthey, J. Refinery (FCC, Hydrocracking, Catalytic Reforming), Synthesis, Polymer & Environmental Catalyst Market - Global Industry Analysis by Material (Zeolites, Metal, Others), by Type (Homogenous & Heterogeneous), Catalyst Regeneration (Off-site & On-site), Size, Share, Growth, Trends and Forecast 2012 - 2018 [Online]. Available from: http://www.transparencymarketresearch.com/global-refinery-catalyst-market.html

[2] Topka, P., Karban, J., Soukup, K., Jirátová, K., and Šolcová, O. Preparation of Al–SBA-15 pellets with low amount of additives: Effect of binder content on texture and mechanical properties. Application to Friedel–Crafts alkylation. Chemical Engineering Journal 168(1) (2011): 433-440.

[3] Joseph, L.H.C. Incorporating zeolites in microchemical systems. Chemical Engineering Journal 88 (2002): 187–200.

[4] Xia, S., Peng, Y., and Wang, Z. Microstructure manipulation of MFI-type zeolite membranes on hollow fibers for ethanol–water separation. Journal of Membrane Science 498 (2016): 324-335.

[5] Zhang, Y., Hirata, A., Nakasaka, Y., Tago, T., Taniguchi, T., and Masuda, T. Effects of crystal morphology, Si/Al ratio and thickness of an MTW zeolite membrane on water/2-propanol separation by pervaporation. Microporous and Mesoporous Materials 222 (2016): 178-184.

[6] Ning, X., Zhao, C.L., Yang, J., and Chan, C.C. Zeolite thin film-coated spherical end-face fiber sensors for detection of trace organic vapors. Optics Communications 364 (2016): 55-59.

[7] Baimpos, T., Nikolakis, V., and Kouzoudis, D. A new method for measuring the adsorption induced stresses of zeolite films using magnetoelastic sensors. Journal of Membrane Science 390-391 (2012): 130-140.

[8] Wang, X., Yang, Z., Yu, C., Yin, L., Zhang, C., and Gu, X. Preparation of T-type zeolite membranes using a dip-coating seeding suspension containing colloidal SiO2. Microporous and Mesoporous Materials 197 (2014): 17-25.

[9] Barbera, D., et al. The control of selectivity in benzene hydroxylation catalyzed by TS-1: The solvent effect and the role of crystallite size. Journal of Catalysis 275(1) (2010): 158-169.

[10] Feng, X., et al. Au/uncalcined TS-1 catalysts for direct propene epoxidation with H2 and O2: Effects of Si/Ti molar ratio and Au loading. Chemical Engineering Journal 278 (2015): 234-239.

[11] Reichinger, M., et al. Alkene epoxidation with mesoporous materials assembled from TS-1 seeds – Is there a hierarchical pore system? Journal of Catalysis 269(2) (2010): 367-375.

[12] Zhan, G., et al. Kinetics of liquid phase oxidation of benzyl alcohol with hydrogen peroxide over bio-reduced Au/TS-1 catalysts. Journal of Molecular Catalysis A: Chemical 366 (2013): 215-221.

[13] Li, B., Wu, N., Wu, K., Liu, J., Han, C., and Li, X. Bimetallic V and Ti incorporated MCM-41 molecular sieves and their catalytic properties. RSC Adv. 5(21) (2015): 16598-16603.

[14] Zhang, Y., et al. Synthesis, characterization of bimetallic Ce–Fe-SBA-15 and its catalytic performance in the phenol hydroxylation. Microporous and Mesoporous Materials 113(1-3) (2008): 393-401.

[15] Zhang, H., et al. Direct synthesis, characterization and catalytic performance of bimetallic Fe–Mo-SBA-15 materials in selective catalytic reduction of NO with NH3. Microporous and Mesoporous Materials 151 (2012): 44-55.

[16] Taramasso, M. and Notari, B. PREPARATION OF POROUS CRYSTALLINE SYNTHETIC MATERIAL COMPRISED OF SILICON AND TITANIUM OXIDES. in *United States Patent*. 1983, Snamprogetti S.p.A. : Milan, Italy.

[17] Vasile, A., Busuio, A.M., and Tomoiaga. A new route for the synthesis of titanium silicalite-1. Materials Research Bulletin 47 (2012): 35-41.

[18] Deng, X., Wang, Y., Shen, L., Wu, H., Liu, Y., and He, M. Low-Cost Synthesis of Titanium Silicalite‑1 (TS-1) with Highly Catalytic Oxidation Performance through a Controlled Hydrolysis Process. Industrial & Engneering Chemistry Research 52 (2013): 1190-1196.

[19] Zhang, H., Liu, Y., Jiao, Z., He, M., and Wu, P. Hydrothermal Synthesis of Titanium Silicalite-1 Structurally Directed by Hexamethyleneimine. Industrial & Engneering Chemistry Research 48 (2009): 4334–4339.

[20] Zuo, Y., Wang, X., and Guo, X. Synthesis of titanium silicalite-1 with small crystal size by using mother liquor of titanium silicalite-1 as seeds (II): Influence of synthesis conditions on properties of titanium silicalite-1. Microporous and Mesoporous Materials 162 (2012): 105-114.

[21] Xue, T., Liu, H., Wang, Y., Wu, H., Wu, P., and He, M. Seed-induced synthesis of small-crystal TS-1 using ammonia as alkali source. Chinese Journal of Catalysis 36(11) (2015): 1928-1935.

[22] Prasetyoko, D., Royani, C.E., Fansuri, H., Ramli, Z., and Nur, H. CATALYTIC PERFORMANCES OF Fe2O3/TS-1 CATALYST IN PHENOL HYDROXYLATION REACTION. Indonesian Journal of Chemistry 10 (2010): 149-155.

[23] Wu, M., Chou, L., and Song, H. Effect of metals on titanium silicalite TS-1 for butadiene epoxidation. Chinese Journal of Catalysis 34(4) (2013): 789-797.

[24] Mulyatun. Vanadium Contribution to the Surface Modification of Titanium Silicalite for Conversion of Benzene to Phenol. The Journal for Technology and Science 22 (2011): 95-101.

[25] Song, S., et al. One-step synthesis of Ti-MSU and its catalytic performance on phenol hydroxylation. J Colloid Interface Sci 354(2) (2011): 686-90.

[26] Wróblewska, A. Water as the solvent for the process of phenol hydroxylation over the Ti-MWW catalyst. Reaction Kinetics, Mechanisms and Catalysis 108(2) (2012): 491-505.

[27] Jiang, Y., et al. Fe-MCM-41 nanoparticles as versatile catalysts for phenol hydroxylation and for Friedel–Crafts alkylation. Applied Catalysis A: General 445-446 (2012): 172-179.

[28] Kumar, A. and Srinivas, D. Hydroxylation of phenol with hydrogen peroxide catalyzed by Ti-SBA-12 and Ti-SBA-16. Journal of Molecular Catalysis A: Chemical 368-369 (2013): 112-118.

[29] Wang, X., Zhang, X., Liu, H., Yeung, K.L., and Wang, J. Preparation of titanium silicalite-1 catalytic films and application as catalytic membrane reactors. Chemical Engineering Journal 156(3) (2010): 562-570.

[30] Jiang, X., She, F., Jiang, H., Chen, R., Xing, W., and Jin, W. Continuous phenol hydroxylation over ultrafine TS-1 in a side-stream ceramic membrane reactor. Korean Journal of Chemical Engineering 30(4) (2013): 852-859.

[31] Yan, Y., Jiang, S., Zhang, H., and Zhang, X. Preparation of novel Fe-ZSM-5 zeolite membrane catalysts for catalytic wet peroxide oxidation of phenol in a membrane reactor. Chemical Engineering Journal 259 (2015): 243-251.

[32] Types of catalysis [Online]. Available from: http://www.chemguide.co.uk/physical/catalysis/introduction.html [15 November]

[33] Venceslau, K. The Structure of Zeolite and Aluminophosphase Molecular Seives. Croacita Chemica Acta 67 (1994): 241-261.

[34] Structure of zeolite [Online]. Available from: http://www.gordeszeolite.com/zeolite--clinoptilolite-

[35] Secondary Building Units (SBU's) in zeolites [Online]. Available from: http://www.ch.ic.ac.uk/vchemlib/course/zeolite/structure.html [30 June]

[36] Flanigen, E.M., Broach, R.W., and Wilson, S.T. Zeolites in Industrial Separation and Catalysis. WILEY-VCH Verlag GmbH & Co. KGaA (2010).

[37] Schematic representation of the three types of shape selectivity. [Online]. Available from: http://what-when-how.com/nanoscience-and-nanotechnology/catalytic-properties-of-micro-and-mesoporous-nanomaterials-part-2-nanotechnology/ [30 June]

[38] Fazhi, Z., et al. Preparation of titanium-containing zeolites with MEL structure from B-ZSM-11 and their characterization. Applied Catalysis A: General 192 (2000): 157-163.

[39] Framework Type MFI [Online]. Available from: http://izasc.ethz.ch/fmi/xsl/IZA-SC/ftc_main_image.xsl?-db=Atlas_main&-lay=fw&STC=MFI&-find [30 June]

[40] Bergé-Lefranc, D., et al. Adsorption of small uremic toxin molecules on MFI type zeolites from aqueous solution. Adsorption 14(2-3) (2008): 377-387.

[41] Notari, B. Microporous Crystalline Titanium Silicates. in D.D. Eley, W.O.H. and Bruce, G. (eds.),Advances in Catalysis, pp. 253-334: Academic Press, 1996.

[42] Park, J.-N., Wang, J., Choi, K.Y., Dong, W.-Y., Hong, S.-I., and Lee, C.W. Hydroxylation of phenol with H2O2 over Fe2+ and/or Co2+ ion-exchanged NaY catalyst in the fixed-bed flow reactor. Journal of Molecular Catalysis A: Chemical 247(1-2) (2006): 73-79.

[43] Choi, J.-S., Yoon, S.-S., Jang, S.-H., and Ahn, W.-S. Phenol hydroxylation using Fe-MCM-41 catalysts. Catalysis Today 111(3-4) (2006): 280-287.

[44] Meng, L., Guo, H., Dong, Z., Jiang, H., Xing, W., and Jin, W. Ceramic hollow fiber membrane distributor for heterogeneous catalysis: Effects of membrane structure and operating conditions. Chemical Engineering Journal 223 (2013): 356-363.

[45] Wilkenhöner, U., et al. Influence of Pore and Crystal Size of Crystalline Titanosilicates on Phenol Hydroxylation in Different Solvents. Journal of Catalysis 203(1) (2001): 201-212.

[46] Fultz, B. and Howe, J. Diffraction and the X-Ray Powder Diffractometer. (2013): 1-57.

[47] JOSÉ, T. and VIDAL, B. Diffuse Reflectance Spectroscopy. 2008.

[48] Thommes, M. Physical Adsorption Characterization of Nanoporous Materials. Chemie Ingenieur Technik 82(7) (2010): 1059-1073.

[49] The IUPAC classification of isotherms [Online]. Available from: https://gasadsorptiontech.wordpress.com/2016/01/08/adsorption-equilibrium/ [2 July]

[50] Vernon-Parry, K.D. Scanning electron microscopy: an introduction. III-Vs Review 13(4) (2000): 40-44.

[51] Scanning Electron Microscope [Online]. Available from: https://www.purdue.edu/ehps/rem/rs/sem.htm [13 November]

[52] Introduction the ICP-MS [Online]. Available from: http://crustal.usgs.gov/laboratories/icpms/intro.html [22 October]

[53] The ICP Torch showing the fate of the sample [Online]. Available from: http://crustal.usgs.gov/laboratories/icpms/intro.html [22 October]

[54] Nanda, S. Reactors and Fundamentals of Reactors Design for Chemical Reaction. PHARMACEUTICAL ENGINEERING (2008).

[55] Figure 1 Illustrating a batch reactor. [Online]. Available from: http://www.essentialchemicalindustry.org/processes/chemical-reactors.html [22 October]

[56] Model-based reaction engineering [Online]. Available from: https://www.psenterprise.com/sectors/chemicals/reaction [13 November]

[57] Figure 5 Illustrating a fixed bed reactor [Online]. Available from: http://www.essentialchemicalindustry.org/processes/chemical-reactors.html [22 October]

[58] Schematic of the anaerobic fluidized bed process used in Vegetated Submerged Bed Septic System Designs [Online]. Available from: http://inspectapedia.com/septic/Vegetated_Submerged_Bed_Septic_Design.php [22 October]

[59] Wan, Y. 1-Pentene epoxidation in catalytic microfabricated reactors. Journal of Catalysis 223(2) (2004): 241-249.

[60] L.V. Pirutko, A.K.U., V.S. Chernyavsky, A.S. Kharitonov, G.I. Panov. Preparation and catalytic study of metal modified TS-1 in the oxidation of benzene to phenol by N2O. Microporous and Mesoporous Materials 48 (2001): 345-353.

[61] Duprey, E., et al. Characterization of Catalysts Based on Titanium Silicalite, TS-1, by Physicochemical Techniques. JOURNAL OF CATALYSIS 165 (1997): 22-32.

[62] Laizhi Sun, Xiaodong Zhang, Lei Chen, Baofeng Zhao, Shuangxia Yang, and Xie, X. Comparision of catalytic fast pyrolysis of biomass to aromatichydrocarbons over ZSM-5 and Fe/ZSM-5 catalysts. Journal of Analytical and Applied Pyrolysis 121 (2016): 342-346.

[63] Chen, L., Wang, Y.M., and He, M.-Y. Hydrothermal synthesis of hierarchical titanium silicalite-1 using single template. Materials Research Bulletin 46(5) (2011): 698-701.

[64] Weibin Fan, Ren-Guan Duan, Toshiyuki Yokoi, Peng Wu, Yoshihiro Kubota, and Tatsumi, T. Synthesis, Crystallization Mechanism, and Catalytic Properties of Titanium-Rich TS-1 Free of Extraframework Titanium Species. Journal American Chemical Society 130 (2007): 10150–10164.

[65] Li, B., Xu, J., Liu, J., Zuo, S., Pan, Z., and Wu, Z. Preparation of mesoporous ferrisilicate with high content of framework iron by pH-modification method and its catalytic performance. J Colloid Interface Sci 366(1) (2012): 114-9.

[66] Laha, S.C. and Kumar, R. Promoter-induced synthesis of MCM-41 type mesoporous materials including Ti- and V-MCM-41 and their catalytic properties in oxidation reactions. Microporous and Mesoporous Materials 53 (2002): 163–177.

[67] Liu, M., Chang, Z., Wei, H., Li, B., Wang, X., and Wen, Y. Low-cost synthesis of size-controlled TS-1 by using suspended seeds: From screening to scale-up. Applied Catalysis A: General 525 (2016): 59-67.

[68] Au, L.T.Y., Chau, J.L.H., Ariso, C.T., and Yeung, K.L. Preparation of supported Sil-1, TS-1 and VS-1 membranes: Effects of Ti and V metal ions on the membrane synthesis and permeation properties. Journal of Membrane Science 183(2) (2001): 269-291.

[69] El-Hamshary, H., El-Newehy, M.H., and Al-Deyab, S.S. Oxidation of phenol by hydrogen peroxide catalyzed by metal-containing poly(amidoxime) grafted starch. Molecules 16(12) (2011): 9900-11.

[70] Jung-Nam Park, Jun Wang, Kyu Yong Choi, Wei-Yang Donga, S.-I.H., and Lee, C.W. Hydroxylation of phenol with H2O2 over Fe2+ and/or Co2+ ion-exchanged NaY catalyst in the fixed-bed flow reactor. Journal of Molecular Catalysis A: Chemical 247 (2006): 73-79.

[71] Ying Yan, S.J., Huiping Zhang, Xinya Zhang. Preparation of novel Fe-ZSM-5 zeolite membrane catalysts for catalytic wet peroxide oxidation of phenol in a membrane reactor. Chemical Engineering Journal 259 (2015): 243-251.

[72] Yube, K., Furuta, M., and Mae, K. Selective oxidation of phenol with hydrogen peroxide using two types of catalytic microreactor. Catalysis Today 125(1-2) (2007): 56-63.

APPENDICES

1. Calculation of %conversion of reactant and selectivity of products

$$\%\text{conversion} = \frac{\text{Reacted mole of phenol}}{\text{Initial mole of phenol}} \times 100$$

$$\%\text{selectivity to hydroquinone} = \frac{\text{mole of hydroquinone}}{\text{total mole of all products}} \times 100$$

$$\%\text{selectivity to catechol} = \frac{\text{mole of catechol}}{\text{total mole of all products}} \times 100$$

$$\%\text{selectivity to benzoquinone} = \frac{\text{mole of benzoquinone}}{\text{total mole of all products}} \times 100$$

2. Calibration calculation

2.1 Phenol calibration curve

The standard curve of equation is expressed as following

$$y = 0.8707x - 0.1482$$

Where y is M_{Ph}/M_{Isd}; M_{Ph} = mass of phenol (g)

M_{Isd} = mass of internal standard (cycloheptanone, g)

x is A_{Ph}/A_{Isd}; A_{Ph} = peak area of phenol

A_{Isd} = peak area of internal standard

The correlation coefficient R^2 value for phenol calibration curve is 0.9947.

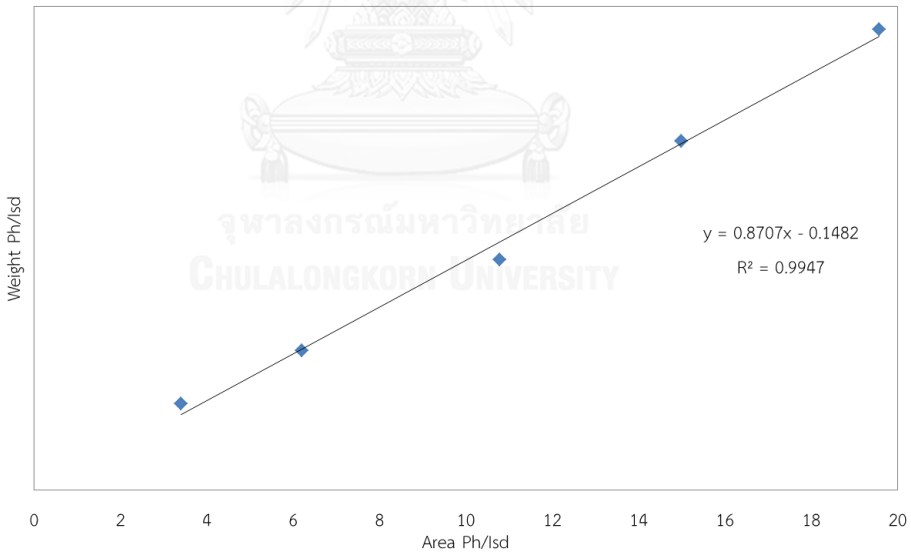

Figure A-1 Calibration curve of phenol

2.2 Hydroquinone calibration curve

The standard curve of equation is expressed as following

$$y = 0.7632x + 0.1807$$

Where y is M_{HQ}/M_{Isd}; M_{HQ} = mass of hydroquinone (g)

M_{Isd} = mass of internal standard (cycloheptanone, g)

x is A_{HQ}/A_{Isd}; A_{HQ} = peak area of hydroquinone

A_{Isd} = peak area of internal standard

The correlation coefficient R^2 value for hydroquinone calibration curve is 0.999.

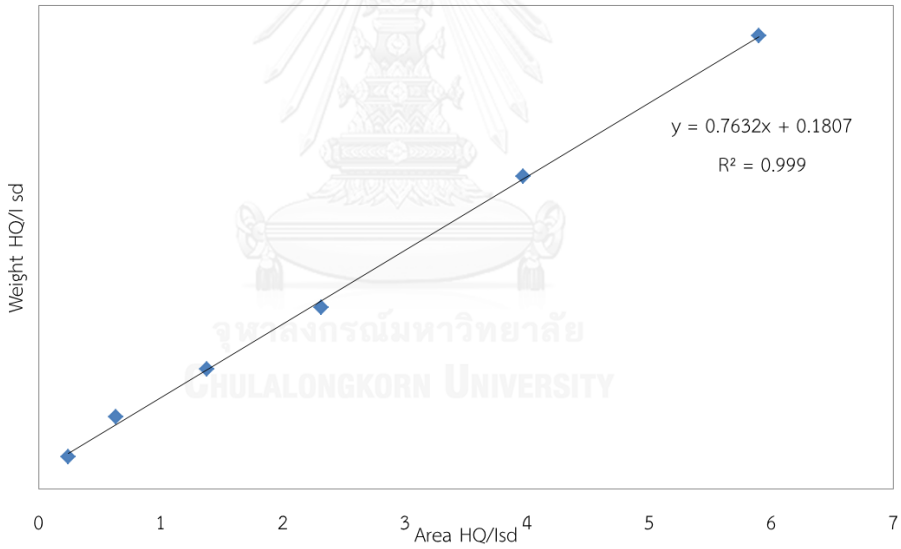

Figure A- 1 Calibration curve of hydroquinone

2.3 Catechol calibration curve

The standard curve of equation is expressed as following

$$y = 0.7312x + 0.1113$$

Where y is M_{CT}/M_{Isd}; M_{CT} = mass of catechol (g)

M_{Isd} = mass of internal standard (cycloheptanone, g)

x is A_{CT}/A_{Isd}; A_{CT} = peak area of catechol

A_{Isd} = peak area of internal standard

The correlation coefficient R^2 value for catechol calibration curve is 0.9993.

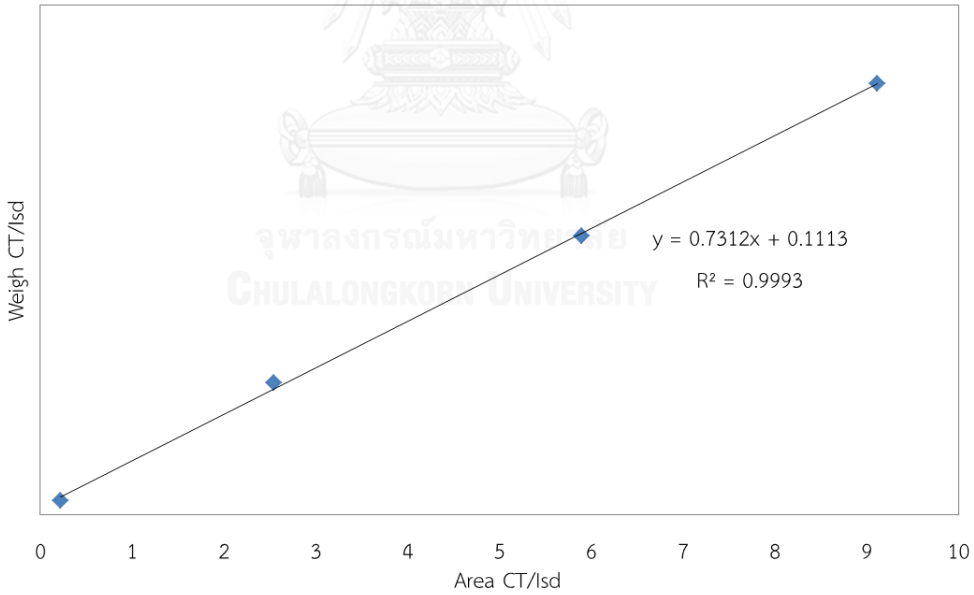

Figure A- 2 Calibration curve of catechol

2.4 Benzoquinone calibration curve

The standard curve of equation is expressed as following

$$y = 1.1257x + 0.0053$$

Where y is M_{BQ}/M_{Isd}; M_{BQ} = mass of benzoquinone (g)

M_{Isd} = mass of internal standard (cycloheptanone, g)

x is A_{HQ}/A_{Isd}; A_{HQ} = peak area of benzoquinone

A_{Isd} = peak area of internal standard

The correlation coefficient R^2 value for benzoquinone calibration curve is 0.9994.

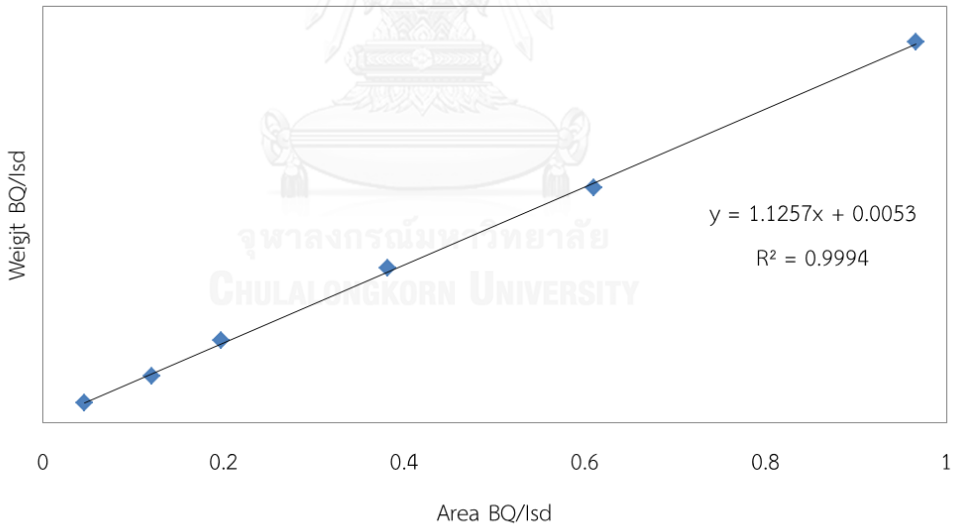

Figure A- 3 Calibration curve of benzoquinone

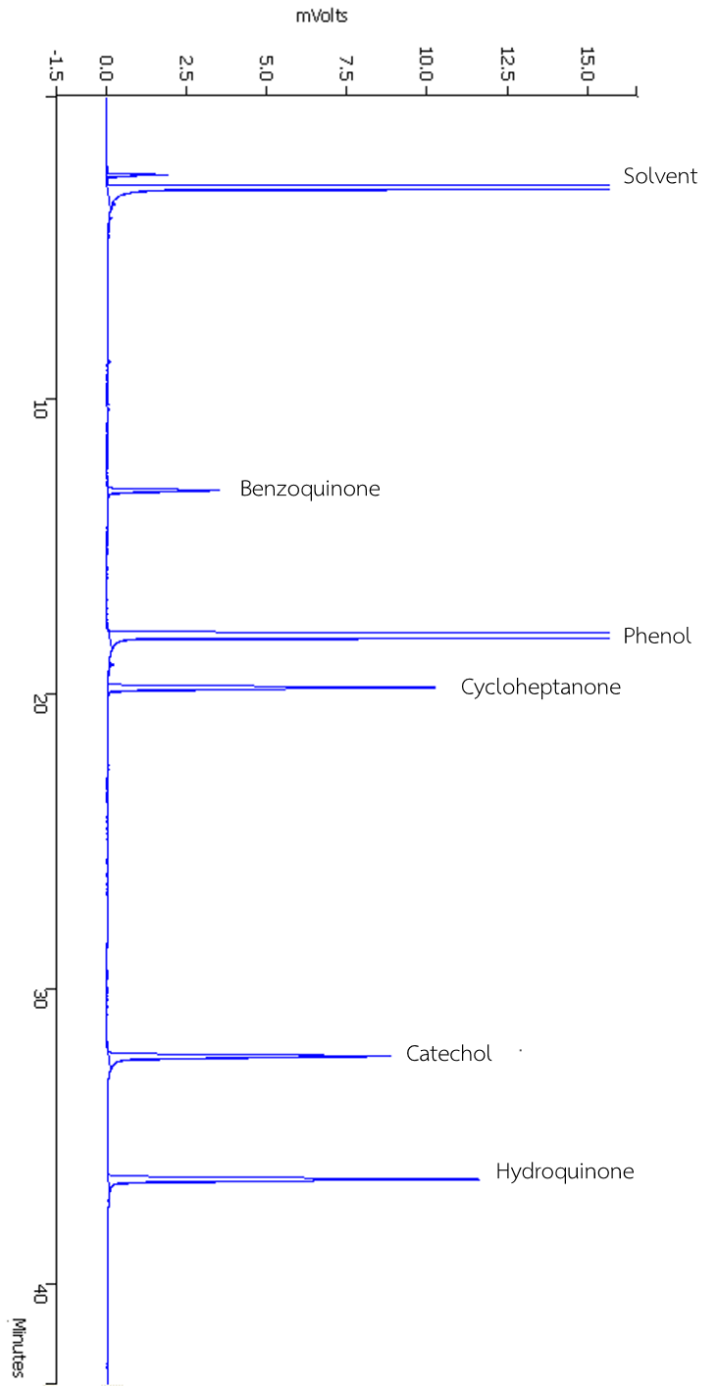

Figure A- 4 GC chromatogram of products from phenol hydroxylation using the cycloheptanone as solvent and cycloheptanone as internal standard

VITA

Miss Kusuma Sriyanai was born on March 8, 1990 in Surin, Thailand. She received a Bachelor Degree of Science, major in Chemistry from Srinakarinwirot University in 2012. And then she has been a graduate student in the program of Petrochemical and Polymer Science, Factually of Science, Chulalongkorn University. She completed of the Master of Science Degree in 2016.

In 9-11 February 2016, she joints the Pure and Applied Chemistry International Conference (PACCON 2016) at Bitec, Bangkok, Thailand. The approval of proceeding and poster presentation was in the title of “Growth and characterizations of titanosilicate porous thin films on silicon substrates”.